Imperial College London

COACTIVATOR BINDING INHIBITORS TARGETING THE ANDROGEN RECEPTOR

Chenming Qian

Supervisor: Prof. Alan C. Spivey

2020-10-23

THESIS SUBMITTED TO IMPERIAL COLLEGE LONDON TO FULLFILL A MPHIL DEGREE

Acknowledgement

Firstly, I would like to express my sincere gratitude to my supervisor, Prof. Alan Spivey, who supported me a lot and offered me this precious chance to have great research experience at Imperial College London.

Secondly, I would like to thank Prof. Charlotte Bevan from the Department of Surgery and Cancer, who is collaborating with this project and kindly offered us a chance to work in her laboratory at Imperial Hammersmith Campus.

Thirdly, I am pleased to acknowledge Ms. Sue Powell from Bevan group, and Dr. Mahesh Mohan from Spivey group for their kind help and huge support during this project.

Besides, I would like to thank people from Imperial College London, Dr. Lisa Haigh and Mr. Peter Haycock from Chemistry Department, and Dr. Anke Nijhuis from the Institute of Reproductive and Developmental Biology for their kind help during this project.

Then, I would like to extend my thanks to everyone in the Spivey group and my friends inside or outside Imperial College London, especially Dr. Deng who initially motivated me for conducting research here.

I also would like to thank my parents, Prof. Qian and Ms. Zhang, who not only financially support my study at Imperial College, but also provide me love and trust.

Finally, please allow me to deliver my greatest gratitude to my deceased grandpa, Mr. Zhang, in memorial of his understanding and support.

Declaration of Originality

I hereby declare that this work and this thesis was completed by me, Chenming Qian. The other materials included in this thesis are all cited with appropriate reference.

5

Copyright Declaration

The copyright of this thesis rests with the author. Unless otherwise indicated, its contents are licensed under a Creative Commons Attribution-Non-Commercial 4.0 International License (CC BY-NC). Under this license, you may copy and redistribute the material in any medium or format. You may also create and distribute modified versions of the work. This is on the condition that: you credit the author and do not use it, or any derivative works, for a commercial purpose. When reusing or sharing this work, ensure you make the license terms clear to others by naming the license and linking to the license text. Where a work has been , , you should indicate that the work has been changed and describe those changes.

Please seek permission from the copyright holder for uses of this work that are not included in this license or permitted under UK Copyright Law.'

Abstract

The Androgen receptor (AR) transcription pathway is known to be a key biological process in the growth of prostate cancer. To specifically interrupt this biological process without side effects, coactivator binding inhibitors (CBIs) have been developed which are designed to target a unique binding site called activation function 2 (AF-2) which is located in the AR ligand-binding domain (LBD).

In this thesis, research was carried out to synthesize compounds which are able to block this protein-protein interface (PPI) and to develop a binding assay to quantify their effectiveness as blocking agents.

In the synthetic work, to obtain a model compound for use as a positive control during the development of the CBI binding assay, a six-step synthesis of a known pyrimidine-based CBI with a 'FXXLF' motif was completed. The final product was characterized spectroscopically and shown to be identical to that reported in the literature. In addition, to target another interesting binding site, binding function 3 (BF-3), several analogs of an indoline-indole based lead compound were designed and were successfully synthesized. An investigation into the oxidation of these to give indole-indole control compounds was also conducted. These BF-3 antagonists are ready for screening in the cell-based assay to produce inhibition data.

For the biology part, a luciferase reporter (LR) assay and a fluorescence polarization (FP) assay were performed on both the AF-2 and BF-3 targeted model compounds. These two assays generated good inhibition data against the AR transcriptional activity and binding towards rat AR-LDB, respectively. The optimization of the FP assay was also successfully achieved with respect to the buffer components and the protocol.

Finally, having successfully recorded the activities of the mentioned model compounds in the FP assay, an alpha-helix mimetic CBI which had been designed and synthesized

previously in the Spivey research group was tested using the FP assay platform and shown to produce good binding data towards AR. It gave a micromolar level IC_{50}, 18.72 ± 3.94 μM. This promising result provides a strong impetus for further investigation of this type of compound for the modulation of AR activity.

5

Abbreviation List

AF-2	*Activation Function 2*
AR	*Androgen Receptor*
BF-3	*Binding Function 3*
Boc	*Di-tert-butyl pyrocarbonate*
conc.	*Concentration*
DCM	*Dichloromethane*
DHT	*Dihydrotestosterone*
DMF	*N,N-Dimethylformamide*
DMSO	*Dimethyl sulfoxide*
DNA	*Deoxyribonucleic acid*
FP	*Fluorescence Polarization*
LBD	*Ligand Binding Domain*
LBP	*Ligand Binding Pocket*
LR	*Luciferase Reporter*
MS	*Mass Spectrometry*
NMR	*Nuclear Magnetic Resonance*
PPI	*Protein-protein Interaction*
PSA	*Prostate Specific Antigen*
RNA	*Ribonucleic acid*
r.t.	*Room Temperature*
SAR	*Structural-activity Relationship*
SM	*Starting Material*
THF	*Tetrahydrofuran*
m.p.	*Melting Point*

Content

Acknowledgement **2**

Declaration of Originality **3**

Copyright Declaration **4**

Abstract **5**

Abbreviation List **7**

Content **8**

List of Figures, Schemes and Tables **10**

Figures 10

Schemes 12

Tables 12

Graphs 13

Chapter 1. The Androgen Receptor as a Therapeutic Target for Prostate Cancer **15**

Introduction 15

Nuclear Receptors (NRs) 15

Androgen Receptor and Prostate Cancer 16

The Androgen Receptor (AR) Transcriptional Pathway 17

Current Anti-Prostate Cancer (PC) Drugs 18

Alternative Target Sites 19

Aim 23

Results and Discussion 27

Synthesis of Model CBIs Following Published Procedures 27

Investigation of Alternative Methods to Obtain CBI-S3 30

Investigation of the Key Step and Synthesis of Model CBI 32

Targeting Binding Function 3 (BF-3) 36

Oxidation Investigations 44

Chapter 2. Development of the Assay **48**

Introduction 48
Luciferase Reporter Assay 48
Time-Resolved Fluorescence Resonance Energy Transfer (TR-FRET) Assay 49
Fluorescence Polarization (FP) Assay 50
Aim 53
Results and Discussion 55
Luciferase Reporter Assay Results 55
Excitation and Emission Scan of the Fluoromone™ 58
First Attempt at Performing the FP Assay 60
Investigation Between Fluoromone™ and AR-LBD, A Direct Binding Assay 67
Optimization of the Protocol 71
Known Anti-androgen Drug Binding 73
Re-testing the model control compound 75
Reach to the Milestone 77
Chapter 3. Conclusions 81
Chapter 4. Future Work 83
Chapter 5. Experimental 85
Biology Assays 85
Chemistry Experimental 86
Chapter 6. Reference List 105
Appendix 110
List of Supporting Information (SI), Figures and Tables 110
SI Figures 110
SI Tables 111
SI Figures and Tables 112

List of Figures, Schemes and Tables

Figures

Figure 1. Universal bar structure of nuclear receptors. It consists of an N-terminal domain (**NTD**), a DNA binding domain (**DBD**), a hinge region (**H**) and a ligand binding domain. (**LBD**) [3] 15

Figure 2. The plasmid siRNA transfected control (**A, left**) and the AR-depleted LNCap Cells (**B, right**).[7] More apoptosis was found in **B**, which indicates the importance of AR activity for survival of LNCap Cells. 16

Figure 3. The signaling transcriptional pathway of AR. 17

Figure 4. Structures of flutamide, bicalutamide and nilutamide. 18

Figure 5. The crystal structure of AR-LBD. Highlighted regions are activation function 2 (AF-2 in yellow) and binding function 3 (BF-3 in red). This figure is from Biron *et al*. [4] 19

Figure 6. A Pymol representation of the interaction between AF-2 key residues (K720, M734, M894 and E897 in yellow) and FXXLF motif in orange. One of the phenyl groups is stabilised by a lysine (K720) and a methionine (M734) residue. The combination of glutamic acid residue (E897) as well as lysine (K720) residue also serves as a charge clamp. [PDB: 1T7R] [15, 16] 20

Figure 7. Chemical Structure of Compound **1**.[17] 21

Figure 8. The chemical structure of compound **2** and a Pymol representation of the interaction between BF-3 key residues (P671, I672, F673, L674, P723. P724, N727, F826, E829, L830, N833, Y834, E837 R840 in yellow) and compound **2** in orange. The whole structure was generated by molecular modelling [PDB: 2YLO][19, 20] 22

Figure 9. Chemical structure of Compound **3**. 23

Figure 10. The chemical Structure of **Spivey's CBI**[22]. 24

Figure 11. The chemical structures of the selected model CBIs for development of our *in-vitro* assay.[17] 24
Figure 12. The chemical structure of BF-3 inhibitors that were planned to be synthesized. 26
Figure 13. The oxidization of BF-3 inhibitors that planned to be synthesized. ... 26
Figure 14. Synthesis of **CBI-S1**. 27
Figure 15. Synthesis of **CBI-S2**. 27
Figure 16. Synthesis of **CBI-S2.** 28
Figure 17. First alternative synthetic route to obtain **CBI-S3**. 30
Figure 18. Nucleophilic substitution using isobutylamine may generate two regioisomers of **CBI-S4**. 30
Figure 19. Unsuccessful Boc protection. 31
Figure 20. Second alternative synthetic route to obtain **CBI-S3**. 31
Figure 21. Synthesis of **CBI-S4**. 32
Figure 22. Synthesis of **CBI-S7**. 34
Figure 23. Boc deprotectio to generate **CBI-S8**. 34
Figure 24. Comparison of the ^{1}H NMR spectra for the crude product of **CBI-S8**: 35
Figure 25 Synthesis of compound **1**. 35
Figure 26. The plan of synthesis of BF-3 targeting compounds. 36
Figure 27. Synthesis of compound **3**. 37
Figure 28. Synthesis of **BF3-S2**. 39
Figure 29. Synthesis of **BF3-S6**. 41
Figure 30. Synthesis of **BF3-S7**. 42
Figure 31. Planed alternative route to obtain **CBI-S7.** 42
Figure 32. Synthesis of **BF3-S8**. 43
Figure 33. Oxidation of indoline-indole structure into bis-indole. 44
Figure 34. Attempted oxidation of **BF3-S1**. 44
Figure 35. A schematic of luminescence generated by luciferase oxidation. The luciferin reagent is added to the system in non-rate-limiting amounts, and the

luminescence output is proportional to the amount of luciferase enzyme produced by activation of the reporter gene. 48
Figure 36. Schematic representation of the TR-FRET assay.[34] 49
Figure 37. A schematic representation of FP detection. [35] 51
Figure 38. Cartoon showing how a size differences between molecules results in differences in the polarization of emitted light in an FP assay. [35] 52
Figure 39. Structures of compound **1**, compound **3** and **Spivey's CBI**. 53
Figure 40. Schematic of the AR FP competitor assay. 54
Figure 41. The Luciferase Reporter Assay Result for compound **1**..... 56
Figure 42. The Luciferase Reporter Assay Result for compound **3**..... 56
Figure 43. 96-well plate layout and table of resulting final conc. values for the first attempt at the FP assay..... 61
Figure 44. Plates in the original protocol. 71
Figure 45. Plates in the optimized protocol. 71
Figure 46. Structure of Enzalutamide. 73

Schemes

Scheme 1. Planned Synthetic route to model CBI **1** following Gunther's route.[17] 25

Tables

Table 1. Entries of the substitution reaction involves Suzuki coupling product. T = Temperature; R. T. = Reaction Time, N. D. = No data, U. P. = undesired product. 29
Table 2. Entries of the substitution reaction involves Suzuki coupling product. T = Temperature; R. T. = Reaction Time, N. D. = No data, U. P. = undesired product. 33

Table 3. Left is comparison of 1H NMR of reaction mixture with variable equivalent of HFIP. **Blue** (5 eq. of HFIP); **Green** (25 eq. of HFIP); **Red above** (1 eq. of HFIP); **Red below**, NMR of **BF3-S1.** 38

Table 4. Comparison of yield of the reaction to form **BF3-S1** following the original protocol and the modified conditions. 39

Table 5. The resulting yield of indoline-indole analogs (**BF3-S3**, **S4** and **S5**) using modified reaction conditions. 40

Table 6. Synthesis of **BF3-S81.** 43

Table 7. Attempted oxidation of **BF3-S1**. S. M. = starting material (**BF3-S1**), N. D. = no data, N. D. P. = No Desired Product. * 10 eq. of Ammonium formate (HO_2NH_4) was also used. 45

Graphs

Graph 1. Excitation Scan of Fluoromone™ with 1X conc. in 1% DMSO in NR buffer. 58

Graph 2. Excitation Scan of Fluoromone™ with 2X conc. in 1% DMSO in NR buffer. 59

Graph 3. Emission Scan of Fluoromone™ with 1X conc. in 1% DMSO in NR buffer. 59

Graph 4. Emission Scan of Fluoromone™ with 2X conc. in 1% DMSO in NR buffer. 60

Graph 5. Polarization graphed against the conc. of Testosterone with 0.5X NR in 1% DMSO in NR buffer. (2h) 62

Graph 6. Polarization graphed against the conc. of Testosterone with 1X NR in 1% DMSO in NR buffer. (2h) 63

Graph 7. Polarization graphed against the conc. of Testosterone with 2X NR in 1% DMSO in NR buffer. (2h) 63

Graph 8. Polarization graphed against the conc. of Testosterone with 2X NR in 1%

DMSO in NR buffer. (3h) 64

Graph 9. Polarization graphed against the conc. of Testosterone with 2X NR in 1% DMSO in NR buffer. (4h) 64

Graph 10. Polarization graphed against the conc. of KB-CBI with 2X NR in 1% DMSO in NR buffer. (2h) 65

Graph 11. Polarization graphed against the conc. of KB-CBI with 2X NR in 1% DMSO in NR buffer. (3h) 66

Graph 12. Polarization graphed against the conc. of KB-CBI with 2X NR in 1% DMSO in NR buffer. (4h) 66

Graph 13. Polarization graphed against the concentration of NR-LBD in 1% DMSO in NR buffer with Hill binding Model and calculated K_d (0.32 μM) 69

Graph 14. Polarization graphed against the concentration of NR-LBD in 2% DMSO in NR buffer with Hill binding model and calculated K_d (0.16 μM)..... 70

Graph 15. Polarization against the concentration of Enzalutamide in 2% DMSO in NR buffer. (3h)..... 74

Graph 16. Polarization against the concentration of Enzalutamide in 2% DMSO in NR buffer. (4h)..... 74

Graph 17. Polarization against the concentration of compound **1** in 2% DMSO in NR buffer. (3h)..... 75

Graph 18. Polarization against the concentration of **compound 3** in 2% DMSO in NR buffer. (3h)..... 76

Graph 19. Polarization against the concentration of **Testosterone** in 2% DMSO in NR buffer. (3h)..... 77

Graph 20. Polarization against the concentration of **Testosterone** in 2% DMSO in NR buffer. (4h)..... 78

Graph 21. Polarization against the concentration of **Spivey's CBI** in 2% DMSO in NR buffer. (3h)..... 78

Graph 22. Polarization against the concentration of **Spivey's CBI** in 2% DMSO in NR buffer. (4h)..... 79

Chapter 1. The Androgen Receptor as a Therapeutic Target for Prostate Cancer

Introduction

Nuclear Receptors (NRs)

Nuclear Receptors (NRs) are known to be key proteins for regulating complex physiological processes including cell development, differentiation and death.[1] This family of transcription factors comprises a subfamily of steroid receptors, like the androgen receptor (AR) and the estrogen receptor (ER), as well as thyroid, retinoid, vitamin D and other orphan receptors which also belong to the NR superfamily.[2] In the past several decades, the molecular-structures, and mode of activity of these proteins have gradually become better understood, and well-presented. It has become apparent that all the NRs share a similar structure. Thus, NRs all contain a series of common functional domains. (**Figure 1**)



Figure 1. Universal bar structure of nuclear receptors. It consists of an N-terminal domain (NTD), a DNA binding domain (DBD), a hinge region (H) and a ligand binding domain. (LBD) [3]

Starting from the N-terminus, there is an N-terminal domain (NTD) which contains a transcriptional activation function and mediates direct binding with certain regulatory proteins. Next is a DNA binding domain (DBD) which allows DNA binding to modulate gene expression. The DBD is linked by a hinge region (H) to the ligand binding domain

(LBD) which possesses a key conserved ligand binding pocket for the endogenous ligand.[3]

Androgen Receptor and Prostate Cancer

The AR is comprised of approximately 919 amino acids and shares a similar structure to the other NR family proteins.[4] The ligand binding pocket that is conserved inside the AR-LDB enables the AR to become a cytoplasmic carrier for the androgens and plays a key role not only in cell differentiation, but also in growth of the male reproductive systems.[5]

The AR is also known as a key transcriptional factor not only for the growth of the male reproductive system but also for the growth of prostate cancer (PC). To investigate this, Yang *et al*.[6] have demonstrated a control experiment that emphasizes the importance of AR to PCs. By utilizing vector-based small interfering RNA (siRNA) to target AR mRNA, they were aiming to suppress AR expression. After transfection with pre-constructed vectors, AR protein levels and activity in these LNCaP cells was removed. After incubation and counting of apoptotic bodies, they found that the AR-depleted cancer cells undergo more apoptosis than the control. (**Figure 2**)

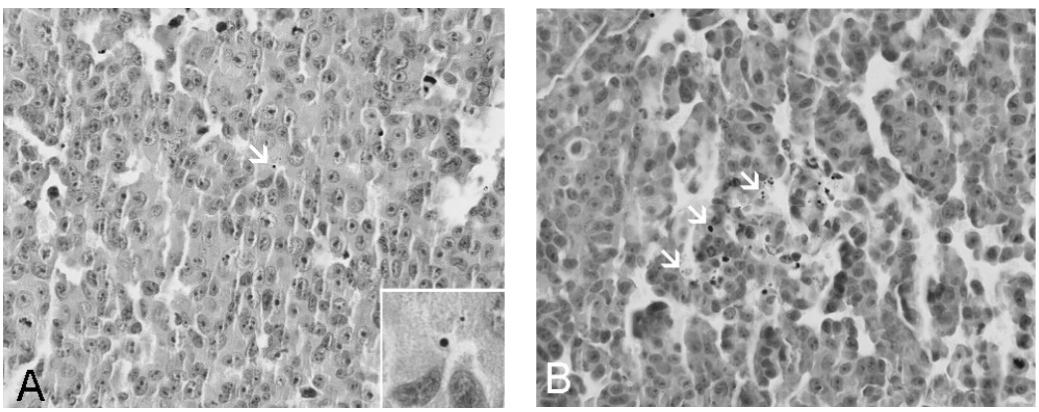


Figure 2. The plasmid siRNA transfected control (**A, left**) and the AR-depleted LNCap Cells (**B, right**).[6] More apoptosis was found in **B**, which indicates the importance of AR activity for survival of LNCap Cells. The cells were stained with hematoxylin for

observation of the apoptosis.

This result demonstrates the importance of the AR for the survival of PC cells and reinforces the prospect of suppressing the AR activity for PC treatment.

The Androgen Receptor (AR) Transcriptional Pathway

As a key component of a ligand-dependent signaling transcriptional pathway, the AR plays an important role in the growth and proliferation not only of healthy prostate cells, but also PC cells. An overview of the transcriptional pathway is shown below (**Figure 3**).

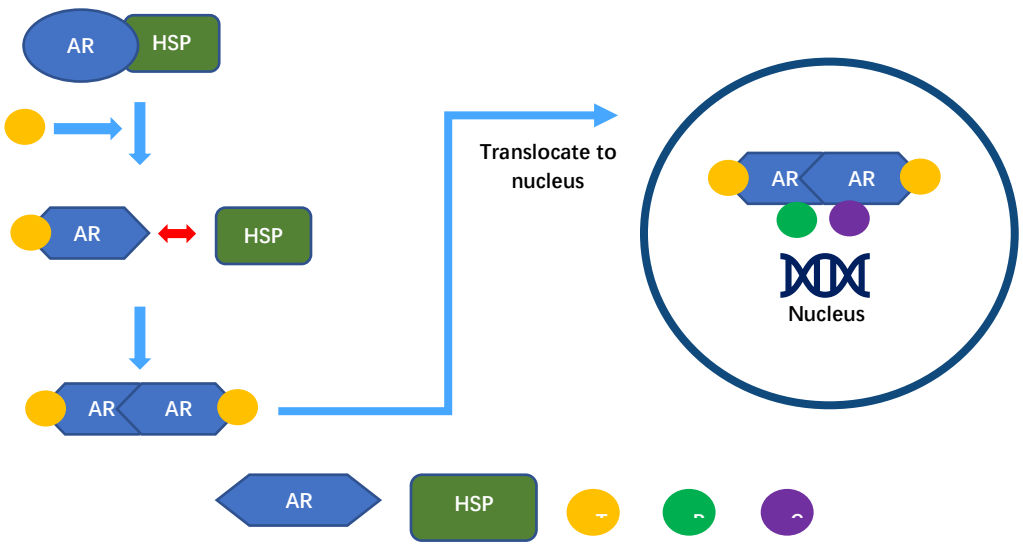


Figure 3. The signaling transcriptional pathway of AR.

AR; HSP; Androgen; Coregulator; Coactivator

The transcriptional pathway is initiated by the interaction between AR and an androgen ligand (e.g. testosterone or DHT). After the androgen enters into the AR ligand binding pocket (LBP), the LBD helix-12 starts to fold which leads to a conformational change of the protein. The shape changes of the protein structure lead to a structural rearrangement which triggers the dissociation of the ligand-bound

receptor from the heat shock protein (HSP). The dissociated ARs can then dimerize, and also the nuclear localization signal in the hinge region is exposed. The complex can be translocated into the nucleus for further activation by binding to the DNA for gene expression before recruitment of coregulators and coactivators[7, 8].

Current Anti-Prostate Cancer (PC) Drugs

Conventional therapies for PC mainly target the LBP directly. By blocking the interaction between an androgen and the AR, the whole transcriptional pathway can be interrupted since no trigger condition exists.

These therapies generally employ non-steroidal antiandrogen drugs, for example: flutamide, bicalutamide and nilutamide. (**Figure 4**)

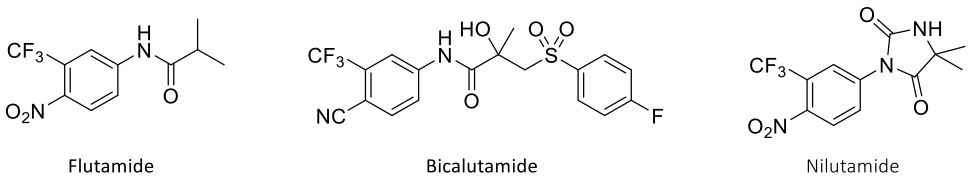


Figure 4. Structures of flutamide, bicalutamide and nilutamide.

Without the agonist properties of androgens[9], these drugs have been proven to be effective for the suppression of PCs and are widely used in current therapies.

However, it has been reported that this strategy is not efficient in castration-resistant prostate cancers (CRPCs). This intractable form of PC may arise in many cases due to two features.

The first of these is increased AR expression in cancer cells which results from AR gene amplification. The increased amount of AR contributes to the increasing sensitivity of AR in the PC cells under androgen deprivation therapy. Secondly, the AR can be mutated in its LBD, resulting in a decrease of ligand specificity and selectivity. One well-characterized mutation is T877A, where it has been shown that an LBP targeting

antagonists e.g. flutamide can become an agonist as the result of the mutation. Furthermore, the X-ray structure of the AR-LBD bound to DHT was refined at 2.0 Å resolution by Sack *et al*.[5] They found that the structural differences could explain how the treatment can lose control resulting in enhanced rather than suppressed transcriptional pathway activity[10].

Alternative Target Sites

To gain better suppression of AR activity and avoid the impact from the above-mentioned LBD mutations, researches have looked for other attractive target sites including activation function 2 (AF-2) and binding function 3 (BF-3). (**Figure 5**)

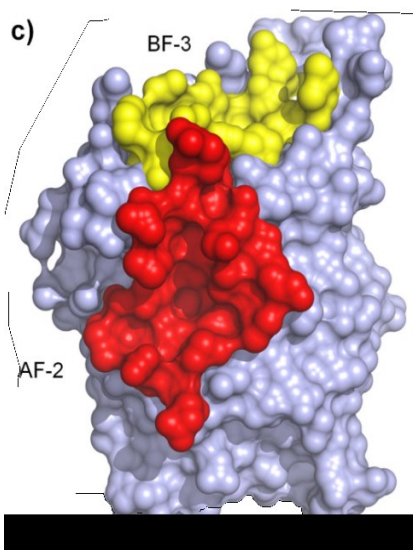


Figure 5. The crystal structure of AR-LBD. Highlighted regions are activation function 2 (AF-2 in yellow) and binding function 3 (BF-3 in red). This figure is from Biron *et al*.[11]

AF-2 is a surface-exposed region that is located on the AR-LBD and forms a binding interface with coactivator and corepressor proteins. Small molecules that bind to this region have the potential to prevent the recruitment of these coregulator proteins that are essential for the transcriptional function of the receptor. The hypothesis therefore

is that compounds that can selectively block this interaction may suppress growth of PC without the intractable side-effects of the current drugs. [12, 11]

To gain better understanding and to interact with the hydrophobic domain of AF-2, previous work has employed phage display technology and structural studies. These have revealed that alpha-helical peptides or peptide-like molecules with 'LXXLL' (L = leucine, X = any amino acid) and 'FXXLF' (F = phenylalanine) motifs can bind strongly at this protein-protein interface. Thus molecules bearing an alpha-helix structural motif with side chains (e.g. leucine or phenylalanine) at unique positions (*e.g. i*, *i*+3 and *i*+4) also have a potential for strong binding. [13, 14, 11] (**Figure 6**)

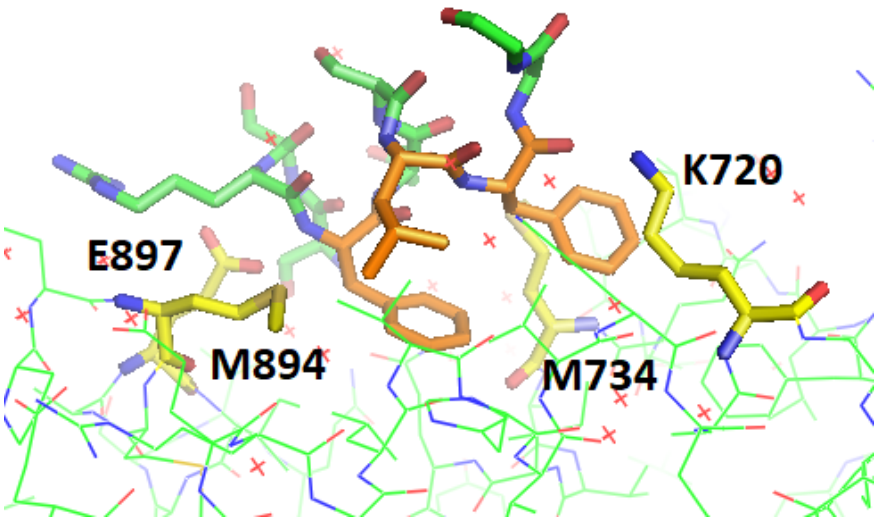


Figure 6. A Pymol representation of the interaction between AF-2 key residues (K720, M734, M894 and E897 in yellow) and FXXLF motif in orange. One of the phenyl groups is stabilized by a lysine (K720) and a methionine (M734) residue. The combination of glutamic acid residue (E897) as well as lysine (K720) residue also serves as a charge clamp. [PDB: 1T7R] [15, 16]

Based on their successful work developing coactivator binding inhibitors (CBIs) targeting the estrogen receptor (ER), Parent *et al*. have extended the use of their previous potent scaffold to interrupt the AR signaling transcriptional pathway.[12] They

have reported the results of a time-resolved fluorescence energy transfer (TR-FRET)-based-assay of a library of 2,4,6-trisubstitued pyrimidine core CBIs. CBI derivatives bearing bulky and hydrophobic aromatic side chains showed promising IC_{50} values in the micromolar range. Among all of them, compound **1** bearing the 'FXXLF' motif has the best inhibition of transcriptional activity of both wild-type AR and mutant AR (T877A), with IC_{50} values of 2.6 μM and 3.5 μM, respectively.[17] (**Figure 7**)

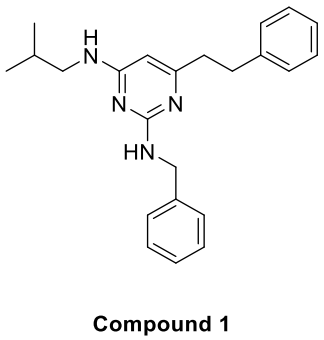
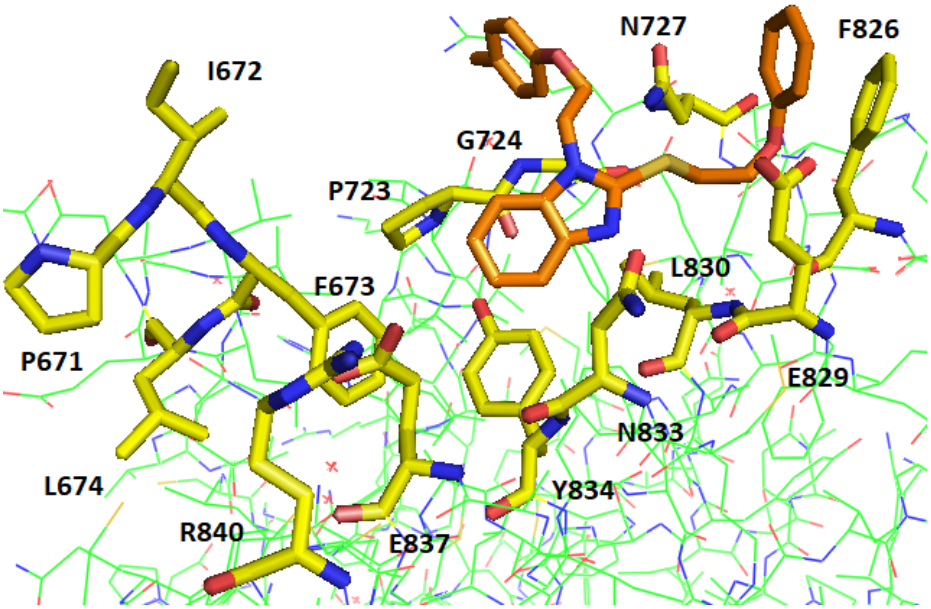


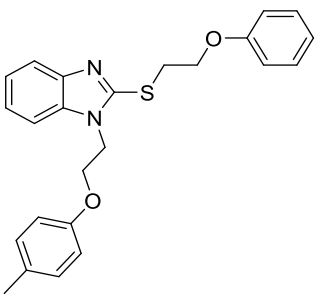
Figure 7. Chemical Structure of Compound **1**.[17]

Apart from AF-2, BF-3 is also an interesting potential target site, which is located beside AF-2 in the AR-LBD. Although the natural role in biological processes of BF-3 remains unclear, it has been reported that BF-3 can have an allosteric impact on the AF-2 region[18]. It can be involved in recruitment of key AR activators like the FKPB52 protein.[19] Previous papers revealed that inhibitors often bind to both BF-3 and AF-2 and have off-target effects.[11] The IC_{50} values of these drug candidates were also moderate (>50 μM). Therefore, the development of inhibitors that specifically target BF-3 is a necessary and worthwhile pursuit.

Based on structural-activity relationship (SAR) studies in cell-based assays, Cherkasov's group has reported the virtual screening of a library of BF-3 inhibitor candidates using the ZINC database.[11] Following purchase and screening of selected potential hit compounds, they found that some of the molecules (*e.g.* benzo-imidazole-based compound **2**) have no effect on ligand displacement at AF-2 but have relatively potent

activity against AR transcriptional activity (IC_{50} = 0.5 – 100 μM). They determined that these derivatives bind at the BF-3 site and developed a binding model between these screened compounds and the BF-3 binding site.[20] (**Figure 8**)



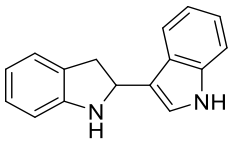


Compound 2

Figure 8. The chemical structure of compound **2** and a Pymol representation of the interaction between BF-3 key residues (P671, I672, F673, L674, P723. P724, N727, F826, E829, L830, N833, Y834, E837 R840 in yellow) and compound **2** in orange. The whole structure was generated by molecular modelling [PDB: 2YLO][20, 21]

SAR studies were conducted by Cherkasov's group through modification of the side chains of compound **2**. The removal of the bulky side chain can decrease the binding energy while the introduction of functional groups on the aromatic rings can increase

the binding affinities.[21] Recently, they reported a potent indoline-indole based structure that targets BF-3 and inhibits AR transcriptional activity with an IC_{50} value of 0.31 μM.[22](**Figure 9**)



Compound 3

Figure 9. Chemical structure of Compound **3**.

Their peptide displacement assay at the BF-3 pocket showed that compound **3** was directly binding to BF-3 rather than AF-2. They also reported that compound **3** displays good inhibition of AR activity by significantly decreasing the expression of prostate specific antigen (PSA) and the expression of AR target genes.[22] This promising lead compound provides impetus to look further at the BF-3 site as a therapeutic target, to develop a better understanding of its function, and to find more potent antagonists which could form the basis of better PC therapies in the near future.

Aim

Our group has successfully synthesized a novel scaffold for alpha-helix mimetic molecules based on the ideas outlined in the introduction to this thesis. These aza-biocyclo[.2, 2] octane-based structures are designed to project five different functional units to mimic the five side chain functions of alpha-helix. The employed side chain residues (*e.g*. *i*, *i*-3, *i-2*, *i*+3 and *i*+4 for five amino residues FEELF, respectively) were designed to project into different directions so as to maximize their binding with the AR AF-2 domain[23]. (**Figure 10**)

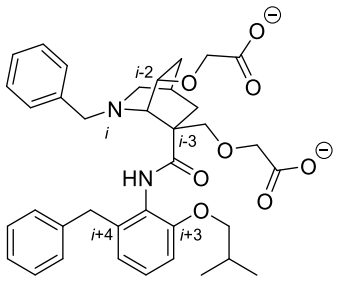


Figure 10. The chemical Structure of **Spivey's CBI**[23].

Nevertheless, the quantity of this novel CBI that was available from the first campaign for its synthesis by a previous post-doctoral researcher in the Spivey group, Dr Christine Tran, was considered unlikely to be sufficient to carry out a whole binding assay to generate reliable IC_{50} values. Thus, to avoid any unnecessary waste of the material, it was considered necessary to select several model structures, designed to target the same motif as the Spivey CBI, for development of the assay.

To this end, two published structures of CBIs from Gunther's work[17] were selected for synthesis. These two compounds were proposed to mimic the 'FXXLF' (compound **2**) and 'FXXFF' (compound **4**) motifs, respectively. (**Figure 11**)

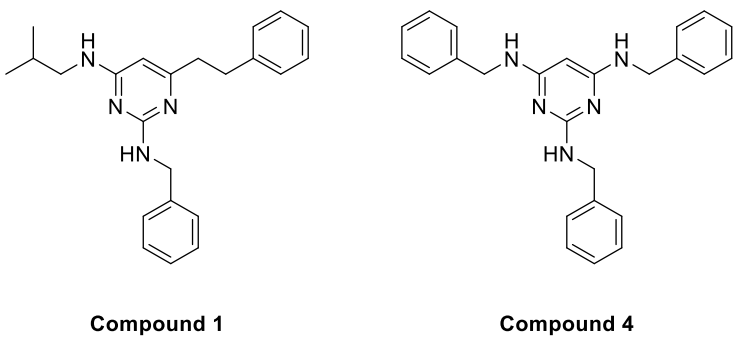
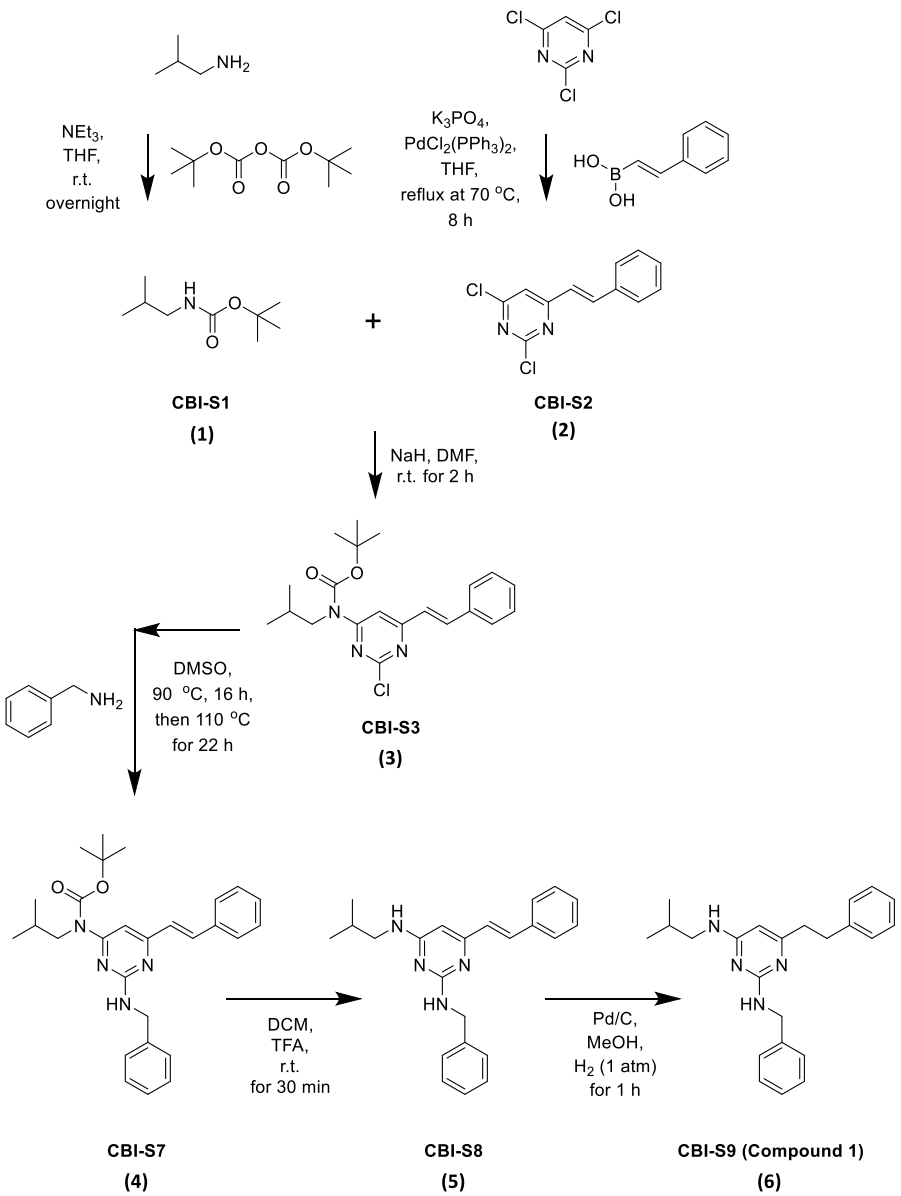


Figure 11. The chemical structures of the selected model CBIs for development of our *in-vitro* assay.[17]

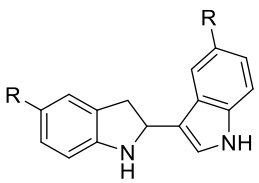
The synthesis of these two compounds had been attempted by a previous MRes

student from our group: Yu Liu.[24] Following the experimental from Gunther's work[17], compound **4** was successfully obtained by Liu while the synthesis of compound **1** was not completed because one of the steps failed. In this work, the synthesis was planned to start by following the published experimental for compound **1**. The planned synthetic route is shown in **Scheme 1**[17].



Scheme 1. Planned Synthetic route to model CBI **1** following Gunther's route.[17]

In addition, as mentioned before, BF-3 is also an interesting target for interrupting AR transcriptional activity. Thus, to see if we could repeat the reported binding and activity data, and gain a better understanding of the BF-3 site, several analogs based on a published indoline-indole structure[22] were scheduled to be synthesized. (**Figure 12**)

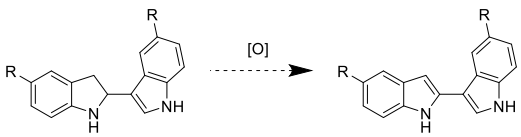


BF3-S1 to S7

R = H, F, Cl, Br, OMe, OH, COOH

Figure 12. The chemical structure of BF-3 inhibitors that were planned to be synthesized.

The indoline-indole structure was thought to be relatively unstable as it can be oxidized into a bis-indole upon exposure to air. (**Figure 13**)



BF3-S1 to S7 **OXBF3-S1 to S7**

R = H, F, Cl, Br, OMe, OH, COOH

Figure 13. The oxidization of BF-3 inhibitors that planned to be synthesized.

The oxidation of these analogs was also therefore planned to be investigated in this work.

Results and Discussion

Synthesis of Model CBIs Following Published Procedures

To obtain compound **1** (**CBI-S9, Scheme 2**), the key step is to obtain a disubstituted pyrimidine through nucleophilic attack of an amine onto a mono-substituted pyrimidine core. The starting materials can be obtained by amine protection and Suzuki coupling, respectively. After the key step, the final product can be achieved by another nucleophilic attack followed by deprotection and hydrogenation. Hence, the work started from protection of isobutyl-amine to reduce its nucleophilicity and gain better regioselectivity in the key step. (**Figure 14**)

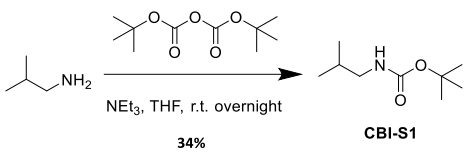


Figure 14. Synthesis of **CBI-S1**.

tert-Butyloxycarbonyl protection of isobutyl-amine took overnight and gave a pale-yellow oil as crude product after work-up. The oil was purified by distillation under reduced pressure and gave the pure product as a colorless oil in34% yield.

At the same time, Suzuki coupling between trichloropyrimidine and phenylvinyl boronic acid was conducted in THF in the presence of potassium phosphate and bis-(triphenylphosphine)-palladium (II) dichloride as catalyst. (**Figure 15**)

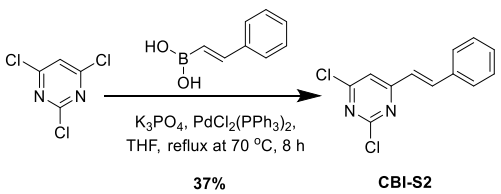


Figure 15. Synthesis of **CBI-S2**.

The reaction took around 8h at reflux and some problems were met during the synthesis. The reaction did not go to completion even when reacted for 1h longer than the published protocol. Besides, after checking by thin layer chromatography (TLC), 2,4,6-trichloro-pyrimidine was found not to be fully consumed even after addition of more boronic acid (0.2 equiv.). Several by-products were also observed by TLC which led to the low yield (37%, *cf.* 73% in the Lit.[17]) and unsatisfactory product purity after flash chromatography. The reason could be the degradation of the boronic acid that generated some impurities. The reaction gave a yellow powder as product (**CBI-S2**).

The third step involved the substitution reaction between **CBI-S1** and **CBI-S2.** The reaction was reported to procced at room temperature (r.t.) for 2h in dimethyl-formamide (DMF) [17] (**Figure 16**).

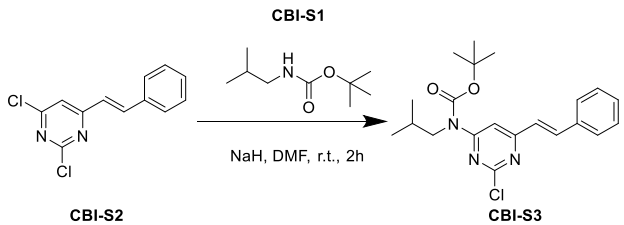
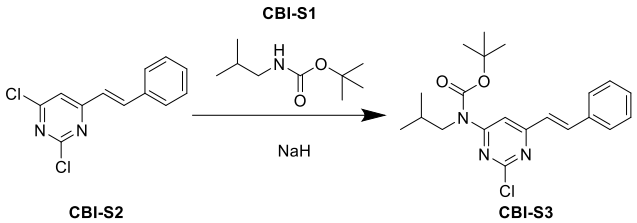


Figure 16. Synthesis of **CBI-S2.**

This reaction was thought to be intractable based on the experience of Yu, the previous MRes student in the group who attempted this transformation. She reported that strong heat (80 ^{o}C) and a long reaction times (6 days) were required to obtain traces of product. The reason for this might be that the protection of the amine significantly reduces the nucleophilicity of the amine. This makes the attack on the pyrimidine unfavorable. However, Boc protection was believed to be necessary since the more nucleophilic unprotected amine was expected to lead to uncontrolled regioselectivity and product purity. This means the reaction would have generated a mixture of di- and tri-substituted products rather than only generating the desired disubstituted pyrimidine. The investigation of this reaction (**Table 1**) started with carrying out the

reaction strictly following the published experimental protocol utilizing sodium hydride (NaH) as the base (**entry 1**).



	Solvent	T/°C	NaH Used	R. T.	Outcome
Entry 1	DMF	r.t. (2h) then 50	1.5 eq.	2+3h	N. D.
Entry 2	DMF	r.t. (2h) then 80	1.5 eq.	2+3h	N. D.
Entry 3	DMF	r.t. (2h) then 90	1.5 eq.	2+overnight	U. P.
Entry 4	THF	r.t. (2h) then 50	1.5 eq.	2+overnight	U. P.

Table 1. Attempted substitution reaction between dichloropyrimidine and N-Boc protected iso-butylamine. T = Temperature; R. T. = Reaction Time, N. D. = No data, U. P. = undesired product.

The reaction was conducted under an atmosphere of nitrogen to prevent ingress of water since NaH is extremely moisture sensitive. However, no evidence of product was obtained by TLC analysis after 2h. The reaction was heated to 50 °C based on the experience from previous report that heating may contribute to the conversion of starting materials. After 3h, TLC still showed no evidence for the product. At this stage, another reaction (**Table 1, entry 2**) was set up, this time applying strong heating to 80 °C. After 2h. stirring at r.t., no reaction was observed, and this situation remained unchanged after a further 3h stirring. Therefore, it was considered that strong heating and a long reaction time was required (**Table 1, entry 3**). A significant solvent effect was also considered likely to affect the outcome. (**Table 1, entry 4**) Unfortunately, both strong heat with long reaction time and changing the solvent from DMF to tetrahydrofuran (THF) gave no desired product as determined by ^{1}H NMR spectroscopy

in comparison to the Lit.[17]

Investigation of Alternative Methods to Obtain CBI-S3

Considering the difficulties in substituting **CBI-S1** onto **CBI-S2**, alternative routes were considered.

The investigation started by using isobutylamine itself rather than its protected congener as the reagent to attempt substitution of the pyrimidine core. The plan was to follow this with Boc protection of the product to give **CBI-S3**. (**Figure 17**)

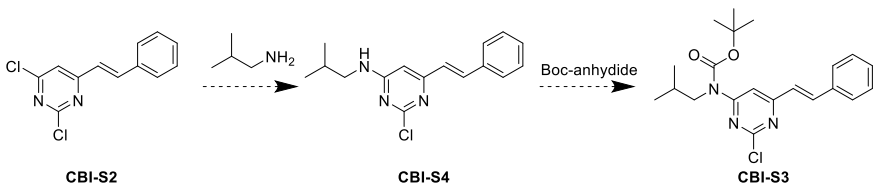


Figure 17. First alternative synthetic route to obtain **CBI-S3**.

The reaction gave a yellow oil but in less than 20% yield. The isobutyl group was clearly present as evidenced by a characteristic doublet for the two methyl groups in the ^{1}H NMR spectrum. This outcome proved the feasibility of this reaction. Nevertheless, due to the strong activity of primary amine, it was suspected that the product in this reaction could be the regioisomer of the desired product. (**Figure 18**)

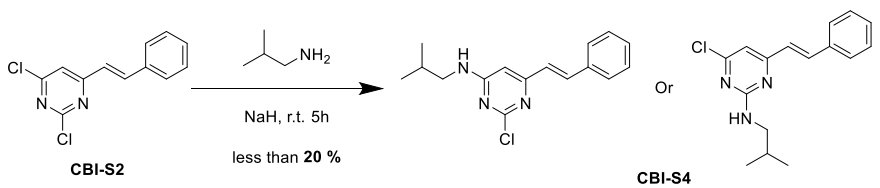


Figure 18. Nucleophilic substitution using isobutylamine may generate two regioisomers of **CBI-S4**.

The lack of a reference spectrum made the confirmation of the structure of the product difficult and several analytical methods were required (*e.g*. 2D NMR).

The investigation was continued with Boc protection of the product to match the reference known compound (**CBI-S3**). However, the protection reaction failed, and no product was obtained. (**Figure 19**)

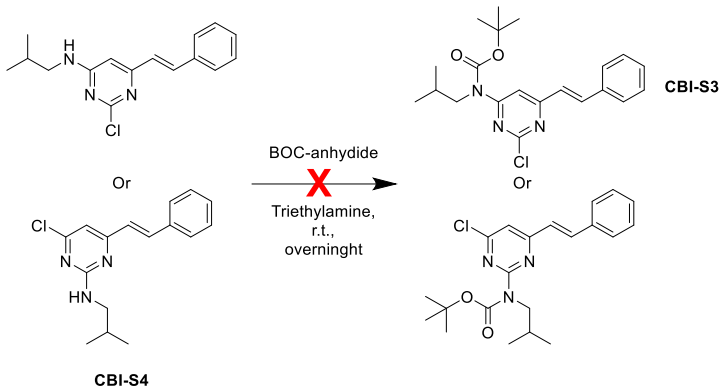


Figure 19. Unsuccessful Boc protection.

An alternative route was attempted next. This involved the substitution reaction of Boc protected isobutylamine with 2,4,6-trichloropyrimidine followed by coupling of the styrenyl group. (**Figure 20**)

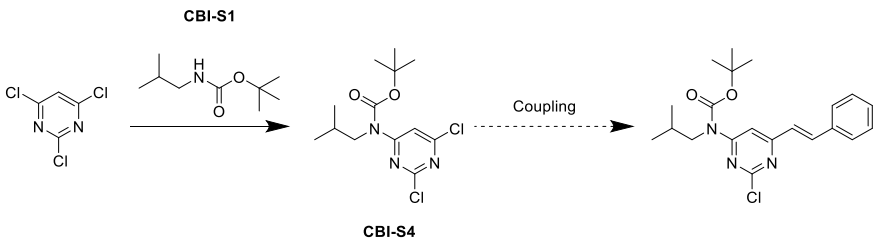


Figure 20. Second alternative synthetic route to obtain **CBI-S3**.

The first reaction provided around 41% of product, the analytical data for which matched the literature reference data.[17] (**Figure 21**)

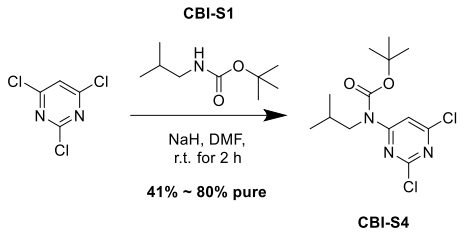


Figure 21. Synthesis of **CBI-S4**.

The outcome suggested that the high reactivity of **CBI-S1** is not fully suppressed by the presence of the Boc group. The next coupling step was anticipated to be difficult due to the presence of the relatively big substituent on the substrate. Consequently, a catalyst with good substrate tolerance would be required to achieve success.

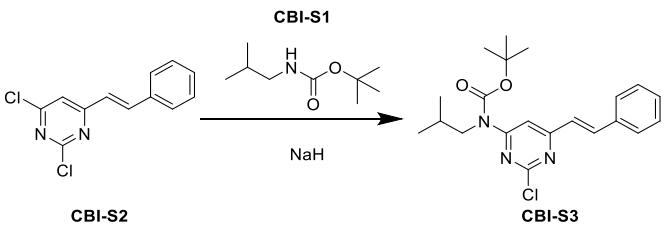
Investigation of the Key Step and Synthesis of Model CBI

At this juncture, the fallback routes to obtain **CBI-S3** were not looking as straightforward as we had hoped and so the investigation of the key step from the original protocol was continued. In light of the fact that the Boc-protected amine had proved sufficiently reactive to participate successfully in S_NAr (second alternative route, see above), It was considered that the failure of the reaction previously might be due to impurities in the starting materials. (**CBI-S1** and **CBI-S2**).

TLC was the first technique used for the purity check. After dipping into potassium permanganate stain, the TLC of protected amine (**CBI-S1**) showed two distinct separated spots. At this stage, a second distillation was performed; unfortunately, two spots were still detected on the TLC plate afterwards. It appeared that distillation under reduced pressure as described in the original protocol, was insufficient to achieve separation presumably because the boiling points of the components in the mixture are quite similar. Therefore, flash column chromatography with pure CH_2Cl_2 was employed to achieve good purity of the amine. A white crystalline solid was obtained after column chromatography. The separated impurity only displayed a single peak at $\delta_H = 1.55$ ppm

in its ^{1}H NMR spectrum, which suggested that it was a simple derivative of Boc anhydride, a by-product from the Boc protection step.

The purified amine was reacted under the same conditions and this time *ca*. 12% product was isolated. (**Table 2, entry 1**). The yield was low compared to the published protocol, hence the conditions were varied with the aim to increase the yield (**Table 2**, **entries 2 – 3**). The solvent was thought to be influential so THF was employed (**Table 2**, **entry 2**), however, an undesired product was obtained after 24h with heating (50 ^{o}C). At this stage, heating was thought to have a negative effect on the resulting yield. Therefore, the original method that uses DMF at room temperature (**Table 2**, **entry 3**) was tested and gave *ca*. 30% yield which was deemed acceptable. TLC analysis also showed that the reaction was completed at the 2h point which is the same as described in the original protocol. Hence, the reaction was repeated using the same conditions (**Table 2**, **entry 4**). A *ca*. 31% yield of CBI-S3 was obtained which is comparable with the literature and shows that the reaction is reproducible.



	Solvent	T/°C	NaH	R. T.	Outcome
Entry 1	DMF	r.t. (2h) then 50	1.5 eq.	2+4h	12%
Entry 2	THF	r.t. (2h) then 50	1.5 eq.	2+22h	U.P.
Entry 3	DMF	r.t.	1.5 eq.	4 (completed at 2)	30%
Entry 4	DMF	r.t.	1.5 eq.	2h	31%

Table 2. The substitution reaction between N-Boc protected isobutylamaine and dichloropyrimidine **CBI-S2**. T = Temperature; R. T. = Reaction Time, N. D. = No data, U. P. = undesired product.

Having successfully overcome of the difficulties from this key S_NAr step, the fourth step in the synthetic scheme was put on schedule. (**Figure 22**)

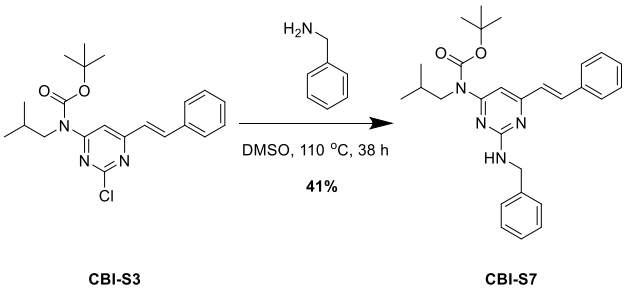


Figure 22. Synthesis of **CBI-S7**.

This reaction involved a substitution reaction between **CBI-S3** and benzyl amine in DMSO at 110 °C for 38h. After this time, the ^{1}H NMR showed evidence of product though the purity of the resulting solid after column chromatography was poor. The solid was further purified by recrystallization (using hexane and ethyl acetate) to finally achieve a purity of 98% (determined by ^{1}H NMR, **SI Figure 7**).

After completion of final substitution on the pyrimidine core, the resulting product required Boc deprotection followed by hydrogenation to obtain the final product **CBI-S9**. The Boc deprotection utilized trifluoroacetic acid (TFA) in CH_2Cl_2 at room temperature. (**Figure 23**)

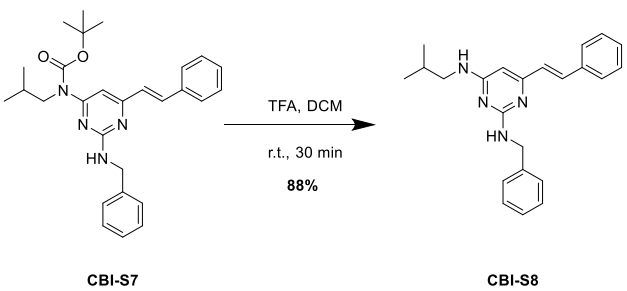


Figure 23. Boc deprotectio to generate **CBI-S8**.

The reaction yielded around 88% of **CBI-S8** after removal of the excess TFA by

distillation. The quality of TFA used in this experiment was important. Use of TFA twice distilled gave a ^{1}H NMR spectrum (**Figure 24 – 1, black**) that was cleaner than when undistilled TFA was used (**Figure 24 – 2, red**). The impurities from undistilled TFA that appear at around δ_H = 1.3 ppm were not present in the distilled reaction.

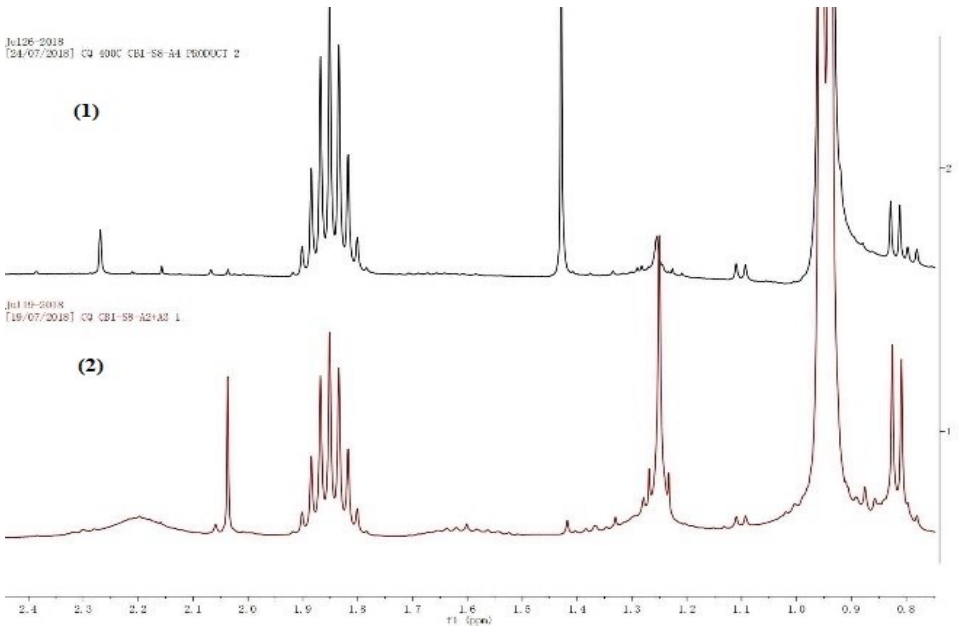


Figure 24. Comparison of the ^{1}H NMR spectra for the crude product of **CBI-S8**: **(1)** Use of twice distilled TFA, **(2)** Use of TFA without distillation.

The final step of the AF-2 coactivator synthesis was a hydrogenation reaction that involved palladium on carbon (Pd/C) as catalyst and hydrogen gas in methanol. (**Figure 25**)

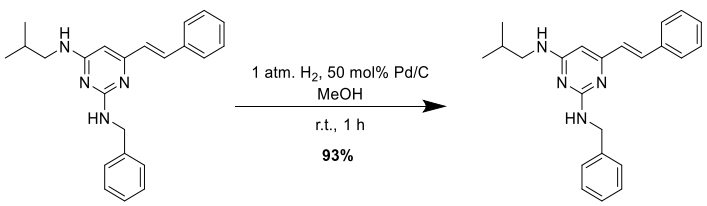


Figure 25 Synthesis of compound **1**.

The reaction gave pure product in 93% yield after column chromatography. The undesired impurity from the previous step was removed since the polarity of the product was dramatically increased after reduction. The success of the hydrogenation was confirmed by inspection of the ^{1}H NMR spectrum of the purified product: the characteristic doublet of the two *trans* alkene protons in the starting material had disappeared and two separated multiplet peaks with an integration of two protons for each had appeared upfield, as expected for the saturated product.

Targeting Binding Function 3 (BF-3)

As indicated above, Cherkasov and colleagues have revealed a series of specific BF-3 inhibitors based on an indoline-indole structure and provided some details of the bioassay they used to determine this activity. In order to obtain some more control compounds for our own assay work and also to perhaps gain an enhanced understanding of the BF-3 site, we aimed to synthesize a couple of their published structures as well as several additional analogs which we hoped might have enhanced activity. Moreover, we planned to also prepare the oxidized partners of each of these compounds as Cherkasov had found that these are also inhibitors, albeit with lower levels of activity, and we needed these therefore as control compounds to ensure our results were not false positives due to inadvertent oxidation of the target compounds. (**Figure 26**)

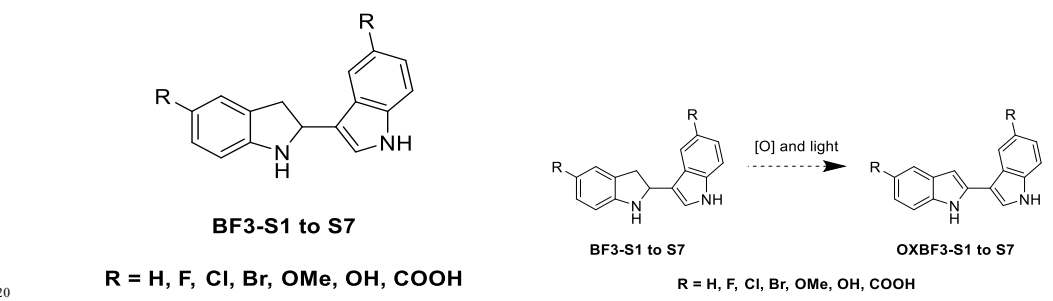


Figure 26. The plan of synthesis of BF-3 targeting compounds.

The work started with the synthesis of 3-(indolin-2-yl)-1H-indole (**BF3-S1**) using the method from the original protocol[22]. (**Figure 27**)

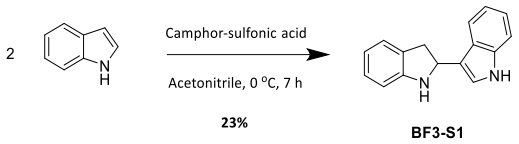
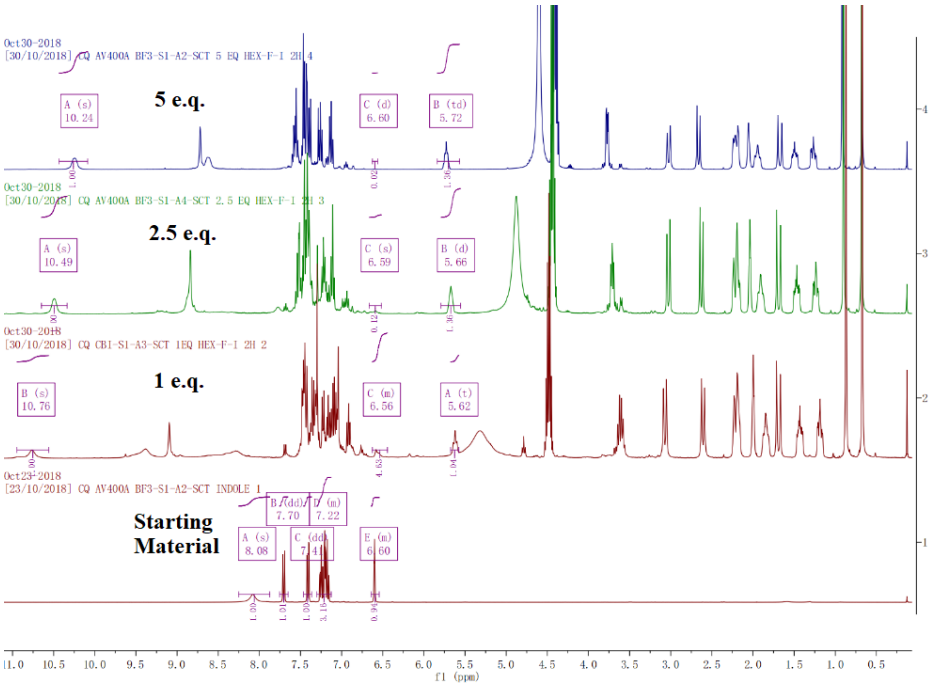
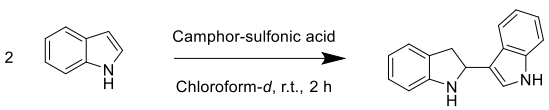


Figure 27. Synthesis of compound **3**.

A modification was made in so far as camphor-sulfonic acid was used in place of *para*-toluene-sulfonic acid. With acetonitrile (MeCN) as solvent, the reaction mixture was allowed to stir at 0 °C and checked at 7h by TLC. The TLC indicated that the reaction was not complete, so a further 0.2 equivalents of camphor-sulfonic acid was added. However, after work up the yield of product was low (23%) and so optimization was undertaken to increase the conversion of indole.

Hexafluoro-2-propanol (HFIP) is known to stabilize carbocations[25] and has been popularly employed in many organic reactions. In this case, HFIP was recruited as a co-solvent to enhance the conversion of indole. The study started with a series of small-scale reactions employing the same amount of camphor-sulfonic acid that was used in the previous reaction and chloroform-*d* as solvent. The reactions were set at room temperature and checked by ^{1}H NMR after 2h. The number of equivalents of HFIP were varied (**Table 3**).





BF3-S1

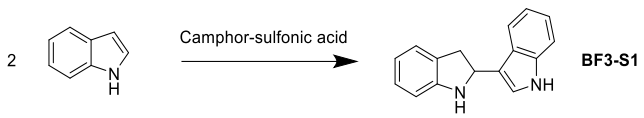
BF3-S1	Indole	Acid	HFIP	Reaction Time	T	Ratio /%
Entry 1	1 eq.	0.55 eq.	5 eq.	2h	r.t.	Approx. 4 : 1
Entry 2	1 eq.	0.55 eq.	1 eq.	2h	r.t.	Approx. 0.1 : 1
Entry 3	1 eq.	0.55 eq.	2.5 eq.	2h	r.t.	Approx. 0.01 : 1

Table 3. A comparison of the ^{1}H NMR spectra of the crude reaction mixtures with variable equivalents of HFIP. **Blue** (5 eq. of HFIP); **Green** (2.5 eq. of HFIP); **Red above** (1 eq. of HFIP); **Red below**, NMR of **BF3-S1.**

With increasing amounts of HFIP from 1 eq. to 5 eq., the ratio of indole and product decreases from ~4:1 to 0.01:1. This suggested that the reaction only reaches completion when at least 5 eq. of HFIP is present; this is likely because several molecules of HFIP are required to provide significant stabilization to the intermediate

carbocation in these reactions.

The modified reaction conditions were examined on a preparative scale in chloroform (**Table 4**).



	Solvent	T /°C	Equivalent of HFIP used/eq.	Time/h	Yield/%
Entry 1	MeCN	0	0	7	23
Entry 2	$CHCl_3$	r.t.	5	3	56

Table 4. Comparison of yield of the reaction to form **BF3-S1** following the original protocol and the modified conditions.

The reaction yielded 56% isolated yield (**Table 4**, **entry 2**) which was a two-fold increase from the original protocol (**Table 4, entry 1**) The reaction time could also be decreased from 7h to 3h without any unconverted starting material (indole) remaining.

Considering that addition of 5 eq. of HFIP gave an encouraging outcome, 5-bromoindole was tested as a substrate to give **BF3-S2 (Figure 28**).

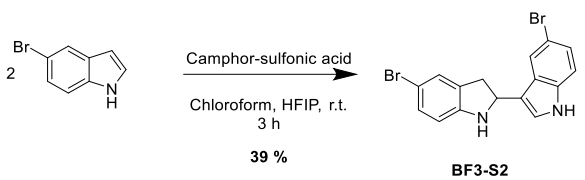
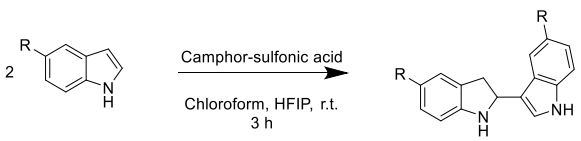


Figure 28. Synthesis of **BF3-S2**.

The consumption of starting material appeared by TLC to be sufficient, however, the isolated yield after flash column chromatography was just 39% as compared to 56%

for the unsubstituted indole.

The method was used with additional substituted indole substrates: 5-chlroro-indole, 5-fluoro-indole and 5-methoxy-indole to give **CBI-S3**, **CBI-S4** and **CBI-S5**, respectively. (**Table 5**)



R = Cl, F. OMe BF3-S3, S4, S5

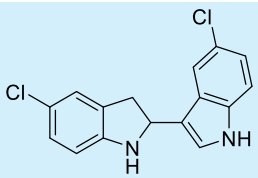
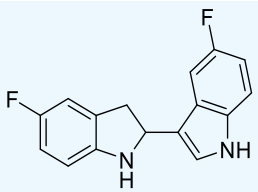
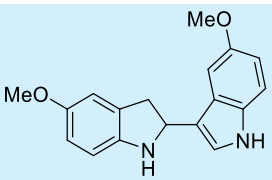
Sample Reference	Chemical Structure	Yield
BF3-S3		31%
BF3-S4		43%
BF3-S5		27%

Table 5. The resulting yield of indoline-indole analogs (**BF3-S3**, **S4** and **S5**) using modified reaction conditions.

The yield of **BF3-S4** was higher than that of **BF3-S3** (43% *vs*. 31%, respectively) which indicated that the HFIP may have a different effect on dimerization of 5-fuoroindole compared to 5-chloroindole. The dropwise addition of HFIP and reacting in dark for **BF3-S4** may also have contributed to the increased yield. The synthesis of **BF3-S5** gave a brown powdery solid. Two separate sharp-singlet signals were observed at around

δ_H = 3.65 ppm in the ^{1}H NMR spectrum (**SI Figure 24**) which were assigned as the two methoxy groups. The total integration of these two peaks corresponded to 6 protons which indicated that the dimerization was successful. The synthesis was then continued with 5-hydroxy indole to give **BF3-S6.** (**Figure 29**)

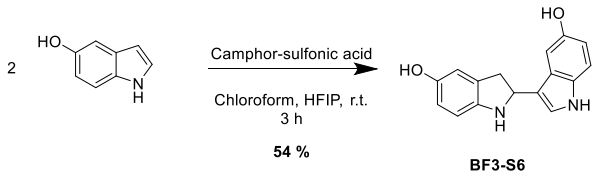


Figure 29. Synthesis of **BF3-S6**.

After loading of the starting material (5-hydroxyindole) and the acid (camphor-sulfonic acid), a pink precipitate was formed during dropwise addition of HFIP into chloroform. The precipitate was taken out of the reaction mixture and then analyzed by TLC and ^{1}H NMR which confirmed this precipitate to be the desired dimeric product. Considering its poor solubility in ethyl acetate, a large volume of solvent was used in the extraction following the neutralization of the reaction medium during work-up. After work-up, flash column chromatography was planned to be used to purify the product since its R_f value was 0.13 (50% ethyl acetate in hexane). However, wet loading of the crude reaction product failed both with methanol and with ethyl acetate as solvent due to insolubility. Thus, recrystallization was attempted. A suspension was formed at 60 ^{o}C, and undissolved solid was filtered and collected. ^{1}H NMR and mass spectrometry analysis of the collected powder confirmed the structure of the product: in particular, the product showed two characteristic double doublet peaks around δ_H = 3.00 ppm in the ^{1}H NMR (hydrogens of methylene from the indoline ring) and a *m/z* [MH^+] = 267.1139 (calculated 267.1134).

Next, the synthesis of **BF3-S7** was attempted. (**Figure 30**)

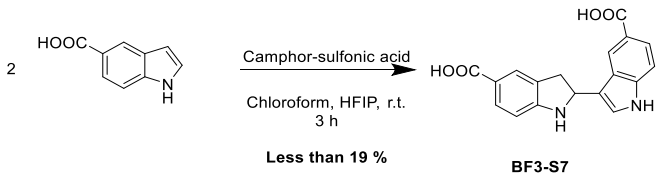


Figure 30. Synthesis of **BF3-S7**.

Due to the poor solubility of the indole-5-carboxylic acid in chloroform, 5 eq. more HFIP was added into reaction mixture (10 eq. total). Due to the presence of carboxylic acid groups, the resulting product was relatively polar and moving sluggishly during flash chromatography though 0.1% of formic acid was added into elution solvent. Besides, the resulting yield of **BF3-S7** was relatively low (*ca*. 19%) compared with other analogs. The purity of the product was also unsatisfactory even after column chromatography and further purification was required.

To achieve a better result, an alternative way to obtain **BF3-S7** and avoid the difficult purification was required. Since the presence of the carboxylic acid groups was the main challenge, esterification of 5-indole carboxylic acid was planned, such that after dimerization the resulting analogs could be hydrolyzed to give **BF3-S7.** (**Figure 31**)

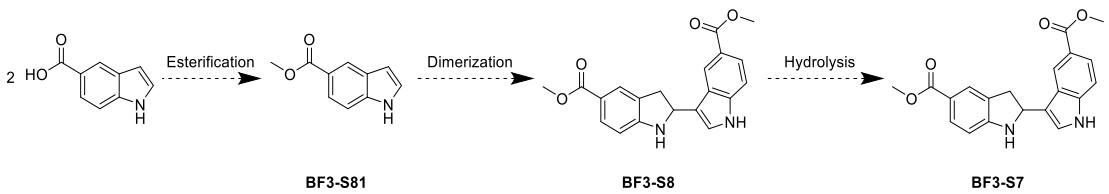
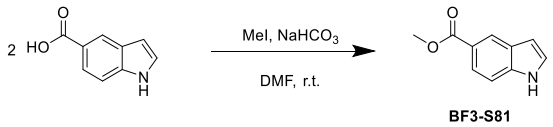


Figure 31. Planed alternative route to obtain **CBI-S7.**

Based on the work of Kong[26], methyl iodide was employed for the methylation and sodium bicarbonate as base and an almost quantitative yield of ester was obtained (98%) on both occasions the reaction was carried out. **(Table 6)**

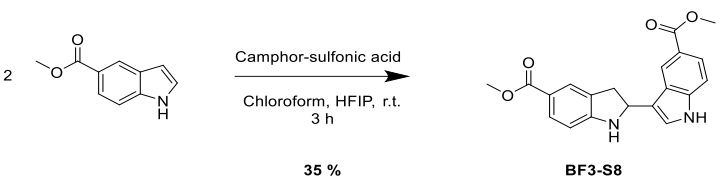


BF3-S81

	SM/ Amount	Reaction Time/ h	Yield
Entry 1	3.1 mmol/ 500 mg	3 days	98%
Entry 2	31 mmol/ 5 g	3 days	98%

Table 6. Synthesis of **BF3-S81.**

The presence of a singlet peak at δ_H = 3.83 ppm in the ^{1}H NMR spectrum indicated the successful formation of product as this peak was assigned as arising from the methyl ester; no column was required as the compound appeared pure. After successful esterification, the resulting dark orange powder was used as a substrate for the dimerization reaction. (**Figure 32**)



BF3-S8

Figure 32. Synthesis of **BF3-S8**.

This gave an off-white powder as product in 35% yield. The reaction was proven to be successful with the presence of two close singlet peaks in the ^{1}H NMR at δ_H = 3.79 ppm and δ_H = 3.76 ppm, corresponding to the two esters groups. The process of flash column chromatography was much more simple compared to the carboxylic acid one and no acetic acid was required to acidify the eluent.

Oxidation Investigations

As stated before, the indoline-indole structures have been reported to be oxidized into bis-indoles upon exposure to air. (**Figure 33**).

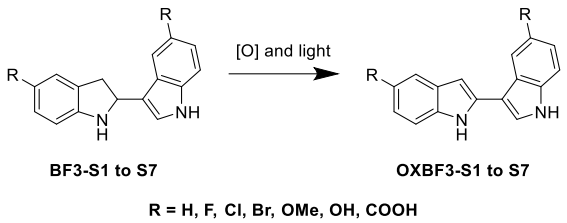


Figure 33. Oxidation of indoline-indole structure into bis-indole.

To obtain the necessary controls for the binding assays of these BF-3 target inhibitors, the oxidized version of all analogs was required. The investigation of oxidization was started from **BF3-S1**. Air was bubbled into a solution of **BF3-S1** in methanol (MeOH) and the reaction was stirred overnight before being checked by TLC. (**Figure 34 & Table 7, entry 1**)

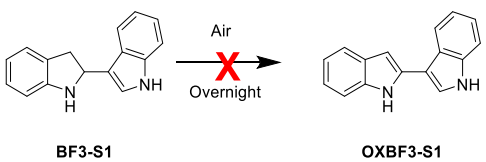
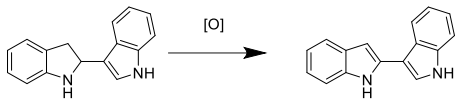


Figure 34. Attempted oxidation of **BF3-S1**.

However, no spot of product was observed by TLC. Hence, other conditions were explored for oxidation of the indoline-indole structure based on **BF3-S1.** (**Table 7**)



BF3-S1 OXBF3-S1

	S. M. / mmol	Oxidant/ Catalyst Loading	Solvent	Time	T	Outcome
Entry 1	0.213	-	MeOH	ON	r.t.	N. D.
Entry 2	0.213	MnO_2/ 6+0.2 eq.	CH_2Cl_2	ON	r.t.	N. D. P
Entry 3	0.213	MnO_2/ 6+0.4 eq.	Toluene	ON	r.t.	N. D. P.
Entry 4	0.213	S_8/ 8 eq. to excess	MeOH	2d	r.t.	34%
Entry 5	0.213	S_8/ excess	Toluene	3d	50°C	N. D. P
Entry 6	0.213	S_8/ excess	EtOH	3d	r.t.	40%
Entry 7	0.213	S_8/ excess	^{i}PrOH	3d	r.t.	NDP
Entry 8	1,70	Excess S_8	MeOH	3d	r.t.	10%
Entry 9*	0.213	0.1 eq. 10% Pd/C*	MeOH	4h	65 °C	45%
Entry 10*	2.13	0.1 eq. 10% Pd/C*	MeOH	4h	65 °C	50%

Table 7. Attempted oxidation of **BF3-S1**. S. M. = starting material (**BF3-S1**), ON = overnight. N. D. = no data, N. D. P. = No Desired Product. * 10 eq. of Ammonium formate (HCO_2NH_4) was also used.

Firstly, manganese dioxide (MnO_2) was employed as oxidant in this reaction, inspired by the work of Melnyk[27] (**Entries 2-3**). When the reaction was carried out in CH_2Cl_2 the starting material was found not to be fully consumed during 4h reaction time. Consequently, 0.2 equivalents of MnO_2 were added into the reaction mixture and the reaction was left overnight. After being filtered through Celite©, no evidence of desired product was found in the ^{1}H NMR spectrum (**Entry 2**). Next, Dupeyre's work[28] inspired the use of toluene as solvent (**Entry 3**). However, the ^{1}H NMR spectrum of the crude product after filtration gave uninterpretable results since too much noise and

impurities were present. Thus, it appeared that MnO_2 was not active enough in this reaction and that other oxidants would be required to be tested.

Elemental sulfur (S_8) was explored as an alternative oxidant in this reaction (**Entries 4-8, Table 7**). Using MeOH as solvent with 8 eq. of S_8, the starting material was still observed by TLC even after 2 days and even after adding additional amounts of sulfur. The resulting crude product was obtained after filtration through Celite© and removal of solvent. After flash column chromatography, the resulting dark purple solid was confirmed to be the oxidized product (**Entry 4**). The ^{1}H NMR showed that the two doublet peaks corresponding to the saturated indoline ring protons at around $\delta_H = 3.0$ ppm had disappeared. To improve the conversion of starting material, additional changes were made including changing the solvent. Toluene was used to improve the solubility of sulfur according to Ren's work (**Entry 5**).[29] However, no desired product was observed by TLC after 3 days. At this stage, two alcohols, ethanol (EtOH) (**Entry 6**) and isopropanol (**Entry 7**) were evaluated as possible solvents. After 3 days, only EtOH gave the spot of product by TLC while isopropanol gave no desired product. The resulting yield of product was slightly increased in comparison with using MeOH (*cf.* **Entry 6** *vs.* **Entry 4**). Although the purity of isolated product was not high. Moreover, in the EtOH reaction the starting material was found not to be fully consumed when the reaction was terminated. Thus, loading of relatively more starting material wa necessary to obtain the desired quantity of product. A scaled-up version of the reaction in MeOH (**Entry 8**), however resulted in the isolation of just 10% product (*cf.* 34% in **Entry 4**). Some undesired polar spots were observed on the TLC plate which might have contributed to the low yield.

Finally, considering the low yields obtained with S_8, an alternative oxidant for this reaction was sought. Kiguchi[30] has described a one-pot procedure for hydrogenolysis of the N-benzyl group of an indoline followed by *in situ* oxidation to the indole utilizing palladium on carbon as catalyst and ammonium formate as the hydrogen source in MeOH at 65 °C. Therefore, those conditions were adapted for our reaction (**Table 7,**

Entry 9). The resulting crude product was obtained after filtration through Celite© and removal of solvent. After flash column chromatography, the resulting dark purple solid was confirmed to be the oxidized product using the previous spectrum as a reference. Although 45% final yield was obtained, the separated product was not as pure as expected which might reflect the poor quality of the ammonium formate). Therefore, another attempt, this time using pure ammonium formate was scheduled[1] (**Table 7, entry 10**). After purification, the quality of the isolated product was significantly improved compared to the previous attempt. The mass spectrum of the product contained a peak at *m/z* = 233.10 (calcualted 233.10) which also indicated the successful formation of the product..

[1] It was recognised only after performing these reactions that the ammoniunm formate is probably not required for our transformation. A reaction in the absence of this component has not however been carried out.

Chapter 2. Development of the Assay

Introduction

Luciferase Reporter Assay

The transcription pathways of the cell are irreplaceable in all organisms and serve countless biological processes by obeying the 'central dogma' for transcription and translation, whereby transcription is the first step in production of DNA-encoded proteins. To monitor and analyze this process in the current research environment, scientists have developed several assay methods, the Luciferase Reporter (LR) assay is one of them.

The LR assay has been popularly employed in biology labs worldwide to study transcriptional pathways by manual gene engineering.[31] LR assays are characterized by being convenient methods which are relatively low cost, and rapidly produce analysis-friendly data which can be quantitative. The LR assay quantifies the response from the reporter gene to a specific activation. The level of activity of the reporter gene expression, and thus the amount of reporter protein, is mirrored by the protein's enzymatic activity. The level of this activity can be indirectly quantified by various kinds of experimental readout luminescence.[32] Normally, researchers take advantage of the measurement of luminescence since it can be readily recorded by standard plate readers. (**Figure 35**)

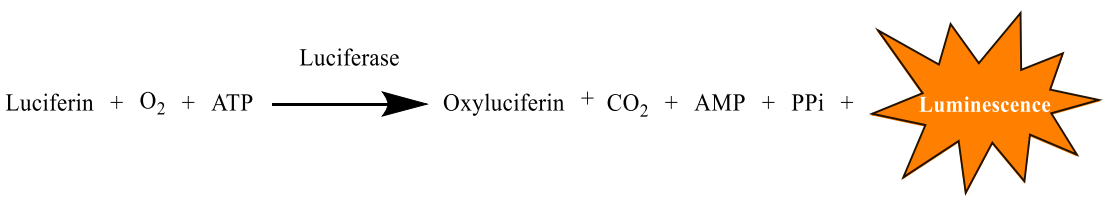


Figure 35. A schematic of luminescence generated by luciferase oxidation. The

luciferin reagent is added to the system in non-rate-limiting amounts, and the luminescence output is proportional to the amount of luciferase enzyme produced by activation of the reporter gene.

Time-Resolved Fluorescence Resonance Energy Transfer (TR-FRET) Assay

Time-resolved fluorescence resonance energy transfer (TR FRET) assays are known to often display high efficiency, and high sensitivity. This technique is widely used for the study of ligand-based biological process including protein-protein interactions and hormone initiated physiological and pathological processes.[33]

Specifically, TR-FRET assays are suited for assessing ligand binding in medicinal chemistry research because they can have high throughput screening capability in pre-clinical investigations. Normally, the assay is principally based on the energy transfer from a donor to an acceptor.[34] For example, a variant of this assay type that that people normally employed is the LanthaScreen® TR-FRET AR Coactivator assay from Thermofisher™.[35] The donor is a lanthanide (*e.g*. Europium, Eu or Terbium, Tb) containing chelate compound, which is covalently linked with a tag-targeting antibody (in this case, glutathione S-transferase, GST) and forms a so-called 'Metal-anti-Tag' antibody, while the acceptor is a fluorescein labeled peptide (FI-peptide). The FI-peptide is designed to mimic an unspecified coactivator binding epitope. A schematic of the TR-FRET assay is shown in **Figure 36**. [35]

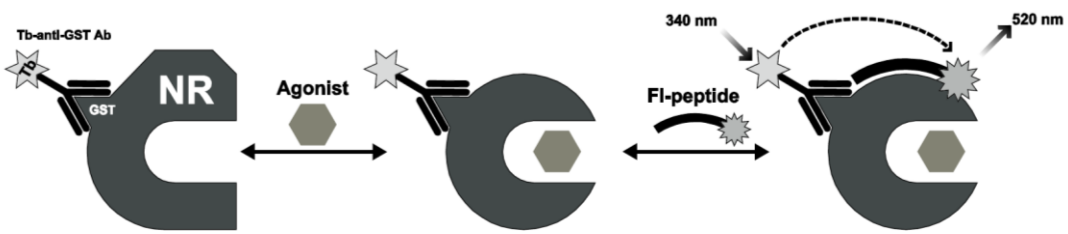


Figure 36. Schematic representation of the TR-FRET assay.[35]

After incubation, the Tb-anti-GST antibody can bind to the GST tagged NR-LBD (NR = nuclear receptor). When a ligand (*i.e*. agonist or antagonist) enters the LBP and causes helix rearrangement, this leads to a conformational change which initiates the recruitment of the coactivator mimic Fl-peptide and results in the proximity of the antibody and the Fl-peptide. After excitation, the energy transfer between the antibody and the Fl-peptide can occur, which finally generates a readout. Compared to the standard FRET assay, the lanthanide chelate (especially Tb) that is employed in this TR-FRET offers distinct long life-time excited state after excitation. The Tb species can also stabilize the energy transfer from the excited lanthanide donor contained antibody to the Fl-peptide acceptor.[36]

Fluorescence Polarization (FP) Assay

Light can be polarized in more than one direction, and the rotation speed of molecules tumbling in solution is mainly dependent on their size. Based on these two principles, the Fluorescence Polarization (FP) assay (or so-called Fluorescence Anisotropic Assay) is also a popular assay format for investigation of ligand-protein interactions.

To take advantage of this highly sensitive assay, an understanding of the two principles of the FP assay is necessary. Firstly, to gain signals in this assay, the polarization of the incident light is crucial. A schematic representation of FP detection is shown in **Figure 37**.[37]

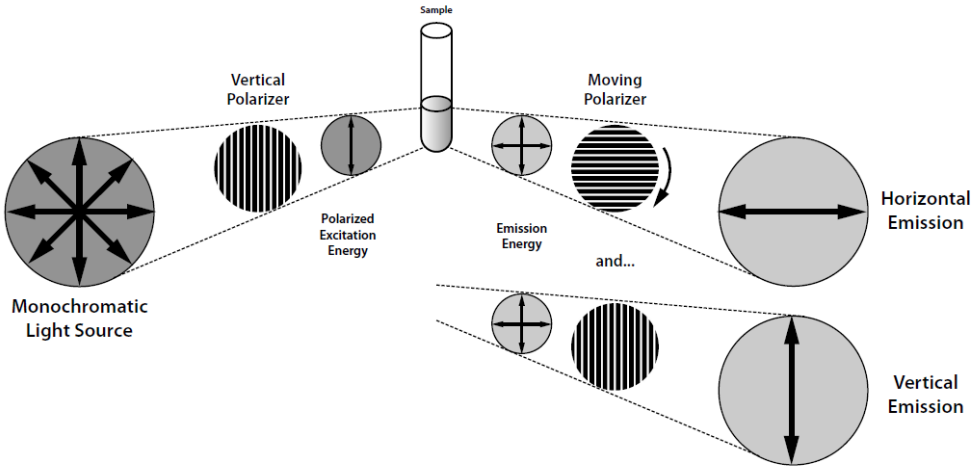


Figure 37. A schematic representation of FP detection. [37]

The light is polarized by a polarizing filter to give anisotropic light which is polarized in one direction before being absorbed by the sample. After excitation, the fluorescence-active sample can emit energy in the form of light which passes through the moving filter and impinges on the detector. The value of polarization (P) can be calculated by applying **Equation 1**,

$$\text{Polarization (P)} = \frac{I_{vertical} - I_{horizontal}}{I_{vertical} + I_{horizontal}} \qquad \textbf{Equation 1}.$$

Where $I_{vertical}$ is the intensity of vertical light and $I_{horizontal}$ is the intensity of horizontal light.

The second principle can be understood by reference to **Figure 38**.[37]

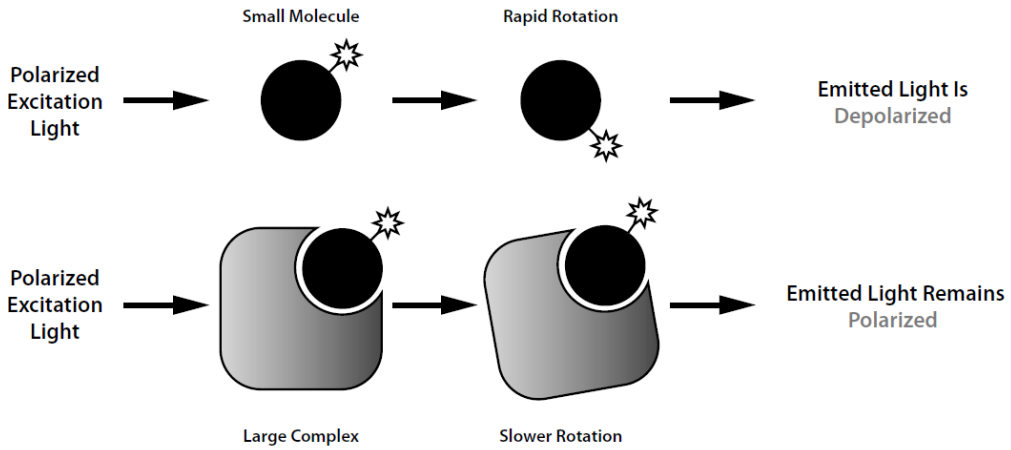


Figure 38. Cartoon showing how a size differences between molecules results in differences in the polarization of emitted light in an FP assay. [37]

The tumbling rotational speed of molecules in solution is proportional to their sizes, hence, after excitation by polarized light, their fluorescent complexes can emit different degrees of polarized light based on their size. A fluorescence-active small molecule which rotates fast will emit more depolarized light compared to the co-complex of a fluorescence-active small molecule that is bound to a macromolecule which rotates slowly.

The FP assay is therefore a versatile research method for studying ligand-protein interactions with high sensitivity. By utilizing *e.g*. fluorescein-labeled ligands, scientists can understand the interaction between ligands and their macro-receptors. Moreover, with the developments in fluorescence chemistry and physics, many fluorescent dyes with excellent chemistry and physics properties for the FAP assays have been developed and validated. These dyes can display emission at long wavelengths (*e.g*. in the green and red regions of the visible spectrum) which allows for good separation between excitation peaks and emission peaks. Molar extinction coefficients larger than 100,000 cm^{-1} M^{-1} can also be achieved. [38]

Aim

With the synthesis part of this project essentially complete, attention focused on the development of biological assays to enable preliminary biological evaluation of the synthesized compounds. (**Figure 39**)

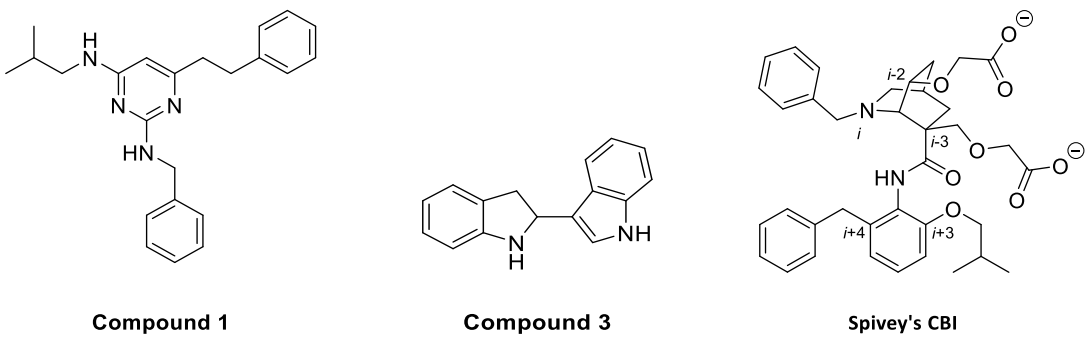


Figure 39. Structures of compound **1**, compound **3** and **Spivey's CBI**.

Capturing data from a cell-based functional assay was the priority at the start as this was anticipated to provide biological data for the model compounds **1** and **3** which would be able to be compared with literature values. It was decided not to test **Spivey's CBI** using this assay at this juncture due to the limited stock of this compound. A LR assay was selected for the testing due to its convenience, low cost, and its ability to provide quantitative outcomes on a short time-scale.

For the *in vitro* binding assay, a FP assay was chosen since this type of assay is suited to the evaluation of small molecule coactivator mimetics which may have an influence on TR-FRET coactivator peptide binding.

Development of the FP assay had been attempted in two previous MRes projects,[24,39] however, overexpression of the NR-LBD had not proved successful because of what was thought to be problems inducing correct protein folding. In light of this previous experience with protein synthesis, a commercially available kit, PolarScreen™ AR Competitor Assay Kit, was purchased from the ThermoFisher Scientific. It contains a

rat NR-LBD along with an Fl-peptide, Fluormone^{TM}, and the NR assay buffers (pH 7.5). A schematic of the assay is shown in **Figure 40**.[40]

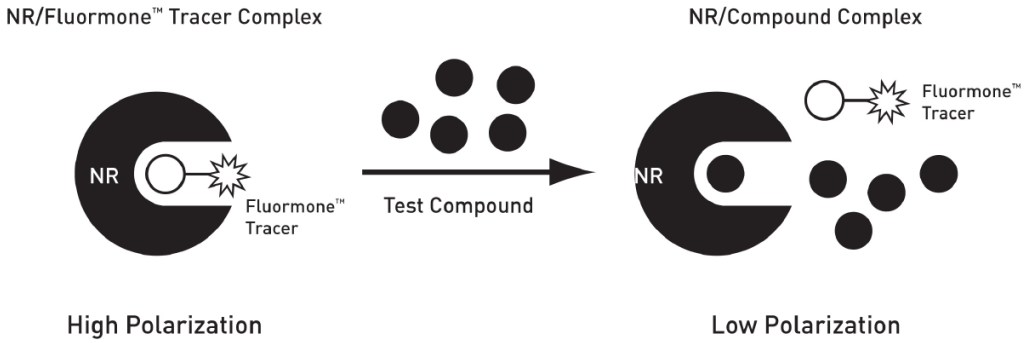


Figure 40. Schematic of the AR FP competitor assay.

The antagonist can bind to its target on the NR-LBD and lead to the dissociation of the peptide (Fluormone^{TM}) which can generate polarization signal differences. The plan was to develop, test and optimize the assay using the model compounds before evaluating the valuable **Spivey CBI** compound.

Results and Discussion

Luciferase Reporter Assay Results

Compounds **1** and **3** are known in the literature and the spectroscopic data for our synthesized samples matched those reported.[17] Testing of these compounds in the LR assay was performed with the group of Prof. Bevan and specifically in collaboration with scientific officer Ms Sue Powell. The expression of the luciferase reporter gene in this case was under the control of a well characterized androgen response element found in the regulatory sequence of the androgen/glucocorticoid-regulated tyrosine aminotransferase (TAT) gene. Two copies of this TAT response element (GRE) were upstream of the luciferase (LUC) element in the reporter vector. This vector, plus an expression vector expressing wild-type androgen receptor, was transfected into COS-1 cells, a cell line transformed from monkey kidney cells. The data for compounds **1**, and **3** are shown in **Figures 41** and **42**, respectively.

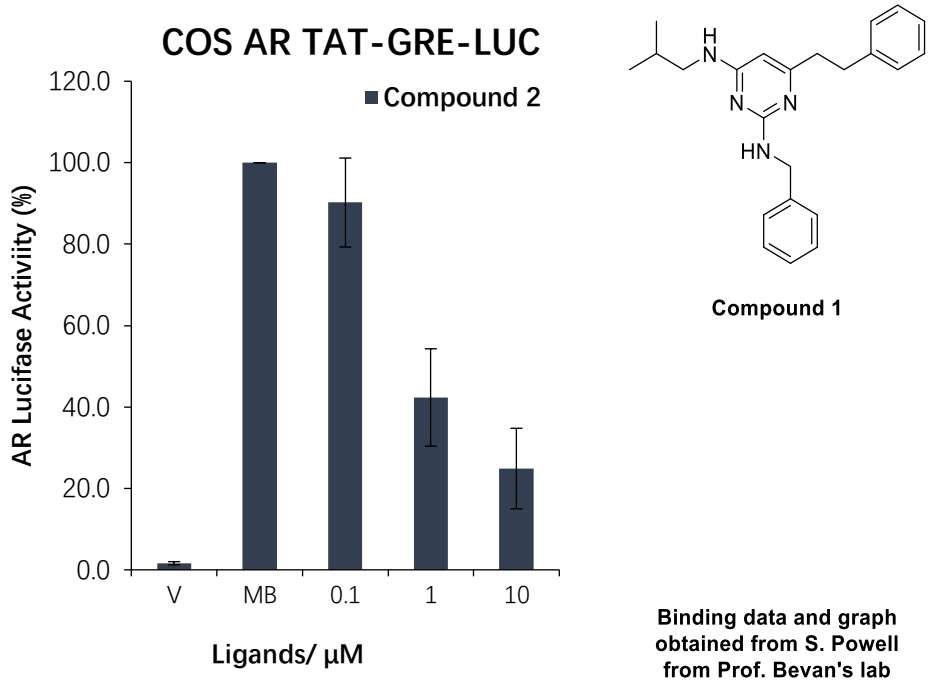


Figure 41. The Luciferase Reporter Assay Result for compound **1**.

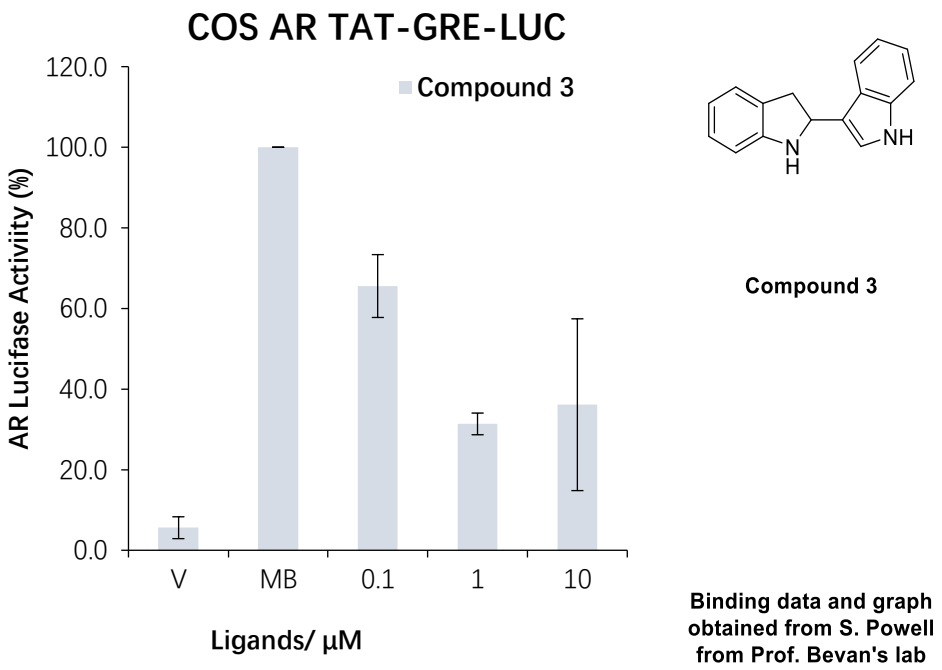


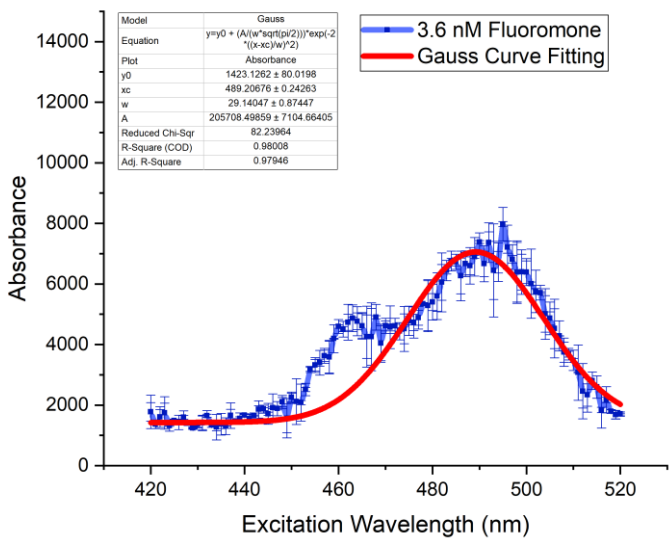
Figure 42. The Luciferase Reporter Assay Result for compound **3**.

Data was produced using a dilution of a 100 µM solution of the test substrate in DMSO. Cells were treated with ethanol vehicle (the control, V) or with Mibolerone (MB, a synthetic androgen) plus increasing concentrations of the inhibitor or vehicle, in this case DMSO, as a negative control. Compound **1** showed a dose-dependent decrease against AR activity. With increasing concentration of the ligand from 0.1 µM to 10 µM, the activity of AR decreased from around 90% to around 25%. Similarly, compound **3** also showed a negative correlation against AR activity. With increasing concentration of the ligand from 0.1 µM to 10 µM, the activity of AR was decreased from around 66% to around 36%. The estimated IC_{50} for compound **1**, and compound **3** are 0.6 µM and 0.1 µM, respectively: (Ref. 1.5 µM[17] and 0.3 µM[22], respectively). This correspondence to the literature assured us that the assay was working correctly and that that these compounds could therefore be used with confidence as positive control compounds in the development of the FP assay.

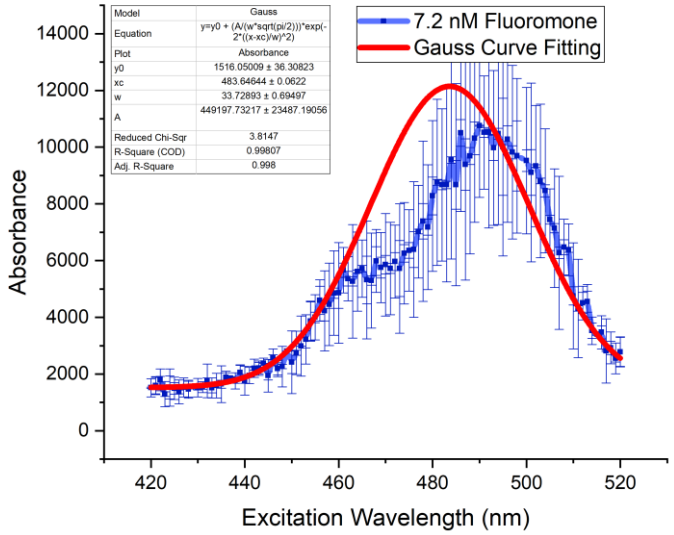
Excitation and Emission Scan of the Fluoromone™

A PHERAStar Plus© instrument from BMG LTD was used for plate reading. The fluorescence polarisation set-up on the plate reader was such that excitation occurred at a wavelength of 485 nm and emission was recorded at a wavelength of 520 nm. The supplied Fluoromone™ has a reported excitation wavelength of 485 nm and an emission wavelength of 520 nm. The 10 nm difference between the instrument optical settings and the reported fluorophore values was not anticipated to have a significant impact on the results. However, it was considered to be necessary to run an excitation and emission scan for the Fluoromone™.

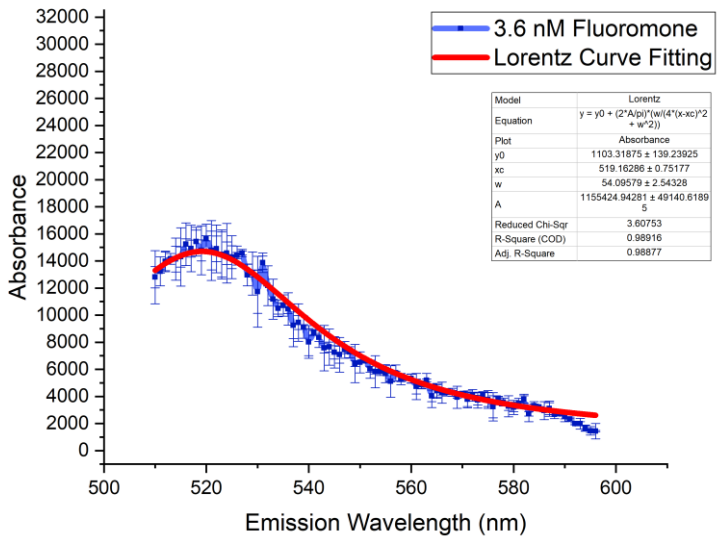
The excitation and emission spectra were scanned using the CLARIOStar© plate reader in triplicate at two different concentrations of the Fluoromone™: 3.6 nM (=1X), and 7.2 nM (=2X) where the former value is the recommended final assay concentration from the protocol. The spectra resulting from these scans together with curve fitting lines are shown below in **Graphs 1, 2, 3** and **4.**



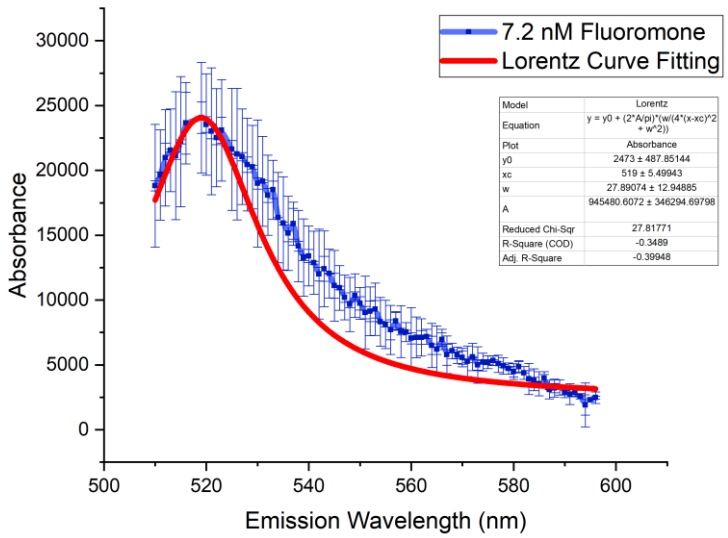
Graph 1. Excitation Scan of Fluoromone™ with 1X conc. in 1% DMSO in NR buffer.



Graph 2. Excitation Scan of Fluoromone™ with 2X conc. in 1% DMSO in NR buffer.



Graph 3. Emission Scan of Fluoromone™ with 1X conc. in 1% DMSO in NR buffer.



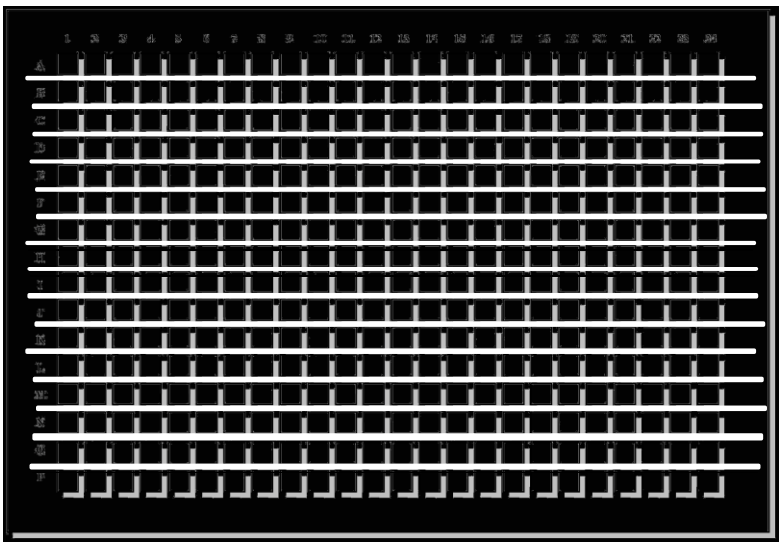
Graph 4. Emission Scan of Fluoromone™ with 2X conc. in 1% DMSO in NR buffer.

Gaussian and Lorentz curve fitting were employed for maxima determination and most R squares were found to be close to 1 which indicated that the fittings were acceptable. For excitation **Graphs 1** and **2,** an excitation maximum was found at 485 nm which perfectly matched the reference. For emission **Graphs 3** and **4**, an emission maximum of 520 nm was detected which indicated that the use of (485nm/520nm) optics from PHERAStar Plus© should be successful.

First Attempt at Performing the FP Assay

Once we were satisfied that the instrument conditions were suitable for the experiments, the first attempt at the FP assay was scheduled. This was conducted strictly according to the recommended protocol[40] and each test compound was run in duplicate at three different nuclear receptor concentrations (Rat AR-LBD, 0.5 X, 1X and 2X, where 1X is 676 nM, which is the recommended final assay concentration from the certificate of analysis). In this assay, testosterone (**T**) and CBI (compound **3**) from Katzenellenbogen were chosen as test compounds and dihydrotestosterone (**DHT)** was

chosen as control ligand. The total assay plate layout is shown below in **Figure 43**.



Serial Dillution Conc. (nM)
10000.0
3333.33
1111.11
370.370
123.457
41.1523
13.7174
4.57247
1.52416
0.50805
0.16935
0.05645
0.01882
0.00627
0.00209
0.00070

1	2	3	4	5	6	7	8	9	10	11
Absolute Negative Control. Fluoromone™ **ONLY**	*Positive Control.* Fluoromone™ and 0.5X **NR**.	*Positive Control.* Fluoromone™ and 1.0X **NR**.	*Positive Control.* Fluoromone™ and 2.0X **NR**.	*Negative Control.* Fluoromone™ and 0.5X **NR** plus **DHT**	*Negative Control.* Fluoromone™ and 1.0X **NR** plus **DHT**	*Negative Control.* Fluoromone™ and 2.0X **NR** plus **DHT**	Fluoromone™ and 0.5X **NR** plus **T** (16 points SD).		Fluoromone™ and 1.0X **NR** plus **T** (16 points SD).	

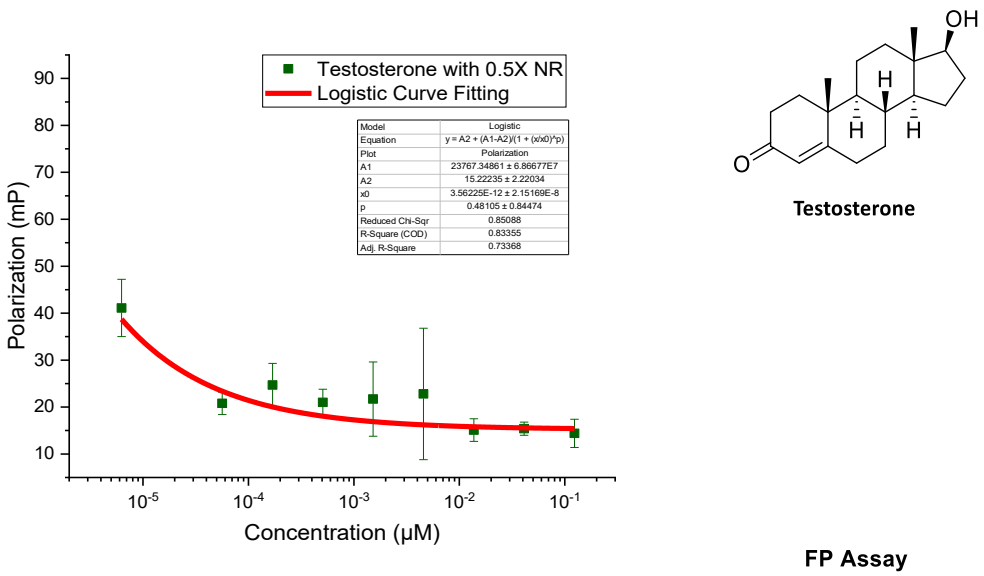
12	13	14	15	16	17	18	19	20	21	22
Fluoromone™ and 2.0X **NR** plus **T** (16 points SD).		Fluoromone™ and 0.5X **NR** plus **KB CBI** (16 points SD).		Fluoromone™ and 1.0X **NR** plus **KB CBI** (16 points SD).		Fluoromone™ and 2.0X **NR** plus **KB CBI** (16 points SD).		*Negative Control.* Fluoromone™ and 0.5X **NR** plus **DHT**	*Negative Control.* Fluoromone™ and 1.0X **NR** plus **DHT**	*Negative Control.* Fluoromone™ and 2.0X **NR** plus **DHT**

Figure 43. 96-well plate layout and table of resulting final conc. values for the first attempt at the FP assay

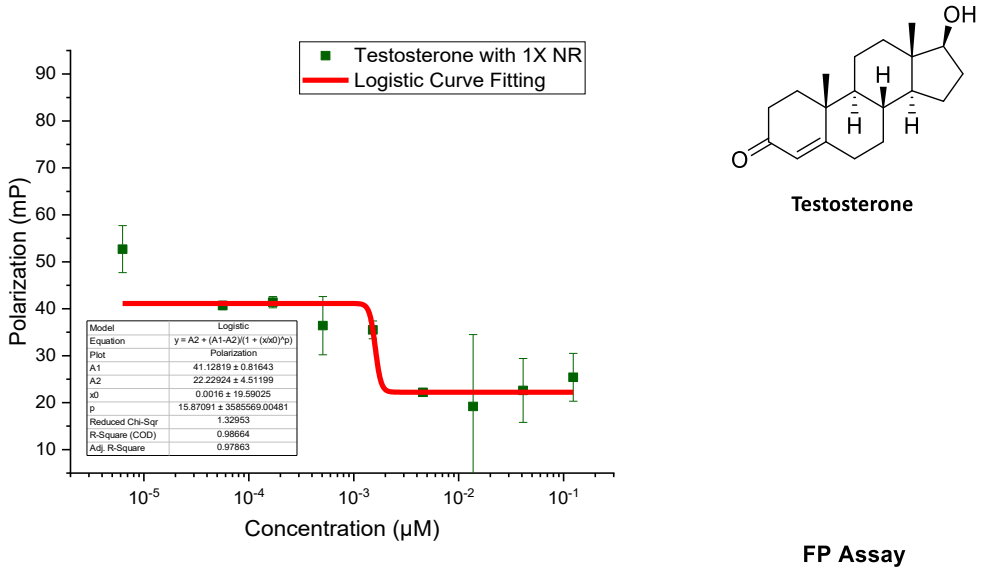
The readings were taken at time points of 2h, 3h and 4h after preparation of the plate, which allowed the plate to have 2h incubation.

After plate reading, the first four dilution points of each compound were found to be

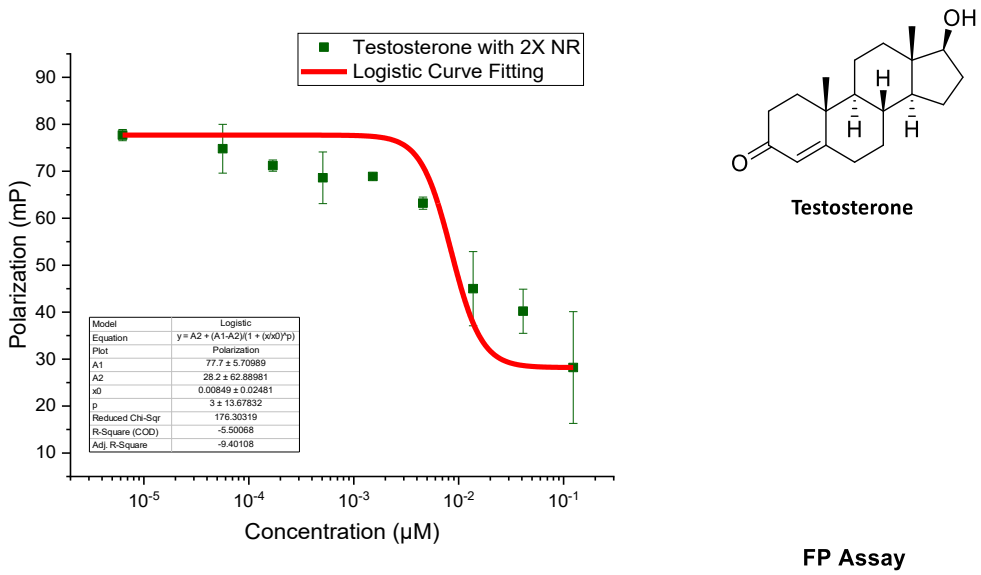
inaccurate since they were inverted. This was found to commonly happen and may result from the precipitation of these hydrophobic test compounds due to the extremely low concentration of DMSO in each well (1% of total volume). Deploying an increased concentration of DMSO is not generally recommended since it may make the binding equilibrium hard to achieve. Therefore, to allow the graph to be analyzed, the values for the first four dilution points were deleted from each graph. After manual optimization, the analyzed graphs are shown below in **Graphs 5** - **7**.



Graph 5. Polarization graphed against the conc. of Testosterone with 0.5X NR in 1% DMSO in NR buffer. (2h)



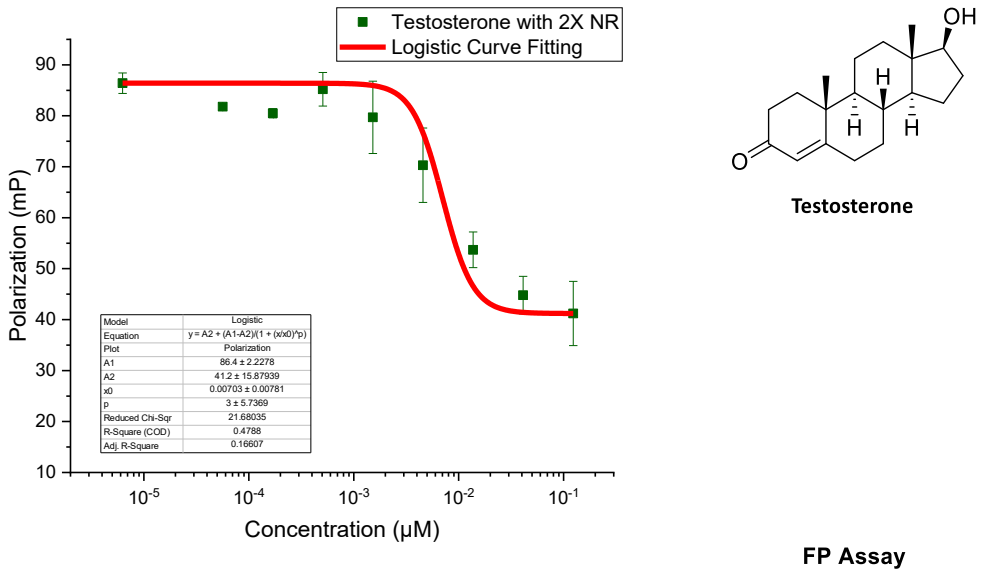
Graph 6. Polarization graphed against the conc. of Testosterone with 1X NR in 1% DMSO in NR buffer. (2h)



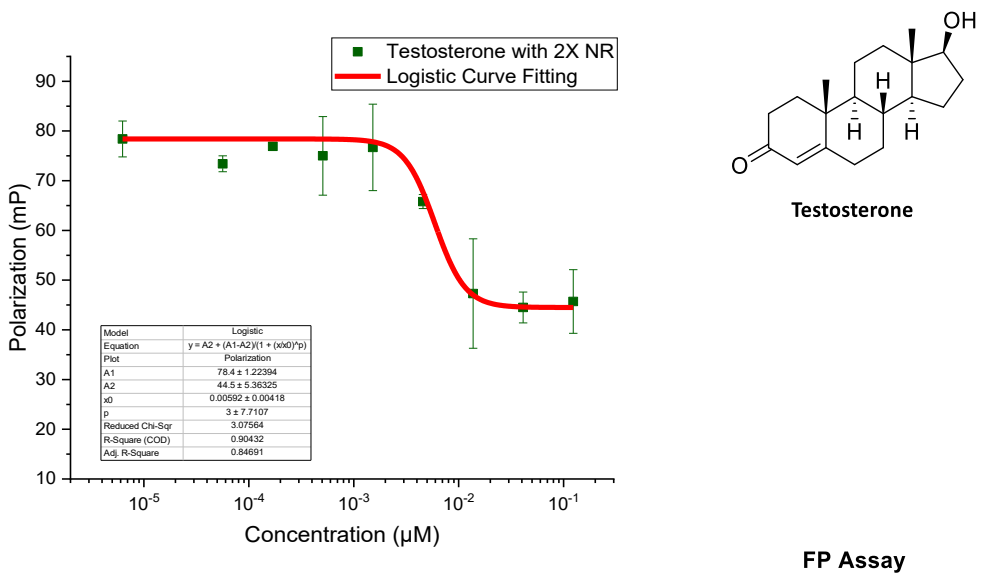
Graph 7. Polarization graphed against the conc. of Testosterone with 2X NR in 1% DMSO in NR buffer. (2h)

Among **Graphs 5 - 7, Graph 7** has the best fitting sigmoid curve, which suggested that the optimized NR concentration is 2X (1352 nM). Furthermore, to investigate the best

equilibrium time point, results recorded at 3h and at 4h were also compared. (**Graphs 8** and **9**, respectively)



Graph 8. Graph of Polarisation *vs.* the conc. of Testosterone with 2X NR in 1% DMSO in NR buffer. (3h)



Graph 9. Graph of Polarisation *vs.* the conc. of Testosterone with 2X NR in 1%

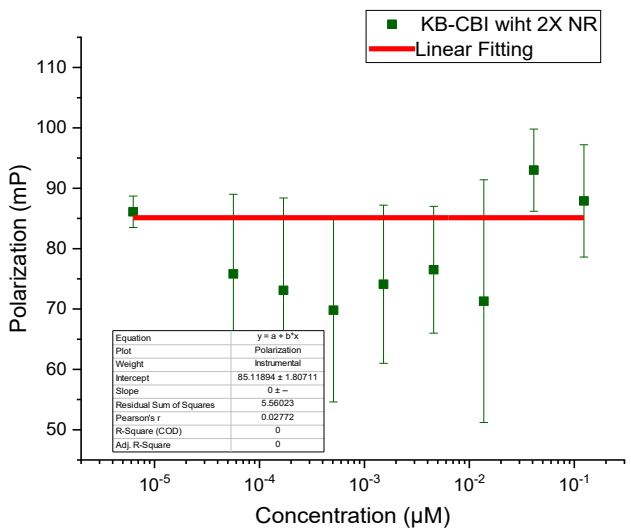
DMSO in NR buffer. (4h)

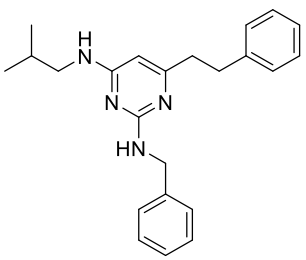
Compared to **Graph 7**, both **Graphs 8** and **9** have better curve fitting which indicates that the equilibrium was reached after 2h and before 3h. The result shown in **Graph 7** appeared to be the most reliable one and therefore the equation for determining the IC_{50} was applied to this fitted curve (**Equation 2)**[41]

$$\text{Polarization (P)} = P_{min} + \frac{(P_{max} - P_{min})}{(1+10^{(\log(conc.) - \log(IC_{50}))})} \qquad \textbf{Equation 2}.^{41}$$

After comparing with the reference value[40], we found that the calculated data (0.007±0.008 μM) is close to the reference data (0.02 μM) which indicates that this assay is working to some extent.

For Katzenellenbogen's compound (compound **3**), the reference IC_{50} is 1.7 μM[12] which means that the deletion of the first four dilution points will not be possible for this compound as it will lead to loss of the sigmoid curve. Hence, linear fitting was applied to these graphs and the results are shown below in **Graphs 10**, **11**and **12**.



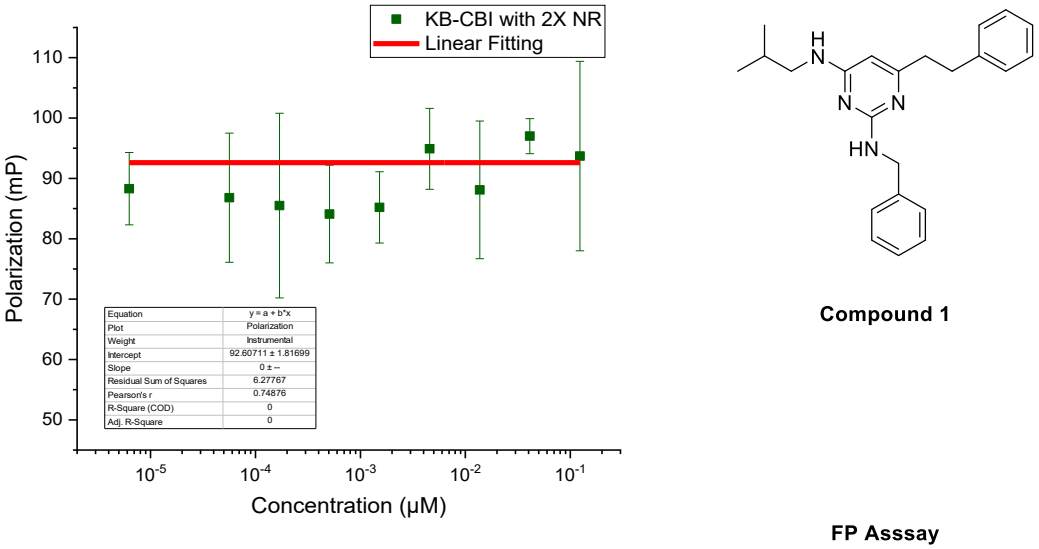


Compound 1

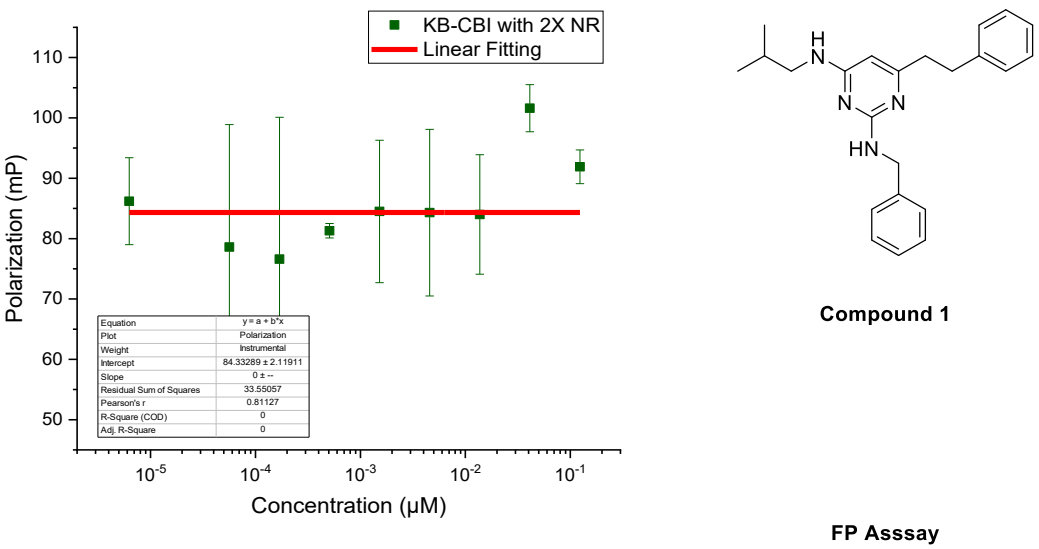
FP Asssay

Graph 10. Graph of Polarization *vs*. the conc. of KB-CBI with 2X NR in 1% DMSO in NR

buffer. (2h)



Graph 11. Graph of Polarization *vs*. the conc. of KB-CBI with 2X NR in 1% DMSO in NR buffer. (3h)



Graph 12. Graph of Polarization *vs*. the conc. of KB-CBI with 2X NR in 1% DMSO in NR buffer. (4h)

It was apparent from these results that the assay in its current form was not satisfactory for detecting the binding of these compounds – the error bars were too large to allow the identification of any sigmoidal binding behavior.

Investigation Between Fluoromone™ and AR-LBD, A Direct Binding Assay

Although the emission and excitation spectra of the Fluorenone™ from the PolarScreen™ AR Competitor Assay Kit had been found to be appropriate, the outcome of the first attempt to run the FP assay was unsatisfactory. Hence, work was continued to optimize the direct binding assay of the Fluoromone™ and AR-LBD. Unlike in a competition binding FP assay (assay mode 1, below), a direct binding assay is based on the interaction only between the Fluorescein labeled peptide and the NR (assay mode 2, below).[42]

Assay mode 1:

$$\text{Peptide} + \text{NR} \leftrightharpoons \text{Peptide:NR}$$

$$\text{Testee} + \text{NR} \leftrightharpoons \text{Testee:NR}$$

$$\text{Testee} + \text{Peptide:NR} \leftrightharpoons \text{Testee:NR} + \text{Peptide}$$

Assay mode 2:

$$\text{Peptide} + \text{NR} \leftrightharpoons \text{Peptide:NR}$$

In was decided that a direct binding assay was preferred in our case since the ligand dissociation constant (K_d) is required in order to interpret a competition assay. In order to improve upon the initial assay conditions, it was considered important to achieve better solubility of the protein by increasing the buffer concentration of the DMSO in the assay.

Our initial protocol had been based on Vaz's work[41] using a constant peptide concentration and variable protein concentration. However, given the limited concentration of the supplied peptide and protein, it had not been possible to achieve any data points at high protein concentrations.

Based also on the original protocol[40] from Thermofisher™, we looked to establish the optimal concentration at which to perform the assay. The original concentration examined was based on the concentration ratio between peptide and protein indicated in the Thermofisher™ protocol; *i.e.* 4X = 7.508 µM. We now therefore decided to examine 5-fold and 10-fold diluted variants of this assay (**Table 8**).

Original Protocol Assay Conc.		5-fold diluted Designed Assay Conc.		10-fold diluted Designed Assay Conc.	
Peptide Conc./µM	Max Protein Conc./µM	Peptide Conc./µM	Max Protein Conc./µM	Peptide Conc./µM	Max Protein Conc./µM
0.1	approx. 30	0.02	6	0.01	3
		Max Assay Peptide Conc./uM		**0.17875** (Dilluted from 0.715 stock)	
		Max Assay Protein Conc./uM		**4.55** (Dilluted from 18.2 stock)	

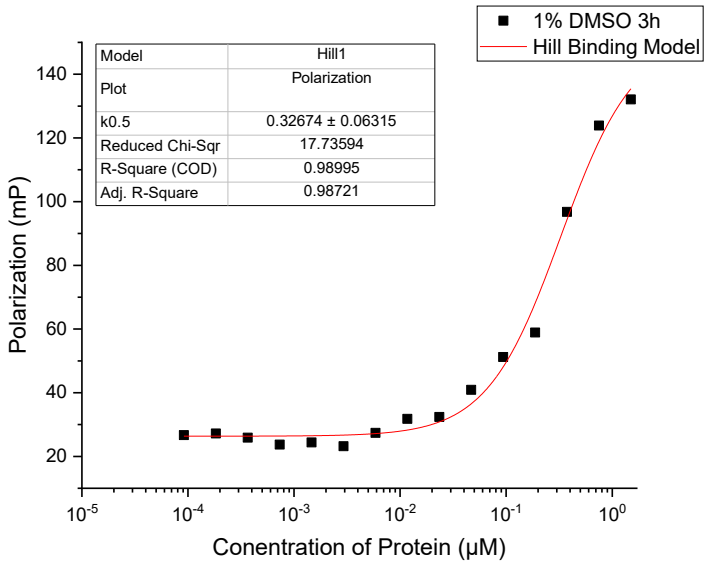
Table 8. Calculated concentrations for the direct binding assay.

In the 10-fold diluted assay, the peptide concentration was set to 0.01 µM and the highest concentration for protein was 3 µM. A 2-fold, 16-point serial dilution of the protein was performed directly in the assay plate with nuclear receptor (NR) buffers in 5 µL of two different volume concentrations of DMSO (2% and 4%) as well as 10 µL of 4X protein stock (12 µM). After serial dilution, 5 µL of neat NR buffer as well as 4X peptide stock (0.04 µM) was added to make the volume into 20 µL. The direct binding assay was performed on the platform of PHERAStar Plus©plate reader using fluorescence polarization. The resulting data were analyzed using Origin© as well as curve fitting to give K_d. The Hill binding model was employed in the curve fitting; this involved applying the Hill equation:

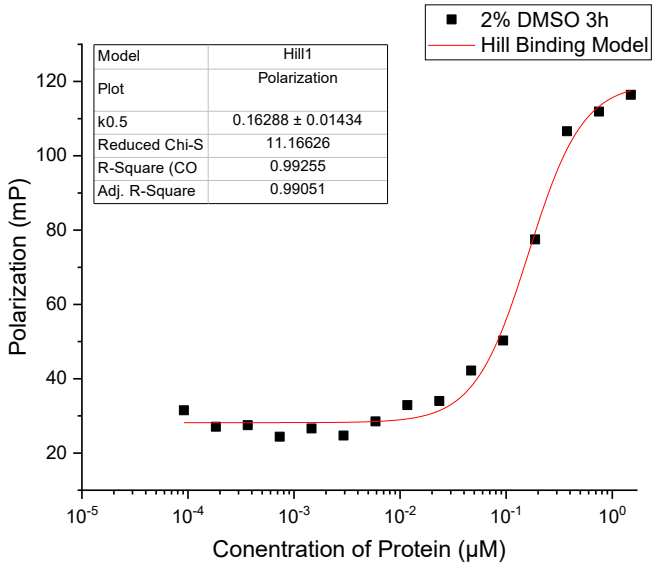
$$V = \frac{V_{max}[S]^n}{(K_{0.5})^n + [S]^n} \ ,$$

Here, V is reaction velocity defined as the rate of reaction progression per unit. V_{max} is

the maximum velocity while [*S*] is substrate concentration. $K_{0.5}$ is the half-maximal concentration constant which in this case, is the dissociation constant K_d. *n* is a unitless Hill coefficient. The graphs are shown below (**Graphs 13 & 14**).



Graph 13. Graph of Polarization *vs*. the concentration of NR-LBD in 1% DMSO in NR buffer with Hill binding Model and calculated K_d (0.32 μM)



Graph 14. Graph of Polarization *vs*. the concentration of NR-LBD in 2% DMSO in NR buffer with Hill binding model and calculated K_d (0.16 μM)

The similar shape of the graphs indicated that the increased amount of DMSO has a limited effect on the binding. The two K_ds obtained in the different concentrations of DMSO were also comparable. Consequently, it was decided to use 2% DMSO in the NR buffer for future assays (instead of 1%).

Optimization of the Protocol

The original protocol recommends two plates in advance of the final assay plate for use of dilutions. (**Figure 44**)

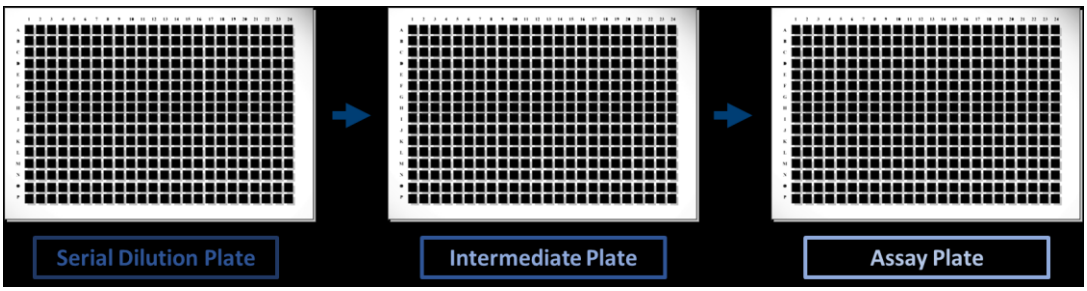


Figure 44. Plates in the original protocol.

The serial dilution plate is designed for 16 points, 3-fold serial dilution for testing compounds with neat DMSO. The intermediate is designed for further dilution with the NR buffer for NR capability. However, this method requires the use of automated multichannel micropipettes. Due to the limitation of the lab and avoiding unexpected waste of materials, based on the method in the original protocol, we optimized it with the method shown in **Figure 45**.

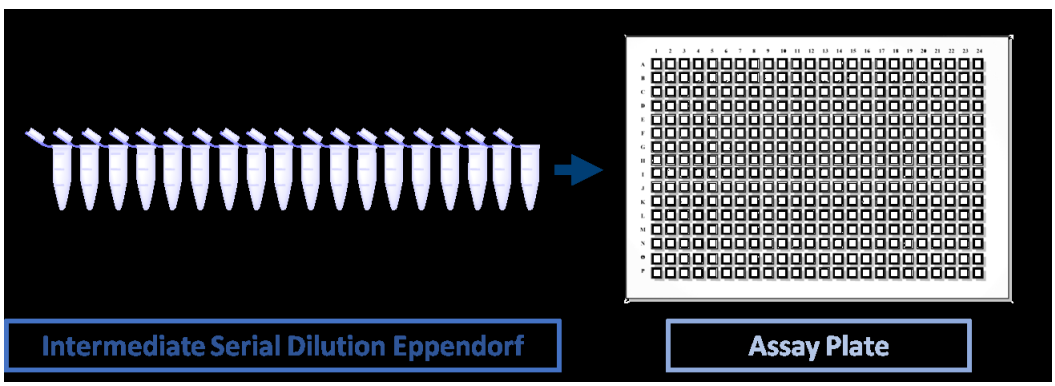


Figure 45. Plates in the optimized protocol.

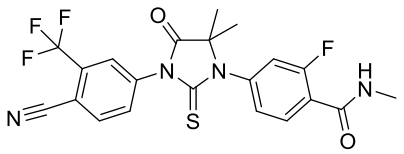
Instead of a Serial dilution plate plus an intermediate dilution plate, a series of Eppendorf tubes was recruited. Since the total dilution from the start point (serial

dilution plate) to the intermediate dilution plate is 50-fold, the degree of dilution in the Eppendorf was fixed to 50-fold as compared to the stock solution. The ratio of DMSO and NR buffer in the Eppendorf was also fixed to match the ratio in the original intermediate dilution plate.

The advantages of this optimized format can be described as: that it is convenient, it has low cost of consumable components, and generates clean experimental data. This method doesn't require multichannel micro pipetting for inter-plate transfers which also leads to time-saving. The low cost of Eppendorf tubes compared to the high cost of DMSO resistant 384-well plate was significant. The original protocol only used 2 µL out of 100 µL from the serial dilution plate to populate the intermediate dilution plate, which results in a large loss of the testing compound. However, in the Eppendorf method, the remaining materials can stay inside the Eppendorf which allows it to be re-frozen and stored so as to allow for subsequent re-use at any time without concern about decomposition. The reliability of the data generated benefits from the shorter duration of the method since the dissociation constant (or IC_{50}) may vary with time. Due to the addition of several components (NR, peptide, and compound) into the assay plate, it can be extremely time-consuming loading a 384-well plate, hence, this method minimizes the time for preparing the plate and obtaining a reliable outcome.

Known Anti-androgen Drug Binding

Having successfully optimized the protocol as described in the previous section, we moved on to test another known anti-androgen drug, Enzalutamide. (**Figure 46**)



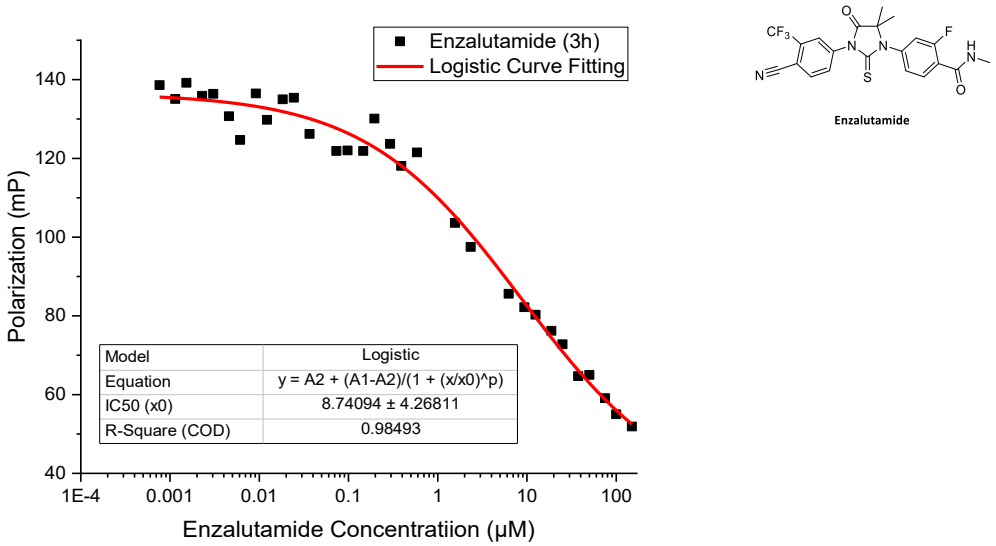
Enzalutamide

Figure 46. Structure of Enzalutamide.

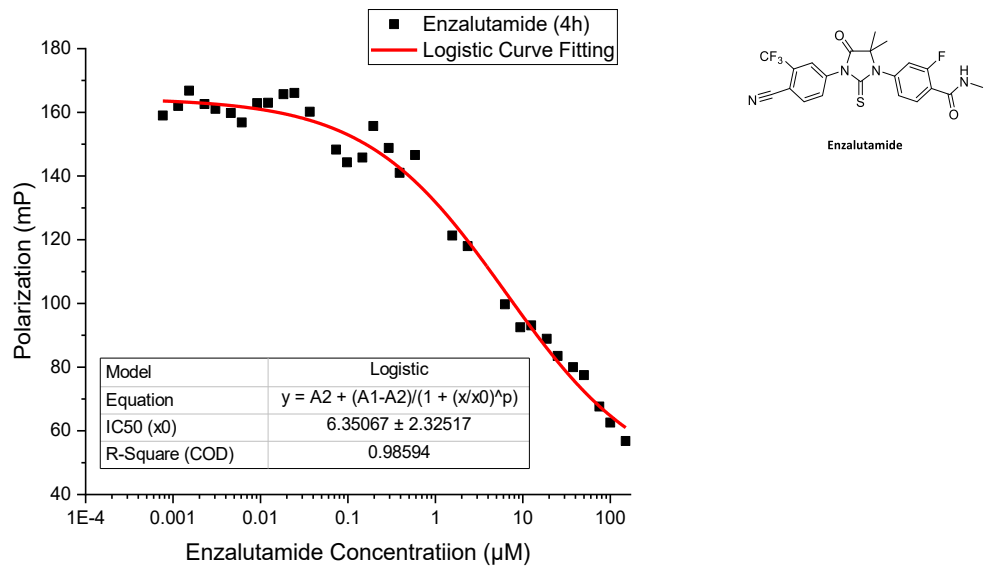
Unlike testosterone and DHT, which have nM level affinities for the AR LBD, this drug has just μM level affinity and so was considered likely to be a more useful positive control in the concentration ranges relevant to our compounds.

Considering the volume percentage of DMSO had been fixed to 2% in NR buffer from the previous direct binding assay, the highest assay well concentration, in this case, was set at 150 μM (*cf*. 100 μM previously). Two-fold serial dilution was performed rather than the 3-fold serial dilution described in the original protocol. In addition, to obtain better scatters distribution and curve fitting, two series of two-fold serial dilutions were operated with different highest Eppendorf concentrations, 200 μM and 300 μM, respectively.

After delivering 10 μL of Eppendorf serial dilution stock into the assay region on the assay plate, 5 μL of 4X Fluromone^{TM} stock was delivered followed by the delivery of 5 μL 8X NR stock. The plate was placed on an orbital shaker for a 2h incubation. Readings were taken at 3h and 4h time points. After analyzing, the resulting curves are shown below in **Graphs 15** and **16**.



Graph 15. Graph of Polarization against the concentration of Enzalutamide in 2% DMSO in NR buffer. (3h)



Graph 16. Graph of Polarization against the concentration of Enzalutamide in 2% DMSO in NR buffer. (4h)

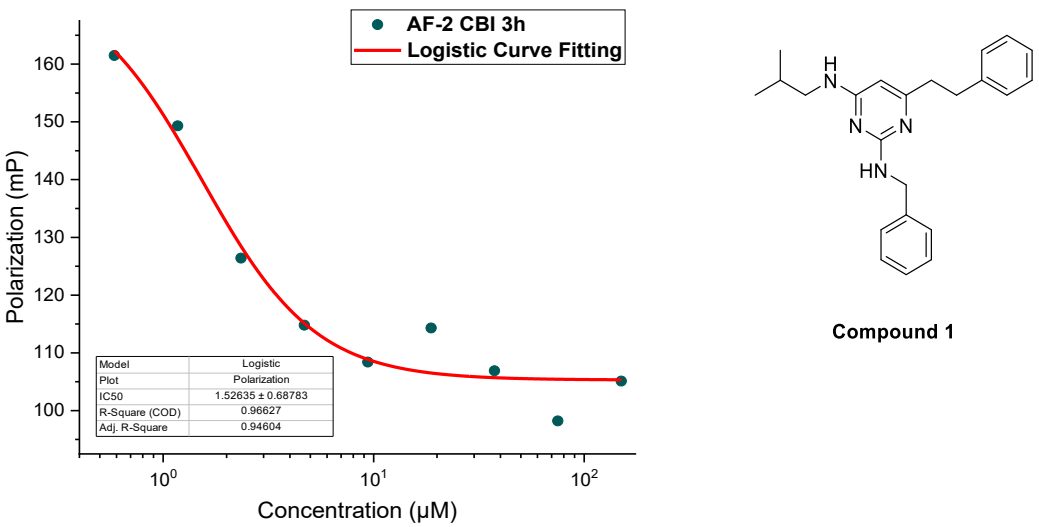
The IC_{50} was calculated from the curve fitting results using **Equation 2** and gave a value

of 8.7± 4.3 µM for 3h incubation and 6.4 ± 2.3 µM and 4h incubation. The reference IC_{50} from the VCaP cell line function assay is 10 µM.[43] The outcome was considered to be in good agreement with the published data.. The R squares of the curves are also close to 1 which emphasizes the good quality of the data. Interestingly, the IC_{50} at 4h is lower than that at 3h which may indicate that the equilibrium maximum is achieved between 3h and 4h incubation.

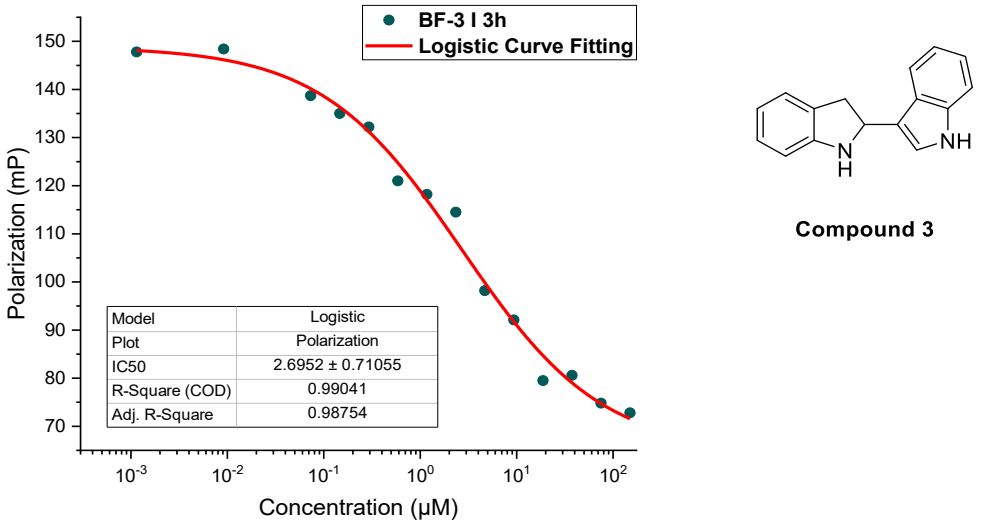
Re-testing the model control compound

Encouraged by the good curves from enzalutamide, we decided to move on with our FXXLF model compound, compound **1** and the indole-indoline control compound **3**.

The serial dilution applied for these compounds followed that in the previous enzalutamide assays. After comparison of the data from the time point of 2h to 4h, a binding equilibrium was found at a 3h point for both compounds. The resulting graphs with curving fitting are shown below in **Graph 17** and **18**.



Graph 17. Graph of Polarization against the concentration of compound **1** in 2% DMSO in NR buffer. (3h)

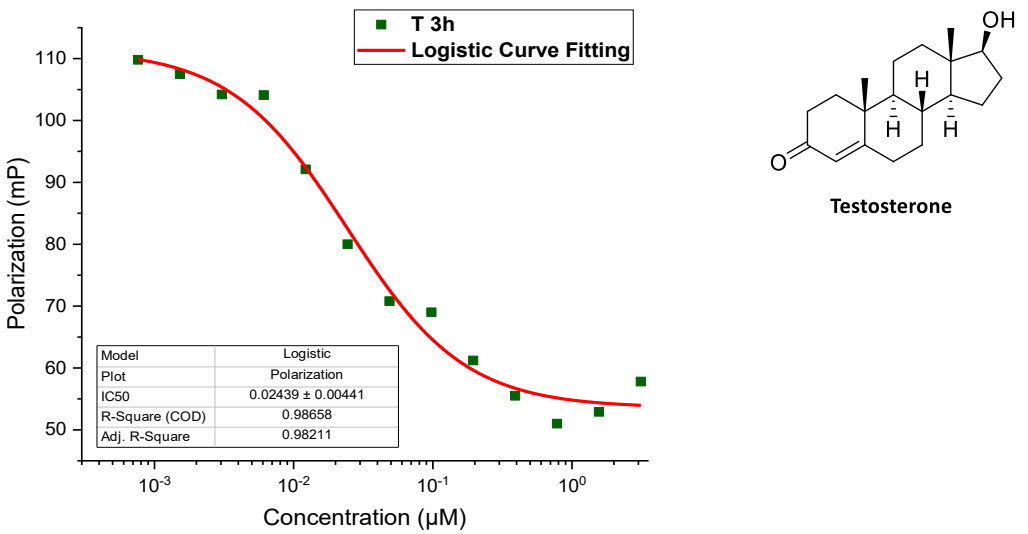


Graph 18. Graph of Polarization against the concentration of **compound 3** in 2% DMSO in NR buffer. (3h)

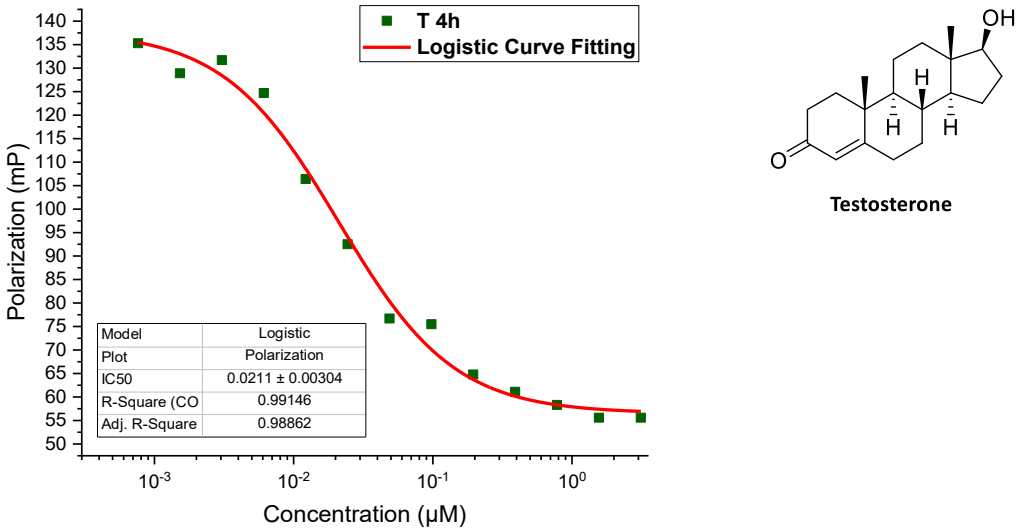
After curve fitting and the application of **Equation 2**, the IC_{50} of compound **1** and compound **3** were calculated to be 1.5 ± 0.7 μM and 2.6 ± 0.7 μM, respectively. These IC_{50}s are in good agreement with their reference values. For compound **1**, its IC_{50} in an ER TR-FRET assay[17] is reported to be 1.5 μM which is perfectly matched with this AR FP assay. The binding interfaces of both AR and ER are found to have structural similarity which contributes to the similarity of IC_{50}. For compound **3**, its reference[22] IC_{50} is 0.3 μM. The difference between the experimental data and the reference data likely results from the different types of assay used, *i.e*. our FP assay *vs*. the literature cell-based functional assay.

Reach to the Milestone

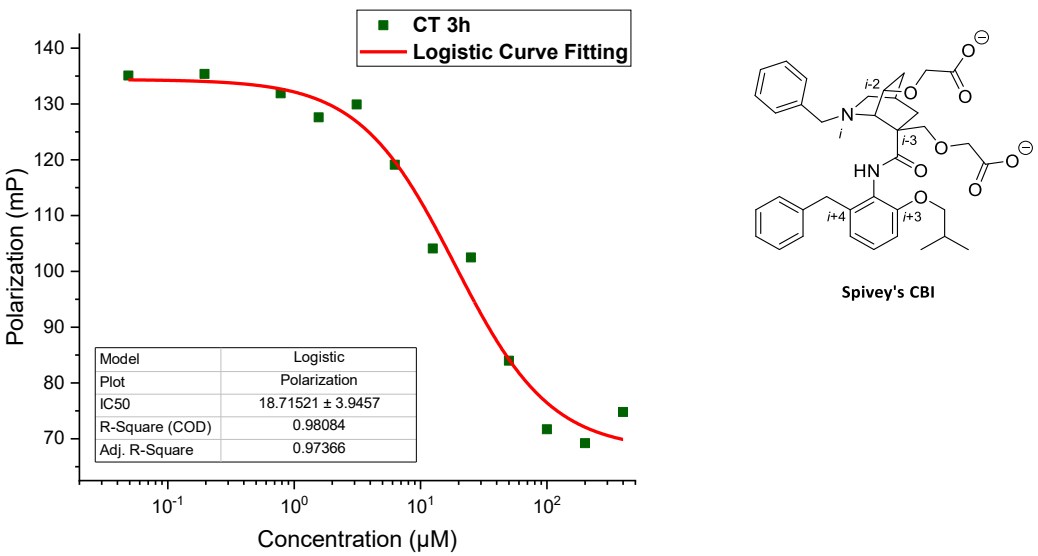
Considering the encouraging outcome from the model control compounds, we decided to move on to our final goal, the **Spivey's CBI** (reference, **CT**, synthesized by Christine Tran, a previous postdoc from the Spivey group). It was also decided to retest testosterone as a positive control since the data from the first attempt was not satisfactory. The assay was performed following the previously optimized protocol using the Eppendorf tube-based method. The highest assay concentration for both compounds was fixed at 200 µM. A 2-fold, 24-point serial dilution was applied, and the data was collected after a 3h incubation period. After analyzing and curve fitting, the resulting graphs are shown in **Graphs 19** and **20** for **Testosterone**, **Graphs 21** and **22** for **Spivey's CBI (CT)**.



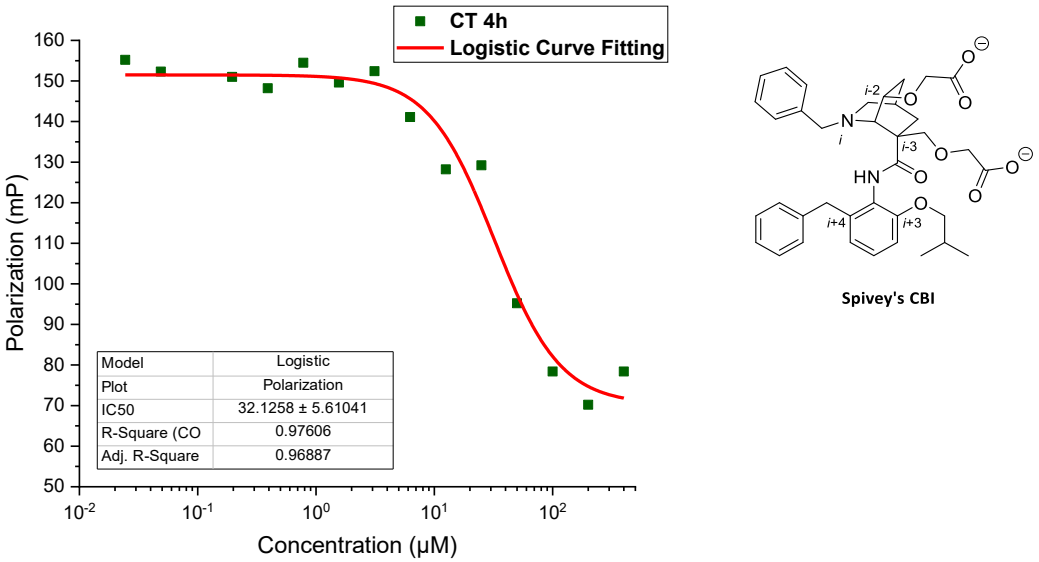
Graph 19. Graph of Polarization against the concentration of testosterone in 2% DMSO in NR buffer. (3h)



Graph 20. Graph of Polarization against the concentration of testosterone in 2% DMSO in NR buffer. (4h)



Graph 21. Graph of Polarization against the concentration of **Spivey's CBI** in 2% DMSO in NR buffer. (3h)



Graph 22. Graph of Polarization against the concentration of **Spivey's CBI** in 2% DMSO in NR buffer. (4h)

After applying a similar method to the collected data, the IC_{50}s of both compounds were calculated. The testosterone, interestingly, showed IC_{50} values very similar to the published ones. The IC_{50}s are 24.4 ± 4.4 nM (3h and 21.1 ± 3.0 nM (4h) while the reference value[40] is 20.0 nM. This result further increased our confidence in the reliability of the assay. It is notable that in this case the IC_{50} value was similar after both 3h and 4h incubation times which may indicate that the androgen enters the LGP of LBD and stabilizes the conformational change thereby preventing the rebound of the peptide.

For **Spivey's CBI (CT)**, it appeared that the equilibrium had already been reached after 3h incubation and gave an IC_{50} value of 18.7 ± 3.9 μM. Considering that this result had been obtained in parallel with the results for testosterone (*i.e.* on the same plate, using the same reagents *etc*.) the data was thought to be reliable and demonstrates that the compound has affinity for the AR. The micromolar level IC_{50} indicates that it could constitute a useful lead for the development of compounds that interfere with AR

transcriptional activity and therefore be of interest for the development of potential therapeutics for PCs. The reading taken at 4h incubation gave IC_{50} of 32.1 ± 5.6 μM. The evaporation of the buffer may contribute to the increase in the value.

Chapter 3. Conclusions

A pyrimidine-based alpha-helix mimetic molecule (compound **1**, CBI S9) designed by Katzenellenbogen to mimic the 'FXXLF' motif which binds to the AR-LBD AF-2 domain was successfully prepared *via* a 5-step synthetic route described in the literature.

Several indoline-indole based compounds that have been reported by Cherkasov to bind to the AR LBD BF-3 domain (e.g. compound **3**, BF3-S1) and some analogues were also successfully synthesized. The synthetic route employed used modified conditions relative to those described in the literature by using HFIP as co-solvent. The oxidation of these compounds to the corresponding bis-indoles was also investigated and conditions using a palladium catalyst and ammonium formate were found to be efficient for this transformation.

These model compounds were sent to our collaborator, Prof. Bevan where they were tested for their ability to inhibit the transcriptional activity of AR. The assay used was a LR assay and this showed that all these compounds had activity as claimed in the literature.

These model compounds were also evaluated in an *in-vitro* FP binding assay based on the inhibition of binding between a fluorescently labelled peptide and rat AR LBD. Optimisation of this assay was required before meaningful data could be obtained, but once optimization had been achieved, the compounds were shown to bind with levels of affinity close to those described in the literature.

Finally, a 5-residue alpha-helix mimetic compound (**Spivey's CBI)** prepared in the Spivey group by Dr Christine Tran and designed to bind to the AR by presenting residues compatible with the 'FXXLF' motif, was also tested for its ability to bind in the FP assay. The compound gave a micromolar level of activity for binding with AR-LBD: IC_{50} = 18.7 ± 3.9 μM. This excellent result encourages us to investigate further

compounds of this type as potential leads for therapeutic agents with activity against the AR transcriptional pathway.

Chapter 4. Future Work

The immediate future work can mainly focus on two areas: 1) repeating the FP assay, and 2) conducting cell-based functional assays.

Given the scarcity of **Spivey's CBI** compound, the FP binding experiment described in this thesis was only conducted on one occasion. In order for confidence in that result to be sufficiently high to allow for publication this experiment needs to be repeated as a triplicate run. This will likely require more of the compound to be prepared by synthesis. This material will also be required for the below-described activity assay work.

The FP assay only indicates the activity of binding to AR. To become a useful lead for development of a therapeutic agent, a positive result in a cell-based function assay is also crucial. The described LR assay should be suitable for this purpose.

The longer-term future work can be divided into three parts:

Firstly, if the cell-based assay for **Spivey's CBI** achieves a good outcome, a study of binding model and target specificity can be put on the schedule. By utilizing solid-phase peptide synthesis (SPPS), a known coactivator mimetic peptide with fluorescein can be produced and another FP assay can be constructed to allow the interaction with the AF-2 domain to be verified. It would also be valuable to try to obtain a single crystal X-ray structure determination of Spivey's CBI bound into the AR protein either by the soaking or co-crystallization techniques.

Secondly, for the so-called BF-3 specific indole-indoline analogs, a series of cell-based LR assay could be developed to produce interesting binding data. A combination of AF-2 target and BF-3 targeting compounds could be an attractive option for combination therapy.

Finally, the structure of **Spivey's CBI** could also be further modified based on the assay results. Some hydrophilic groups can be added into the structure to increase its water solubility. The side chains can also be replaced with other amino acid residues to try to increase its binding affinity.

Chapter 5. Experimental

Biology Assays

LR Assay.

COS-1 cells were transiently transfected with expression vectors for the Androgen receptor, TAT-GRE luciferase reporter and β-galactosidase using the calcium phosphate method[44]. Cells were treated with 0.1nM MB plus increasing concentrations of androgen receptor antagonists for 24h. Luciferase activities were normalized for β-galactosidase activity and presented relative to the corresponding value for vehicle treatment. Data presented are the mean of three independent experiments performed in duplicate ± S.E.

FP Assay

The FP Assay Kit 'PolarScreen™ Androgen Receptor Competitor Assay Kit, Green' was supplied by ThermoFisher™ Scientific. Product Number: A15880 Website: https://www.thermofisher.com/order/catalog/product/A15880

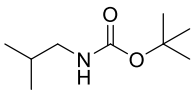
The FP assay protocol is a 'PolarScreen™ Nuclear Receptor Competitor Assays - Universal Protocol' from ThermoFisher™ Scientific Website: https://www.thermofisher.com.

All the biological experimental data were generated using MARS™ software (BMG LABTECH LTD, https://www.bmglabtech.com/mars-data-analysis-software/) and analyzed using Origin Lab™ software (©Origin Lab Corporation, https://www.originlab.com).

Chemistry Experimental

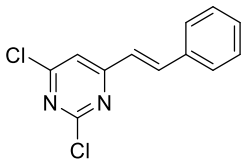
Note: The known compounds are cited with the corresponding reference while the new compounds are not.

tert-Butyl isobutylcarbamate[45]



As described in Millet *et al.*[45], isobutyl-amine (2.20 g, 29.9 mmol) and triethylamine (3.03 g, 29.9 mmol) were dissolved in dry THF (10 mL) before cooled to 0 °C. After di-tert-butyl carbonate (6.400 g, 29.3 mmol) was added portion-wise with continuous string followed by a 10 min more stirring, the mixture was allowed to warm to room temperature. After 16h, 20 mL deionized water was added into mixture before extracted with ethyl acetate (3×30 mL). The combined organic layer was dried ($MgSO_4$) and concentrated under reduced pressure to give crude product follow by a column chromatography (CH_2Cl_2) then gave white crystalline solid (1.81 g, 34%); R_f = 0.51 (CH_2Cl_2); δ_H (400 MHz, $CDCl_3$) 4.56 (bs, 1H, N**H**), 2.94 (t, J = 6.4 Hz, 2H, C**H₂**), 1.72 (sept, J = 6.68 Hz, 1H, C**H**(CH_3)$_2$), 1.44 (s, 9H, O**(CH₃)₃**), 0.90 (d, J = 6.7 Hz, 6H. CH**(CH₃)₂**); δ_C (100 MHz, $CDCl_3$) 156.2 (C=O), 78.9 (O**C**(CH_3)$_3$), 48.1 (**C**H_2NH), 28.9 ((CH_3)2**C**H), 28.5 (OC(**C**H_3)$_3$), 20.0 ((**C**H_3)$_2$CH); low melting point, 27 – 28 °C; υ_{max} /cm^{-1} (FTIR) 3355 (N-H stretching, m, amide), 1688 (C=O stretching, s, amide), 1455 (C-H bending, m, methyl), 1468 (C-H bending, m, methylene).

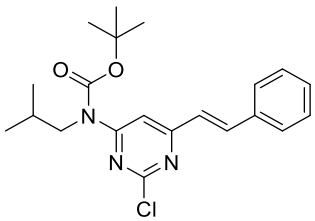
(*E*)-2,4-Dichloro-6-styrylpyrimidine[12]



As described in Parent *et al*[12]., a solution of trans-2-phylvinylboronic acid (1.75 g, 11.83 mmol), K_3PO_4 (5.02 g, 23.66 mmol) and $PdCl_2(PPh_3)_2$ (83.0 mg, 0.11 mmol) in 25 mL dry THF was prepared before the addition of a solution of 2,4,6-trichloropyrimidine (2.16 g, 11.83 mmol) in 25 mL THF with stirring. After adding of 6 mL deionized water, the solution became yellow. The mixture was stirring for 6h at 70 °C under inert atmosphere (N_2) before addition of 0.2 equiv. more boronic acid and 2h more stirring. The reaction was quenched by addition of 20 mL deionized water. The mixture was extracted with ether (3×20 mL) before being washed with brine and dried ($MgSO_4$). The solvent was removed under reduced pressure. The crude product was purified by column chromatography (5-20% EtOAc in hexane) and give pale yellow powder (1.11 g, 37%); R_f = 0.57 (20% EtOAc in hexane); δ_H (400 MHz, $CDCl_3$) 7.98 (d, J = 15.9 Hz, 1H, pyrimidine-C**H**=CH-phenyl), 7.64 – 7.56 (m, 2H, phenyl-**H**), 7.47 – 7.38 (m, 3H, phenyl-**H**), 7.25 (s, 1H, pyrimidine-**H**), 6.97 (d, J = 15.9 Hz, 1H, pyrimidine-CH=C**H**-phenyl); δ_C (100 MHz, $CDCl_3$) 166.7 (pyrimidine), 162.8 (pyrimidine), 160.8 (pyrimidine), 141.0 (Ph), 134.9 (C=C), 130.5 (Ph), 129.2 (Ph), 128.3 (Ph), 123.1 (C=C), 117.1 (pyrimidine); m.p. 108-110 °C (Hexane) [lit.[46], 119-121 °C (EtOAc/Hexane)]; υ_{max} /cm^{-1} (FTIR) 3063 (C-H stretching, m, aromatic), 1950 (aromatic C-H bending, w, overtone), 978 (C=C bending, s, trans alkene), 824 (C-Cl stretching, s); [MS ES-], calculated 251.0143 $[M+H]^+$, found 251.0153 $[M+H]^+$, Δ = 4 ppm.

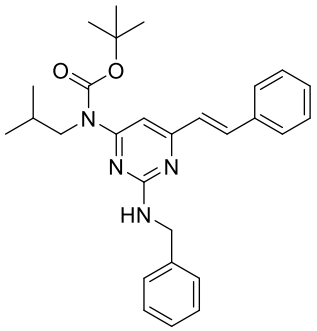
((*E*)-2-Chloro-*N*-(4,4-dimethylpent-1-en-2-yl)-*N*-isobutyl-6-styrylpyrimidin-4-amine)

12



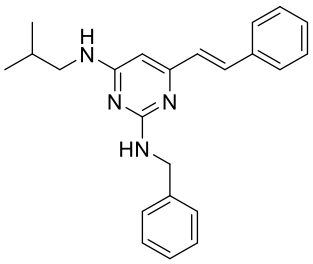
As described in Parent *et al*[12]., CBI-S1 (62.9 mg, 0.36 mmol), CBI-S2 (82.8 mg, 0.33 mmol) and sodium hydride (60% dispersion in mineral oil) (20.0 mg, 0.5 mmol) were dissolved in 5 mL dry DMF with stirring under inert atmosphere (N_2). The mixture was allowed to stir at room temperature for 2h before quenching by addition of 0.1 mL saturated ammonium chloride. The crude product was extracted from 10 mL brine with ether (3×10 mL) before being washed by brine (5×20 mL) and dried ($MgSO_4$) followed by removal of solvent under reduced pressure. After purification by column chromatography (CH_2Cl_2:hexane, 1:1), it gave pale yellow oil (40 mg, 31%); R_f = 0.64 (20% EtOAc in hexane); δ_H (400 MHz, $CDCl_3$) 7.96 (s, 1H, pyrimidine-**H**), 7.88 (d, J = 15.9 Hz, 1H, pyrimidine-C**H**=CH-phenyl), 7.60 – 7.54 (m, 2H, phenyl-**H**), 7.44 – 7.29 (m, 3H, phenyl-**H**), 7.00 (d, J = 15.9 Hz, 1H, pyrimidine-CH=C**H**-phenyl), 3.91 (d, J = 7.3 Hz, 2H, C**H₂**), 2.07 (sept, J = 6.80 Hz, 1H, C**H**$(CH_3)_2$), 1.57 (s, 9H, O**$(CH_3)_3$**), 0.91 (d, J = 6.7 Hz, 6H, CH**$(CH_3)_2$**); δ_C (100 MHz, $CDCl_3$) 165.2, 163.1, 159.7, 153.7, 137.8, 135.7, 129.6, 129.0, 127.9, 125.2, 109.0, 83.1, 52.5, 28.3, 27.9, 20.3; m.p. 118-120 ^oC; υ_{max} /cm^{-1} (FTIR) 3154 (C-H stretching, m, aromatic), 2961 (C-H, stretching, m, alkene), 1953 (aromatic C-H bending, w, overtone), 1714 (C=O stretching, s), 1467 (C-H bending, m, methylene), 1430 (C-H bending, m, methyl), 970 (C=C bending, s, trans alkene), 844 (C-Cl stretching, s); [MS ES+], calculated 388.1792 $[M+H]^+$, found 388.1799 $[M+H]^+$, Δ = 1.8 ppm.

(*tert*-Butyl (*E*)-(2-(benzylamino)-6-styrylpyrimidin-4-yl) (isobutyl) carbamate)[12]



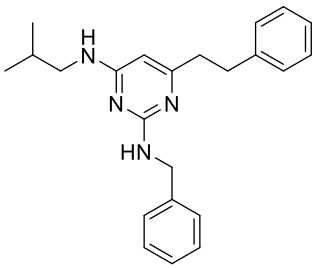
As described in Parent *et al*[12]., CBI-S3 (39.7 mg, 0.102 mmol) and benzyl-amine (32.9 mg, 0.306 mmol) were dissolved in 2 mL DMSO in sealed tube with stirring. The mixture was allowed to stir for 38h at 110 °C. After cooling down, the crude product was extracted from 10 mL brine with ether (3×10 mL) before being washed by brine (5×20 mL) and dried ($MgSO_4$) followed by removal of solvent under reduced pressure. After purification by column chromatography (1-10% EtOAc in hexane), it gave white crystalline solid (19 mg, 41%). R_f = 0.54 (20% EtOAc in hexane); δ_H (400 MHz, $CDCl_3$) 7.73 (d, J = 15.9 Hz, 1H, pyrimidine-C**H**=CH-phenyl), 7.59 – 7.50 (m, 2H, phenyl-**H**), 7.42 – 7.27 (m, 9H, phenyl-**H &** pyrimidine-**H**), 6.95 (d, J = 15.9 Hz, 1H, pyrimidine-CH=C**H**-phenyl), 5.39 (bs, 1H, N**H**), 4.65 (d, J = 6.0 Hz, 2H, C$\mathbf{H_2}$NBOC), 3.80 (d, J = 7.3 Hz, 2H, C$\mathbf{H_2}$-phenyl), 1.99 (sept, J = 6.84 Hz, 1H, C**H**$(CH_3)_2$), 1.55 (s, 9H, O$\mathbf{(CH_3)_3}$), 0.81 (d, J = 6.7 Hz, 6H, CH$\mathbf{(CH_3)_2}$); δ_C (100 MHz, $CDCl_3$) 163.5, 162.4, 161.8, 154.2, 134.0, 136.5, 135.0, 128.8, 128.8, 128.6, 127.6, 127.4, 127.1, 102.5, 81.8, 52.2, 45.7, 28.4, 28.2, 20.3; m.p. 125-127 °C (EtOAc/Hexane); m.p. 125-127 °C; υ_{max} /cm^{-1} (FTIR) 3257 (N-H stretching, m), 3085 (C-H stretching, m, aromatic), 2956 (C-H stretching, m, alkene), 1953 (aromatic C-H bending, w, overtone), 1713 (C=O stretching, s), 1467 (C-H bending, m, methylene), 1415 (C-H bending, m, methyl), 963 (C=C bending, s, trans alkene); [MS ES+], calculated 459.2756 $[M+H]^+$, found 459.2756 $[M+H]^+$, Δ = 0 ppm.

(*E*)-*N*^{2}-Benzyl-*N*^{4}-isobutyl-6-styrylpyrimidine-2,4-diamine[12]



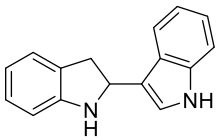
As described in Parent *et al.*[12]., CBI-S7 (107.6 mg, 0.234 mmol) was dissolved in 5 mL CH_2Cl_2 with stirring before addition of 5 mL trifluoroacetic acid. After 30 min, the liquid was removed by nitrogen flow before washed with saturated sodium bicarbonate and extracted with ether (3×10 mL) and dried ($MgSO_4$). The solvent was removed under reduced pressure. The product was purified by column chromatography (20 – 30% EtOAc in hexane) and gave pale yellow oil (less than 73 mg, less than 88%). R_f = 0.41 (40% EtOAc in hexane); δ_H (400 MHz, $CDCl_3$) 7.69 (d, J = 15.9 Hz, 1H, pyrimidine-C**H**=CH-phenyl), 7.58 – 7.51 (m, 2H, phenyl-**H**), 7.41 – 7.23 (m, 8H, phenyl-**H**), 6.84 (d, J = 15.9 Hz, 1H, pyrimidine-CH=C**H**-phenyl), 5.78 (s, 1H, pyrimidine-**H**), 5.21 (bs, 1H, isobutyl-N**H**), 4.78 (bs, 1H, phenyl-N**H**), 4.67 (d, J = 5.8 Hz, 2H, C**H$_2$**-phenyl), 3.12 (t, J = 6.43 Hz, 2H, $(CH_3)_2$CHC**H$_2$**N), 1.87 (sept, J = 6.68 Hz, 1H, C**H**$(CH_3)_2$), 0.96 (d, J = 6.70 Hz, 6H, CH**$(CH_3)_2$**); δ_C (100 MHz, $CDCl_3$) 164.4, 162.4, 140.3, 136.7, 134.2, 128.8, 128.5, 127.8, 127.4, 127.0, 49.1, 45.7, 28.6, 20.4; υ_{max} /cm^{-1} (FTIR) 3230 (N-H stretching, m), 3085 (C-H stretching, m, aromatic), 2956 (C-H stretching, m, alkene), 1953 (aromatic C-H bending, w, overtone), 1468 (C-H bending, m, methylene), 1420 (C-H bending, m, methyl), 963 (C=C bending, s, trans alkene); [MS ES+], calculated 359.2 $[M+H]^+$, found 359.2 $[M+H]^+$.

N^2-Benzyl-N^4-isobutyl-6-phenethylpyrimidine-2,4-diamine[12]



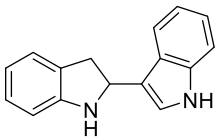
As described in Parent *et al*[12]., compound **CBI-S8** (60.4 mg, 0.168 mmol) was dissolved in 10 mL Methanol with stirring before addition of (10% w/w Pd/C) (90 mg, 0.084 mmol, 0.5 eq.). The mixture was placed under 1 atm of hydrogen gas for 30 min with stirring. The residue was removed by filtration and washed by mixture of CH_2Cl_2 and Methanol (1:1). The filtrate was concentrated under reduced pressure. The product was purified by column chromatography (20 – 40% EtOAc in hexane) to give a yellow oil (56 mg, 93%). R_f = 0.57 (70% EtOAc in hexane); δ_H (400 MHz, $CDCl_3$) 7.38-7.16 (m, 10H, phenyl-**H**), 5.53 (s, 1H, pyramidine-**H**), 5.26 (bs, 1H, phenyl-N**H**), 4.70 (bs, 1H, isobutyl-N**H**), 4.62 (d, J = 5.84 Hz, 2H, C**H_2**-phenyl), 3.04 (t, J= 5.66 Hz, 2H, $(CH_3)_2CHC\mathbf{H_2}N$), 2.98 (m, pyrimidine-C**H_2**-CH_2-phenyl), 2.74 (m, pyrimidine-CH_2-C**H_2**-phenyl), 1.80 (sept, J = 6.72 Hz, 1H, C**H**$(CH_3)_2$), 0.92 (d, J = Hz, 6H, CH**$(CH_3)_2$**); δ_C (100 MHz, $CDCl_3$) 164.0, 162.2, 141.9, 140.3, 128.6, 128.5, 128.4, 127.7, 127.0, 126.0, 49.0, 45.6, 39.6, 34.9, 28.5, 20.4; υ_{max} /cm^{-1} (FTIR) 3258 (N-H stretching, m), 3061 (C-H stretching, m, aromatic), 2955 (C-H stretching, m, alkane), 1955 (aromatic C-H bending, w, overtone), 1452 (C-H bending, m, methylene), 1415 (C-H bending, m, methyl); [MS ES+], calculated 361.2 $[M+H]^+$, found 361.2 $[M+H]^+$.

3-(Indolin-2-yl)-1H-indole Attempt 1[22]



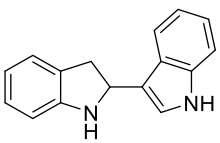
As described in Munuganti *et al*.[22], indole (5.00 g, 42.7 mmol, 1.0 eq.) was dissolved in 150 mL acetonitrile with stirring and gave an orange solution, the solution was allowed to cool to 0 °C before dropwise addition of a 50 mL solution of camphor-sulfonic acid dissolved in acetonitrile (5.45 g, 23.4 mmol, 0.55 eq.). The dark orange mixture was stirring at 0 °C for 7h before checked by TLC. 0.2 eq. more camphor-sulfonic acid was added in due to the reaction was not completed. The reaction was stopped at 8h before filtration of the resulting brown solid and washed with acetonitrile (3×20 mL). The solid was neutralized by saturated sodium bicarbonate (50 mL) and extracted with ethyl acetate (3×50 mL). The organic phase was washed with brine and dried (Na_2SO4). The product was purified by flash column chromatography (5-20% ethyl acetate in hexane) and gave pink solid (1.13 g, 23%); R_f = 0.35 (20% ethyl acetate in hexane); δ_H (400 MHz, DMSO-d_6) 10.86 (s, 1H, N**H** from indole), 7.48 (d, J = 7.88 Hz, 1H, indole), 7.35 – 7.34 (m, 1H, indole), 7.25 (d, J = 2.4 Hz, 1H, indole), 7.10 – 7.00 (m, 2H, aromatic region of indoline), 6.93 – 6.91 (m, 2H, aromatic region of indoline), 6.54 (t, J = 7.2 Hz, 2H, indole), 5.91 (d, J = 2.4 Hz, 1H, N**H** from indoline), 5.12 (t, J = 8.8, 2.4 Hz, 1H, C**H**-indole), 3.37 (q, J = 9.2 Hz, 1H, C$\mathbf{H}_2$ from indoline), 2.98 (dd, J = 8.6 Hz, 1H, C$\mathbf{H}_2$ from indoline).

^{1}H NMR Conversion Experiment Procedure



To a solution of indole (20.0 mg, 0.171 mmol) in chloroform-d, camphor-sulfonic acid (21.8 mg, 0.094 mmol) was added as well as hexafluoro-2-propanol (variable from 18 μL, 0.171 mmol to 90 μL, 0.855 mmol). The mixture was allowed to stir at room temperature for 2h and checked by ^{1}H NMR.

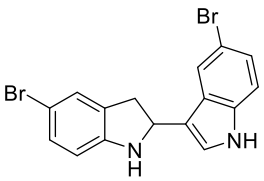
3-(Indolin-2-yl)-1H-indole Attempt 2



Indole (2.01 g, 17.1 mmol, 1.0 eq.) and camphor-sulfonic acid (2.18 g, 9.40 mmol, 0.55 eq.) were dissolved in chloroform (50 mL) before dropwise addition of hexafluoro-2-propanol (9 mL, 85.5 mmol, 5 eq.). The brown mixture was stirring at room temperature in dark for 3h before checked by TLC. The solvent was removed under reduced pressure before neutralization by saturated sodium bicarbonate (50 mL) and extracted with ethyl acetate (3×50 mL). The organic phase was washed with brine and dried (Na_2SO_4). After the removal of solvent under reduced pressure, the crude product was purified by flash column chromatography (5-10% ethyl acetate in hexane) and gave pale yellow sticky oil (1.14 g, 56%); R_f = 0.35 (20% ethyl acetate in hexane); δ_H (400 MHz, DMSO-d_6) 10.87 (s, 1H, N**H** from indole), 7.49 (d, J = 7.88 Hz, 1H, indole), 7.36 – 7.36 (m, 1H, indole), 7.25 (d, J = 2.4 Hz, 1H, indole), 7.11 – 7.01 (m, 2H, aromatic region of indoline), 6.94 – 6.92 (m, 2H, aromatic region of indoline), 6.54 (t, J = 7.2 Hz, 2H, indole), 5.93 (d, J = 2.4 Hz, 1H, N**H** from indoline), 5.12 (t, J = 8.8, 2.4 Hz, 1H, CH-indole), 3.38 (dd, J = 15.5, 8.6 Hz, 1H, C**H**$_2$ from indoline), 2.98 (dd, J = 15.5, 8.6 Hz, 1H, C**H**$_2$ from indoline); δ_C (100 MHz, DMSO-d_6) 152.0, 136.8, 128.2, 127.1, 125.6, 124.1,

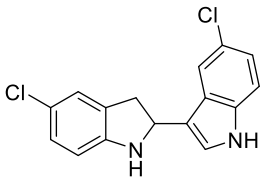
122.0, 121.0, 119.2, 118.3, 118.2, 116.7, 111.5, 108.0, 55.7, 37.4; m.p. 113-115 °C (EtOAc/Hexane) [lit.[47], 110-111 °C]; [MS ES+], calculated 235.1235 $[M+H]^+$, found 235.1243 $[M+H]^+$, Δ = 3.4 ppm.

5-Bromo-3-(5-bromoindolin-2-yl)-1H-indole



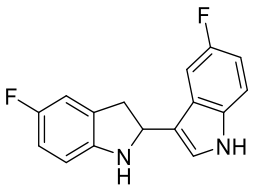
5-bromoIndole (3.35 g, 17.1 mmol, 1.0 eq.) and camphor-sulfonic acid (2.18 g, 9.40 mmol, 0.55 eq.) were dissolved in chloroform (50 mL) before addition of hexafluoro-2-propanol (9 mL, 85.50 mmol, 5 eq.). The orange mixture was stirring at room temperature for 3h before checked by TLC. The solvent was removed under reduced pressure before neutralization by saturated sodium bicarbonate (50 mL) and extracted with ethyl acetate (3×50 mL). The organic phase was washed with brine and dried (Na_2SO_4). The product was purified by flash column chromatography (20% ethyl acetate in hexane) and gave pink solid (1.30 g, 39%); R_f = 0.19 (20% ethyl acetate in hexane); δ_H (400 MHz, DMSO-d_6) 11.12 (s, 1H, N**H** from indole), 7.65 (d, J = 1.9 Hz, 1H, indole), 7.38 – 7.29 (m, 2H, indole), 7.21 – 7.15 (m, 2H, aromatic region of indoline), 7.09 – 7.07 (m, 1H, aromatic region of indoline), 6.48 (d, J = 8.2 Hz, 1H, indole), 6.20 (d, J = 2.3 Hz, 1H, N**H** from indoline), 5.12 (td, J = 8.8, 2.2 Hz, 1H, C**H**-indole), 3.42 (q, J = 9.12 Hz, 1H, C$\mathbf{H}_2$ from indoline), 2.97 (q, J = 8.6 Hz, 1H, C$\mathbf{H}_2$ from indoline); δ_C (100 MHz, DMSO-d_6) 151.3, 135.5, 131.1, 129.6, 127.4, 126.9, 123.8, 123.6, 121.4, 117.6, 113.6, 111.1, 109.5, 107.2, 55.7, 37.0; m.p. 112-118 °C (EtOAc/Hexane) [lit.[48], 127-129 °C]; υ_{max} /cm^{-1} (FTIR) 669 (C-Br stretching, s, halo compound); [MS ES+], calculated 390.9445 $[M+H]^+$, found 390.9445 $[M+H]^+$, Δ = 0 ppm.

5-Chloro-3-(5-chloroindolin-2-yl)-1H-indole



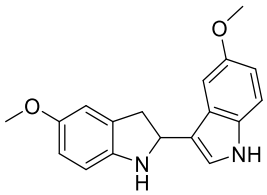
5-ChloroIndole (2.59 g, 17.1 mmol, 1.0 eq.) and camphor-sulfonic acid (2.18 g, 9.40 mmol, 0.55 eq.) were dissolved in chloroform (50 mL) before addition of hexafluoro-2-propanol (9 mL, 85.50 mmol, 5 eq.). The green mixture was stirring at room temperature for 3h before checked by TLC. The solvent was removed under reduced pressure before neutralization by saturated sodium bicarbonate (50 mL) and extracted with ethyl acetate (3×50 mL). The organic phase was washed with brine and dried (Na_2SO_4). The product was purified by flash column chromatography (10 - 20% ethyl acetate in hexane) to give the title product as a brown powder (811 mg, 31%); R_f = 0.30 (30% ethyl acetate in hexane); δ_H (400 MHz, DMSO-*d*$_6$) 11.11 (s, 1H, N**H** from indole), 7.50 (d, J = 2.1 Hz, 1H, indole), 7.37 (d, J = 8.6 Hz, 1H, indole), 7.34 (d, J = 2.4 Hz, 1H, indole), 7.06 - 7.09 (m, 1H, indole), 7.05 – 7.06 (m, 1H, aromatic region of indoline), 6.97 (td, J = 2.2, 8.2 Hz, 1H, aromatic region of indoline), 6.51 (d, J = 8.2 Hz, 1H, aromatic region of indoline), 6.17 (d, J = 2.3 Hz, 1H, N**H** from indoline), 5.13 (td, J = 8.9, 8.8, 2.3 Hz, 1H, C**H**-indole), 3.35 (dd, J = 16.0, 8.6 Hz, 1H, C**H**$_2$ from indoline), 2.96 (dd, J = 16.0, 8.6 Hz, 1H, C**H**$_2$ from indoline); δ_C (100 MHz, DMSO-*d*$_6$) 150.9, 135.2, 130.5, 126.7, 126.6, 124.2, 124.0, 123.0, 121.1, 119.9, 118.4, 117.7, 113.1, 108.8, 55.8, 37.1; m.p. 114-117 ^oC [lit.[48], 123-124 ^oC]; υ_{max} /cm^{-1} (FTIR) 3152 (N-H stretching, m), 2838 (C-H stretching, m, aromatic); [MS ES+], calculated 303.0456 $[M+H]^+$, found 303.0463 $[M+H]^+$, Δ = 2.3 ppm.

5-Fluoro-3-(5-fluoroindolin-2-yl)-1H-indole



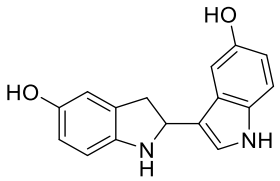
5-FluoroIndole (2.31 g, 17.1 mmol, 1.0 eq.) and camphor-sulfonic acid (2.18 g, 9.40 mmol, 0.55 eq.) were dissolved in chloroform (50 mL) before dropwise addition of hexafluoro-2-propanol (9 mL, 85.50 mmol, 5 eq.). The orange mixture was stirring at room temperature in dark for 3h before checked by TLC. The solvent was removed under reduced pressure before neutralization by saturated sodium bicarbonate (50 mL) and extracted with ethyl acetate (3×50 mL). The organic phase was washed with brine and dried (Na_2SO_4). The product was purified by flash column chromatography (20% ethyl acetate in hexane) to give the title product as a dark brown powder (990 mg, 43%); R_f = 0.34 (30% ethyl acetate in hexane); δ_H (400 MHz, DMSO-d_6) 10.99 (s, 1H, N**H** from indole), 7.33 - 7.36 (m, 2H, indole), 7.19 (dd, J = 2.6, 10.2 Hz, 1H, indole), 6.91 - 6.94 (m, 1H, indole), 6.88 - 6.90 (m, 1H, aromatic region of indoline), 6.76 (td, J = 2.7, 8.6, 2.7 Hz, 1H, aromatic region of indoline), 6.48 (dd, J = 4.5, 8.4 Hz, 1H, aromatic region of indoline), 5.85 (d, J = 2.6 Hz, 1H, N**H** from indoline), 5.09 (td, J = 8.9, 8.8, 2.7 Hz, 1H, C**H**-indole), 3.34 (dd, J = 15.8, 8.7 Hz, 1H, C$\mathbf{H}_2$ from indoline), 2.95 (dd, J = 15.8, 8.7 Hz, 1H, C$\mathbf{H}_2$ from indoline); δ_C (100 MHz, DMSO-d_6) 157.6, 156.5, 155.3, 154.2, 148.4, 133.4, 130.1, 125.8, 124.2, 118.3, 112.9, 109.1, 108.0, 104.0, 56.2, 37.3; m.p. 114-118 °C; υ_{max} /cm^{-1} (FTIR) 3164 (N-H stretching, m), 2848 (C-H stretching, m, aromatic); [MS ES+], calculated 271.1047 $[M+H]^+$, found 271,1049 $[M+H]^+$, Δ = 0.7 ppm.

5-Methoxy-3-(5-methoxyindolin-2-yl)-1H-indole



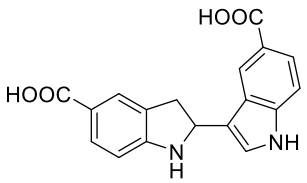
5-MethoxyIndole (2.52 g, 17.1 mmol, 1.0 eq.) and camphor-sulfonic acid (2.18 g, 9.40 mmol, 0.55 eq.) were dissolved in chloroform (50 mL) before dropwise addition of hexafluoro-2-propanol (9 mL, 85.50 mmol, 5 eq.). The orange mixture was stirring at room temperature in dark for 3h before checked by TLC. The solvent was removed under reduced pressure before neutralization by saturated sodium bicarbonate (50 mL) and extracted with ethyl acetate (3×50 mL). The organic phase was washed with brine and dried (Na_2SO_4). The product was purified by flash column chromatography (20% ethyl acetate in hexane) to give the title product as a brown solid (678 mg, 27%); R_f = 0.68 (50% ethyl acetate in hexane); δ_H (400 MHz, DMSO-d_6) 10.69 (s, 1H, N**H** from indole), 7.22 (d, J = 8.7 Hz, 1H, indole), 7.19 (d, J = 2.4 Hz, 1H, indole), 6.90 (d, J = 2.4, 1H, indole), 6.74 (d, J = 2.4 Hz, 1H, indole), 6.70 (dd, J = 2.5, 8.7 Hz, 1H, aromatic region of indoline), 6.56 (d, J = 2.6, 8.3 Hz, 1H, aromatic region of indoline), 6.48 (d, J = 8.3 Hz, 1H, aromatic region of indoline), 5.47 (d, J = 2.5 Hz, 1H, N**H** from indoline), 5.03 (td, J = 8.6, 8.5, 2.6 Hz, 1H, C**H**-indole), 3.65 (s, 6H, C$\mathbf{H}_3$ from methoxy), 3.33 (dd, J = 15.5, 8.0 Hz, 1H, C$\mathbf{H}_2$ from indoline), 2.94 (dd, J = 15.5, 8.0 Hz, 1H, C$\mathbf{H}_2$ from indoline); δ_C (100 MHz, DMSO-d_6) 152.8, 152.0, 146.1, 131.9, 129.9, 125.9, 122.7, 118.2, 112.1, 112.0, 111.2, 111.1, 108.5, 101.2, 56.2, 55.5, 55.2, 37.6; m.p. 163-169 °C [lit.[48], 169-170 °C]; υ_{max} /cm^{-1} (FTIR) 3318 (N-H stretching, m), 2918 (C-H stretching, m, aromatic), 1465 (C-H bending, s, methyl); [MS ES+], calculated 295.1 $[M+H]^+$, found 295.1 $[M+H]^+$.

5-Hydroxy-3-(5-hydroxyindolin-2-yl)-1H-indole



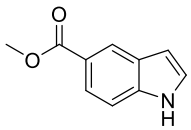
5-HydroxyIndole (2.28 g, 17.1 mmol, 1.0 eq.) and camphor-sulfonic acid (2.18 g, 9.40 mmol, 0.55 eq.) were dissolved in chloroform (50 mL) before dropwise addition of hexafluoro-2-propanol (9 mL, 85.5 mmol, 5 eq.). Pink precipitate was formed during the reaction. The suspension was stirring at room temperature for 3h in dark before checked by TLC. The solvent was removed under reduced pressure. After neutralization with saturated sodium bicarbonate (50 mL), the crude product was extracted with ethyl acetate (3×300 mL) and dried (Na_2SO_4). After the removal of solvent under reduced pressure, the resulting pink solid was recrystallized (ethyl acetate / methanol) at 60 °C to give the title product as a pale pink powder (1.23 g, 54%); R_f = 0.13 (50% ethyl acetate in hexane); δ_H (400 MHz, DMSO-d_6) 10.51 (s, 1H, N**H** from indole), 8.55 (s, 1H, O**H**), 8.39 (s, 1H, O**H**), 7.17-7.04 (m, 2H, indole), 6.87 (d, J = 2.3 Hz, 1H, indole), 6.58 (dd, J = 8.6, 2.3 Hz, 1H, indole), 6.53 (t, J =1.4 Hz, 1H, aromatic region of indoline), 5.22 (s, 1H, N**H** from indoline), 4.94 (t, J = 9.1 Hz, 1H, C**H**-indole), 3.19 (dd, J = 16.5, 9.0 Hz, 1H, C$\mathbf{H}_2$ from indoline), 2.51 (dd, J = 16.5, 9.6 Hz, 1H, C$\mathbf{H}_2$ from indoline); δ_C (100 MHz, DMSO-d_6) 149.9, 149.4, 144.5, 131.3, 129.8, 126.4, 122.5, 117.1, 112.9, 112.1, 111.7, 111.3, 108.9, 103.4, 56.5, 37.7; m.p. 189-192 °C; υ_{max} /cm^{-1} (FTIR) 3298 (N-H stretching, m), 2907 (C-H stretching, m, aromatic); [MS ES+] , calculated 267.1134, found 267.1139 $[M+H]^+$, Δ = 1.9 ppm.

3-(5-Carboxyindolin-2-yl)-1H-indole-5-carboxylic acid



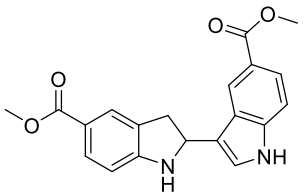
Indole-5-carboxylic acid (2.76 g, 17.1 mmol, 1.0 eq.) and camphor-sulfonic acid (2.18 g, 9.40 mmol, 0.55 eq.) were dissolved in chloroform (50 mL) before dropwise addition of hexafluoro-2-propanol (9 mL, 85.50 mmol, 5 eq.). 5 eq. more hexafluoro-2-propanol was added into mixture to dissolve the starting material. The dark brown mixture was stirring at room temperature for 3h in dark before checked by TLC. The solvent was removed under reduced pressure. After washing with deionized water (3×30 mL), the crude product was extracted with ethyl acetate (3×50 mL) and dried (Na_2SO_4). After the removal of solvent under reduced pressure, the resulting brown solid was purified by flash chromatography (40 - 80% ethyl acetate in hexane with 0.1% formic acid) to give the title product as a pale brown solid (512 mg, 19%); R_f = 0.21 (80% ethyl acetate in hexane); δ_H (400 MHz, DMSO-d_6) 12.32 (bs, 2H, COO**H**), 11.37 – 11.21 (s, 1H, N**H** from indole), 8.22 (d, J = 1.6 Hz, 1H indole), 7.76 – 7.68 (m, 1H, indole), 7.66 – 7.57 (m, 2H, indole), 7.42 (d, J = 8.5 Hz, 1H, aromatic region of indoline), 7.38 (d, J = 2.3 Hz, 1H, aromatic region of indoline), 6.86 (d, J = 1.7 Hz, 1H, aromatic region of indoline), 6.51 (d, J = 8.2 Hz, 1H, NH), 5.29 (t, J = 9.2 Hz, 1H, C**H**-indole), 3.45 (dd, J = 16.0, 9.6 Hz, 1H, C$\mathbf{H}_2$ from indoline), 3.04 (dd, J = 15.9, 8.4 Hz, 1H, C$\mathbf{H}_2$ from indoline); m.p. 203-204 °C.

Methyl 1H-indole-5-carboxylate



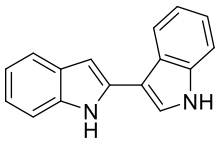
As described in Kong *et al*[26], 5-Indole carboxylic acid (5.03 mg, 31 mmol, 1 eqand sodium bicarbonate (10.4 g, 124 mmol, 4 eq.) were dissolved in dry Dimethylformamide (35 mL) before addition of Iodomethane (12.6 mL, 201 mmol, 6 eq.). The orange mixture was stirring at room temperature for 69h before checked by TLC. The mixture was diluted with water (50 mL) and extracted with ethyl acetate (3×50 mL). The organic phase was washed with saturate sodium bicarbonate (100 mL) and brine (100 mL). The liquid was dried (Na_2SO_4) before removal of solvent under reduced pressure. The resulting solid was brought to high vacuum for 5h and gave orange solid (5.299 g, 98%); R_f = 0.35 (20% ethyl acetate in hexane); δ_H (400 MHz, DMSO-d_6) 11.48 (s, 1H, N**H**), 8.26 (d, J = 1.6 Hz, 1H, indole), 7.72 (dd, J = 8.6, 1.7 Hz, 1H, indole), 7.55 – 7.41 (m, 2H, indole), 6.59 (ddd, J = 3.1, 1.8, 0.8 Hz, 1H, indole), 3.83 (s, 3H, OMe); δ_C (100 MHz, DMSO-d_6) 167.3, 138.5, 127.2, 122.7, 121.9, 120.3, 111.3, 102.6, 51.6; m.p. 118-120 °C [lit.[49], 118-119 °C (propan-2-ol/hexane)]; υ_{max} /cm^{-1} (FTIR) 3318 (N-H stretching, s), 2952 (C-H stretching, m, aromatic), 1694 (C=O stretching, s), 1435 (C-H bending, s, methyl); [MS ES+], calculated 176.0712 $[M+H]^+$, found 176.0715 $[M+H]^+$, Δ = 1.7 ppm.

3-(5-Carboxyindolin-2-yl)-1H-indole-5-carboxylic acid



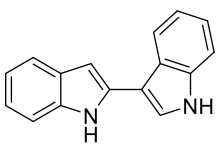
1H-Indole-5-carboxylate (462 mg, 2.64 mmol, 1.0 eq.) and camphor-sulfonic acid (337 mg, 1.45 mmol, 0.55 eq.) were dissolved in chloroform (10 mL) before dropwise addition of hexafluoro-2-propanol (0.89 mL, 13.2 mmol, 5 eq.). 5 eq. more hexafluoro-2-propanol was added into mixture to dissolve the starting material. The dark brown mixture was stirring at room temperature for 3h in dark before checked by TLC. The solvent was removed under reduced pressure. After washing with saturated sodium bicarbonate (20 mL), the crude product was extracted with ethyl acetate (3×20 mL) and dried (Na_2SO_4). After the removal of solvent under reduced pressure, the resulting brown solid was purified by flash chromatography (10 - 30% ethyl acetate in hexane) and gave pale brown solid (162 mg, 35%); R_f = 0.44 (50% ethyl acetate in hexane); δ_H (400 MHz, DMSO-d_6) 11.36 (s, 1H, N**H**), 8.17 (d, J = 1.6 Hz, 1H, indole), 7.77 – 7.67 (m, 1H, indole), 7.64 (d, J = 1.6 Hz, 1H, aromatic region of indoline), 7.51 – 7.37 (m, 2H, aromatic region of indoline), 6.96 (s, 1H), 6.54 (d, J = 8.2 Hz, 1H, C**H**-indole), 5.46 – 5.23 (m, 1H, N**H**), 3.79 (s, 3H, COO**Me**), 3.76 (s, 3H, COO**Me**), 3.48 (dd, J = 16.0, 9.5 Hz, 1H, C**H**$_2$ from indoline), 3.05 (dd, J = 16.1, 7.7 Hz, 1H, C**H**$_2$ from indoline); δ_C (100 MHz, DMSO-d_6) 167.2, 166.5, 156.2, 150.1, 139.5, 130.7, 127.9, 125.5, 124.9, 124.2, 122.3, 121.8, 119.2, 117.0, 111.6, 106.3, 55.5, 51.6, 51.2, 36.5; m.p. 105-110 °C; υ_{max} /cm^{-1} (FTIR) 3332 (N-H stretching, m), 2948 (C-H stretching, m, aromatic), 1684 (C=O stretching, s), 1496 (C-H bending, m, methylene), 1431 (C-H bending, s, methyl); [MS ES+], calculated 351.13 $[M+H]^+$, found 351.1345 $[M+H]^+$, 373.1169 $[M+Na]^+$, Δ = 1.1 ppm.

1H,1'H-2,3'-bi-indole Attempt 1



3-(Indolin-2-yl)-1H-indole (BF3-S1) (50 mg, 0.213 mmol, 1.0 eq.) was dissolved in methanol (10 mL) before addition of oct-sulfur (437 mg, 1.70 mmol, 8 eq.), with stirring at room temperature for 3 days. The purple suspension was further stirred overnight before filtration through Celite©. The solvent was removed under reduced pressure and flash column chromatography (20% - 30% ethyl acetate in hexane) to give dark purple solid (16 mg, 34%); R_f = 0.39 (40% ethyl acetate in hexane); δ_H (400 MHz, DMSO-d_6) 11.40 (s, 1H, N**H**), 11.20 (s, 1H, N**H**), 8.05 – 7.96 (m, 1H, indole), 7.87 (d, J = 2.6 Hz, 1H, indole), 7.55 – 7.44 (m, 3H, indole), 7.38 – 7.33 (m, 1H, indole), 7.17 (ddd, J = 9.3, 7.6, 1.3 Hz, 2H, indole), 7.07 – 6.92 (m, 2H, indole), 6.76 (dd, J = 2.0, 0.8 Hz, 1H, indole).

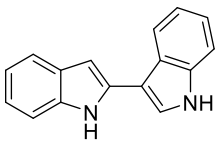
1H,1'H-2,3'-bi-indole Attempt 2



3-(Indolin-2-yl)-1H-indole (BF3-S1) (453 mg, 1.95 mmol, 1.0 eq.) was dissolved in methanol (50 mL) before addition of sulfur (S_8) (excess) and water (5 mL), with stirring at room temperature for 3 days. The purple suspension was filtered through Celite©. The solvent was removed under reduced pressure before extraction by ethyl acetate (3×30 mL) and dried (Na_2SO_4). After the removal of ethyl acetate, the flash column chromatography (10 – 20% ethyl acetate in hexane) gave the title product as a dark purple solid (51 mg, 10%); R_f = 0.39 (40% ethyl acetate in hexane); δ_H (400 MHz, DMSO-d_6) 11.41 (s, 1H, N**H**), 11.22 (s, 1H, N**H**), 8.02 (d, J = 7.5 Hz, 1H, indole), 7.88 (d,

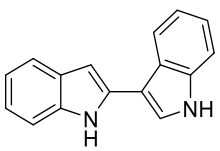
J = 2.6 Hz, 1H, indole), 7.55 – 7.44 (m, 3H, indole), 7.38 – 7.33 (m, 1H, indole), 7.19 (m, 2H, indole), 7.08 – 6.92 (m, 2H, indole), 6.78 (dd, J = 2.2, 0.7 Hz, 1H, indole).

1H,1'H-2,3'-bi-indole Attempt 3



3-(Indolin-2-yl)-1H-indole (BF3-S1) (50.0 mg, 0.213 mmol, 1.0 eq.) was dissolved in methanol (50 mL) before addition of 10% Pd/C (45.0 mg, 0.04 mmol, 0.2 eq) and ammonium formate (304 mg, 2.13 mmol, 10 eq.), with stirring at 65 °C for 4 days. The dark orange suspension was filtered through Celite©. The solvent was removed under reduced pressure before flash column chromatography (10 – 20% ethyl acetate in hexane) gave the title product as a dark purple solid (less than 22 mg, 45%); R_f = 0.39 (40% ethyl acetate in hexane); δ_H (400 MHz, DMSO-d_6) 11.41 (s, 1H, NH), 11.21 (s, 1H, NH), 8.01 (d, J = 7.5 Hz, 1H, indole), 7.87 (d, J = 2.6 Hz, 1H, indole), 7.55 – 7.44 (m, 3H, indole), 7.38 – 7.33 (m, 1H, indole), 7.18 (m, 2H, indole), 7.08 – 6.92 (m, 2H, indole), 6.77 (dd, J = 2.2, 0.7 Hz, 1H, indole).

1H,1'H-2,3'-bi-indole Attempt 4



3-(Indolin-2-yl)-1H-indole (BF3-S1) (200 mg, 0.852 mmol, 1.0 eq.) was dissolved in methanol (50 mL) before addition of 10% Pd/C (45.0 mg, 0.120 mmol, 0.2 eq) and ammonium formate (1.22 g, 8.52 mmol, 10 eq.), with stirring at 65 °C for 4 days. The dark orange suspension was filtered through Celite©. The solvent was removed under reduced pressure before flash column chromatography (10 – 20% ethyl acetate in hexane) gave the title product as a pale brown solid (101 mg, 50%); R_f = 0.39 (40%

ethyl acetate in hexane); δ_H (400 MHz, DMSO-d_6) 11.41 (s, 1H, NH), 11.21 (s, 1H, NH), 8.01 (d, J = 7.5 Hz, 1H, indole), 7.87 (d, J = 2.7 Hz, 1H, indole), 7.55 – 7.44 (m, 3H, indole), 7.38 – 7.33 (m, 1H, indole), 7.18 (m, 2H, indole), 7.09 – 6.90 (m, 2H, indole), 6.77 (dd, J = 2.2, 0.7 Hz, 1H, indole). δ_C (100 MHz, DMSO-d_6) 136.7, 136.0, 134.1, 129.2, 124.7, 123.2, 121.8, 120.3, 119.8, 119.6, 119.1, 118.8, 112.0, 110.4, 108.5, 96.8.; υ_{max} /cm^{-1} (FTIR) 3391 (N-H stretching, m), 2922 (C-H stretching, m, aromatic); m.p. 200-205 ^{o}C [lit.[50], 198-200 ^{o}C]; [MS ES+], calculated 232.1079 $[M+H]^+$, found 232.1086 $[M+H]^+$, Δ = 3.0 ppm.

Chapter 6. Reference List

1 M. Dino and G. Hinrich, *Curr. Opin. Biol.*, 1998, 384–391.

2 J. B. C. Papers, M. Doi, P. M. Matias, P. Donner, R. Coelho, M. Thomaz, C. Peixoto, S. Macedo, N. Otto, S. Joschko, P. Scholz, A. Wegg, S. Ba, U. Egner and M. Arme, *J. Biol. Chem.*, 2000, **275**, 26164–26171.

3 E. P. Gelmann, *J. Clin. Oncol.*, 2002, **20**, 3001–3015.

4 D. N. Lavery and C. L. Bevan, *J. Biomed. Biotechnol.*, 2010, **2011**, 10–12.

5 J. S. Sack, K. F. Kish, C. Wang, R. M. Attar, S. E. Kiefer, Y. An, G. Y. Wu, J. E. Scheffler, M. E. Salvati, S. R. Krystek, R. Weinmann and H. M. Einspahr, *PNAS*, 2001, **98**, 4905–4909.

6 Q. Yang, K. M. Fung, W. V. Day, B. P. Kropp and H. K. Lin, *Cancer Cell Int.*, 2005, **5**, 1–10.

7 L. Ni, C.-S. Yang, D. Gioeli, H. Frierson, D. O. Toft and B. M. Paschal, *Mol. Cell. Biol.*, 2010, **30**, 1243–1253.

8 Y. Chen, C. L. Sawyers and H. I. Scher, *Curr. Opin. Pharmacol.*, 2008, **8**, 440–448.

9 M. E. Tan, J. Li, H. E. Xu, K. Melcher and E. L. Yong, *Acta Pharmacol. Sin.*, 2015, **36**, 3–23.

10 M. Tang, Y. Wu, X. Xu, F. Pan and R. Xu, *Am. J. Transl. Res.*, 2016, **8**, 5141–5150.

11 E. Biron and F. Bédard, *J. Steroid Biochem. Mol. Biol.*, 2016, **161**, 36–44.

12 A. A. Parent, J. R. Gunther and J. A. Katzenellenbogen, *J. Med. Chem.*, 2008, **51**, 6512–6530.

13 J. Trapman, A. O. Brinkmann, A. C. W. Pike, A. C. J. Ziel-van der Made, H. A. G. M. van der Korput, C. A. Berrevoets, J. van Tol, R. Hersmus, C. S. Verma and H. J. Dubbink, *Mol. Endocrinol.*, 2004, **18**, 2132–2150.

14 H.-J. Ting, Y.-C. Kuo, A.-C. Lin, W.-G. Wu, J.-S. Liu, C.-C. Lin, S.-T. Pang, W.-L. Ma, Y.-H. Chang, T.-W. Lin, C.-L. Hsu and L.-Y. Lee, *Oncotarget*, 2017, **8**, 69508–69519.

15 E. Hur, S. J. Pfaff, E. Sturgis Payne, H. Grøn, B. M. Buehrer and R. J. Fletterick, *PLoS Biol.*, 2004, **2**, 1303–1312.

16 N. M. Badders, A. Korff, H. C. Miranda, P. K. Vuppala, R. B. Smith, B. J. Winborn, E. R. Quemin, B. L. Sopher, J. Dearman, J. Messing, N. C. Kim, J. Moore, B. D. Freibaum, A. P. Kanagaraj, B. Fan, H. Tillman, P. C. Chen, Y. Wang, B. B. Freeman, Y. Li, H. J. Kim, A. R. La Spada and J. P. Taylor, *Nat. Med.*, 2018, **24**, 427–437.

17 J. R. Gunther, A. A. Parent and J. A. Katzenellenbogen, *ACS Chem. Biol.*, 2009, **4**, 435–440.

18 V. Buzón, L. R. Carbó, S. B. Estruch, R. J. Fletterick and E. Estébanez-Perpiñ, *Mol. Cell. Endocrinol.*, 2012, **348**, 394–402.

19 J. T. De Leon, A. Iwai, C. Feau, Y. Garcia, H. A. Balsiger, C. L. Storer, R. M. Suro, K. M. Garza, S. Lee, Y. Sang Kim, Y. Chen, Y.-M. Ning, D. L. Riggs, R. J. Fletterick, R. K. Guy, J. B. Trepel, L. M. Neckers and M. B. Cox, *Proc. Natl. Acad. Sci.*, 2011, **108**, 11878–11883.

20 N. A. Lack, P. Axerio-Cilies, P. Tavassoli, F. Q. Han, K. H. Chan, C. Feau, E. LeBlanc,

E. T. Guns, R. K. Guy, P. S. Rennie and A. Cherkasov, *J. Med. Chem.*, 2011, **54**, 8563–8573.

21 R. S. N. Munuganti, E. Leblanc, P. Axerio-Cilies, C. Labriere, K. Frewin, K. Singh, M. D. H. Hassona, N. A. Lack, H. Li, F. Ban, E. Tomlinson Guns, R. Young, P. S. Rennie and A. Cherkasov, *J. Med. Chem.*, 2013, **56**, 1136–1148.

22 R. S. N. Munuganti, M. D. H. Hassona, E. Leblanc, K. Frewin, K. Singh, D. Ma, F. Ban, M. Hsing, H. Adomat, N. Lallous, C. Andre, J. P. S. Jonadass, A. Zoubeidi, R. N. Young, E. Tomlinson Guns, P. S. Rennie and A. Cherkasov, *Chem. Biol.*, 2014, **21**, 1476–1485.

23 C. Tran, *Development and synthesis of five-residue α-helix protein mimetics, Imperial College London Postdoc Report*, 2017.

24 Y. Liu, C. L. Bevan and A. C. Spivey, *Towards the Development of an Assay for Androgen Receptor Antagonists, Imperial College London MRes Manuscript*, 2017.

25 I. Colomer, A. E. R. Chamberlain, M. B. Haughey and T. J. Donohoe, *Nat. Rev. Chem.*, 2017, **1**, 1–12.

26 A. Kong, X. Han and X. Lu, *Org. Lett.*, 2006, **8**, 1339–1342.

27 P. Melnyk, B. Legrand, J. Gasche, P. Ducrot and C. Thal, *Tetrahedron*, 1995, **51**, 1941–1952.

28 X. Dupeyre, G.; Lemoine, P.; Ainseba, N.; Michel, S.; Cachet, *Orangic Biomol. Chem.*, 2011, **9**, 7780–7790.

29 Y. Ren, H. Shui, C. Peng, H. Liu and Y. Hu, *Fluid Phase Equilib.*, 2011, **312**, 31–36.

30 T. Kiguchi, N. Kuninobu, Y. Takahashi, Y. Yoshida, T. Naito and I. Ninomiya, *Synthesis (Stuttg).*, 1989, **10**, 778–781.

31 G. Xiao, D. Jiang, P. Thomas, M. D. Benson, K. Guan, G. Karsenty and R. T. Franceschi, *J. Biol. Chem.*, 2000, **275**, 4453–4459.

32 Z. Cheng, D. Garvin, A. Paguio, P. Stecha, K. Wood and F. Fan, *Curr. Chem. Genomics*, 2012, **4**, 84–91.

33 N. Boute, R. Jockers and T. Issad, *Trends Pharmacol. Sci.*, 2002, **23**, 351–354.

34 T. Chen, W. Xie, M. Agler and M. Banks, *Assay Drug Dev. Technol.*, 2003, **1**, 835–842.

35 *LanthaScreen ® TR-FRET AR Coactivator Assay Protocol*, Thermo Fisher Scientific Inc., 2014.

36 T. W. Moore, J. R. Gunther and J. A. Katzenellengbogen, *Methods Mol Biol*, 2015, **1278**, 545–553.

37 *Technical Resource Guide 4th Edition: Fluorescence Polarization*, 2006.

38 A. Rinken, D. Lavogina and S. Kopanchuk, *Trends Pharmacol. Sci.*, 2017, **39**, 187–199.

39 R. M. Jourdain, G. Brooke, C. L. Bevan and A. C. Spivey, *Towards Novel Peptide Inhibitors for the Treatment of Prostate Cancer, Imperial College London MRes Manuscript*, 2013.

40 *PolarScreen™ Nuclear Receptor Competitor Assays - Universal Protocol*, Thermo Fisher Scientific Inc., 2014.

41 B. Vaz, S. Möcklinghoff, S. Folkertsma, S. Lusher, J. De Vlieg and L. Brunsveld, *Chem. Commun.*, 2009, 5377–5379.

42 J. C. Owicki, *J. Biomol. Screen.*, 2000, **5**, 297–306.

43 Selleck.cn, Enzalutamide (MDV3100), https://www.selleck.cn/products/MDV3100.html.

44 S. M. Powell, V. Christiaens, D. Voulgaraki, J. Waxman, F. Claessens and C. L. Bevan, *Endocr. Relat. Cancer*, 2004, **11**, 117–130.

45 A. Millet, D. Dailler, P. Larini and O. Baudoin, *Angew. Chem.*, 2014, **126**, 2716–2720.

46 A. A. Parent, D. H. Ess and J. A. Katzenellenbogen, *J. Org. Chem.*, 2014, **79**, 5448–5462.

47 V. Bocchi and G. Palla, *Tetrahedron*, 1986, **42**, 5019–5024.

48 T. Guo, S. L. Han, Y. C. Liu, Y. Liu and H. M. Liu, *Tetrahedron Lett.*, 2016, **57**, 1097–1099.

49 K. Masafumi, A. Kojima, K. Nakano, A. Miyagishi, T. Noguchi and N. Ohashi, *Chem. Pharm. Bull.*, 1999, **11**, 1538–1548.

50 Y. L. An, Z. H. Yang, H. H. Zhang and S. Y. Zhao, *Org. Lett.*, 2016, **18**, 152–155.

Appendix

List of Supporting Information (SI), Figures and Tables)

SI Figures

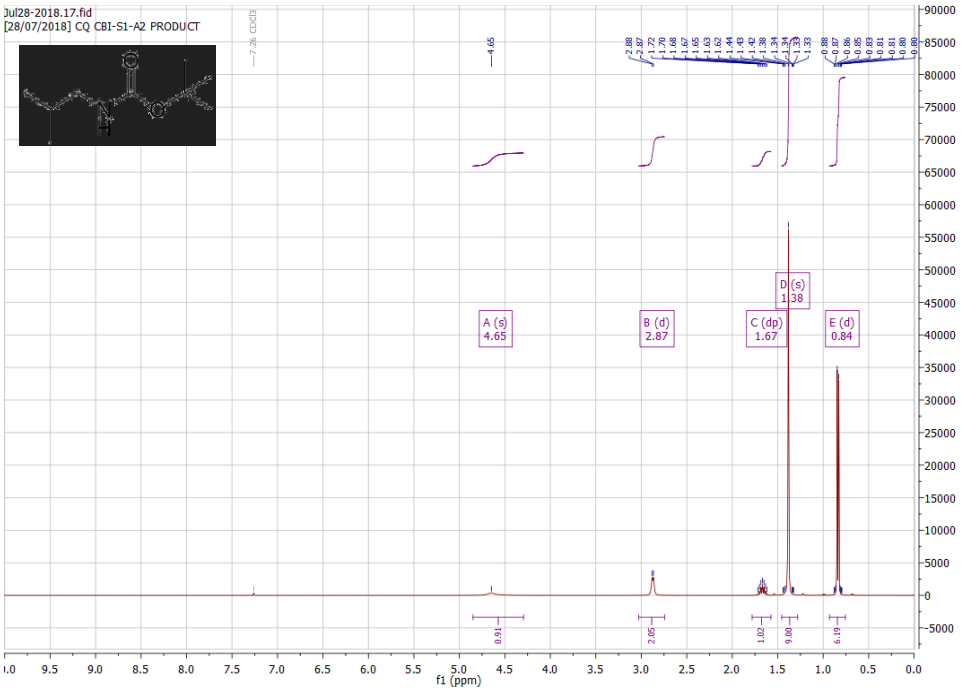
SI Figure 1.....112
SI Figure 2......112
SI Figure 3......113
SI Figure 4......113
SI Figure 5......114
SI Figure 6......114
SI Figure 7......115
SI Figure 8......115
SI Figure 9......116
SI Figure 10......116
SI Figure 11......117
SI Figure 12......117
SI Figure 13......118
SI Figure 14......118
SI Figure 15......119
SI Figure 16......119
SI Figure 17......120
SI Figure 18......121
SI Figure 19......121
SI Figure 20......122
SI Figure 21......123
SI Figure 22......123

SI Figure 23.....124
SI Figure 24.....125
SI Figure 25.....125
SI Figure 26.....126
SI Figure 27.....127
SI Figure 28.....127
SI Figure 29.....128
SI Figure 30.....129
SI Figure 31.....130
SI Figure 32.....130
SI Figure 33.....131
SI Figure 34.....132
SI Figure 35.....132
SI Figure 36. 133
SI Figure 37.....134
SI Figure 38.....134
SI Figure 39.....135

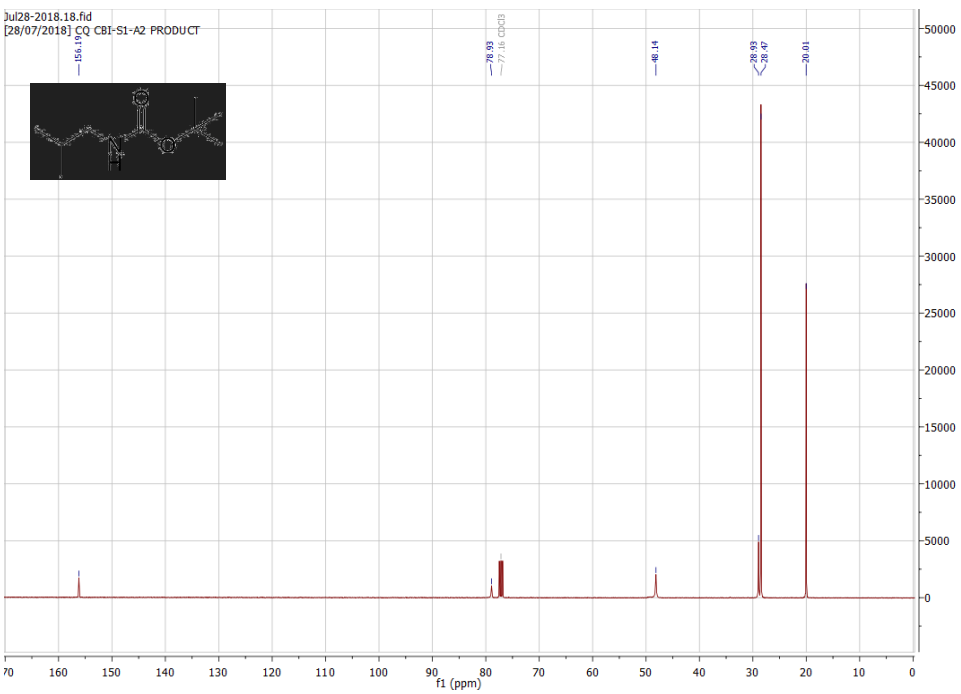
SI Tables

SI Table 1. Enz Serial Dilution Stock concentration (Series A & Series B) (36 in total).... 136
SI Table 2. Compound 1 Stock Concentration (20 in total) 137
SI Table 3. Compound 3 Serial Dilution Stock concentration (20 in total) 138
SI Table 4. T Serial Dilution Stock concentration (22 in total).... 139
SI Table 5. CT Serial Dilution Stock concentration (24 in total).... 140

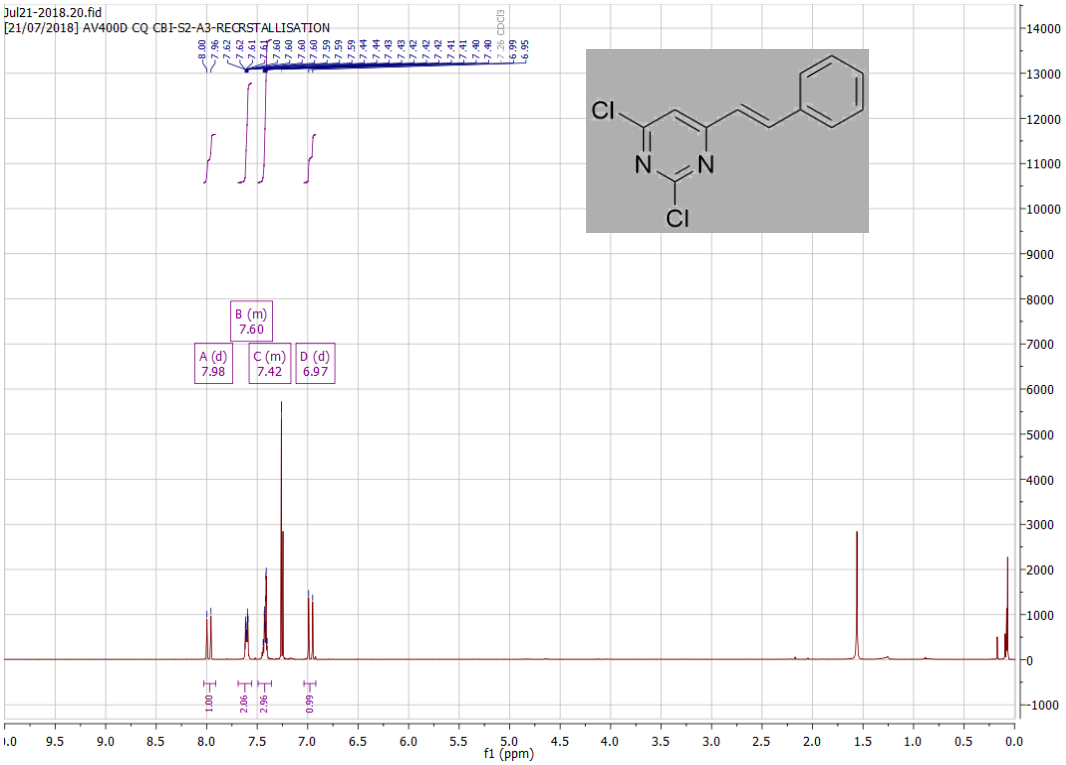
SI Figures and Tables



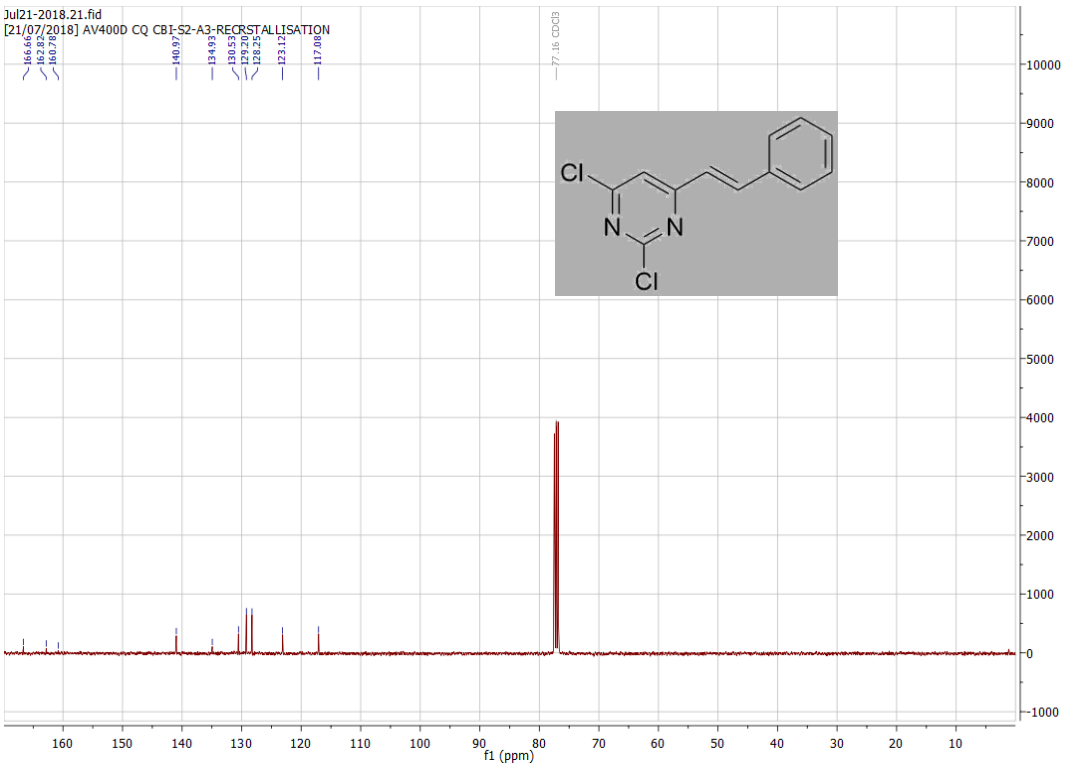
SI Figure 1



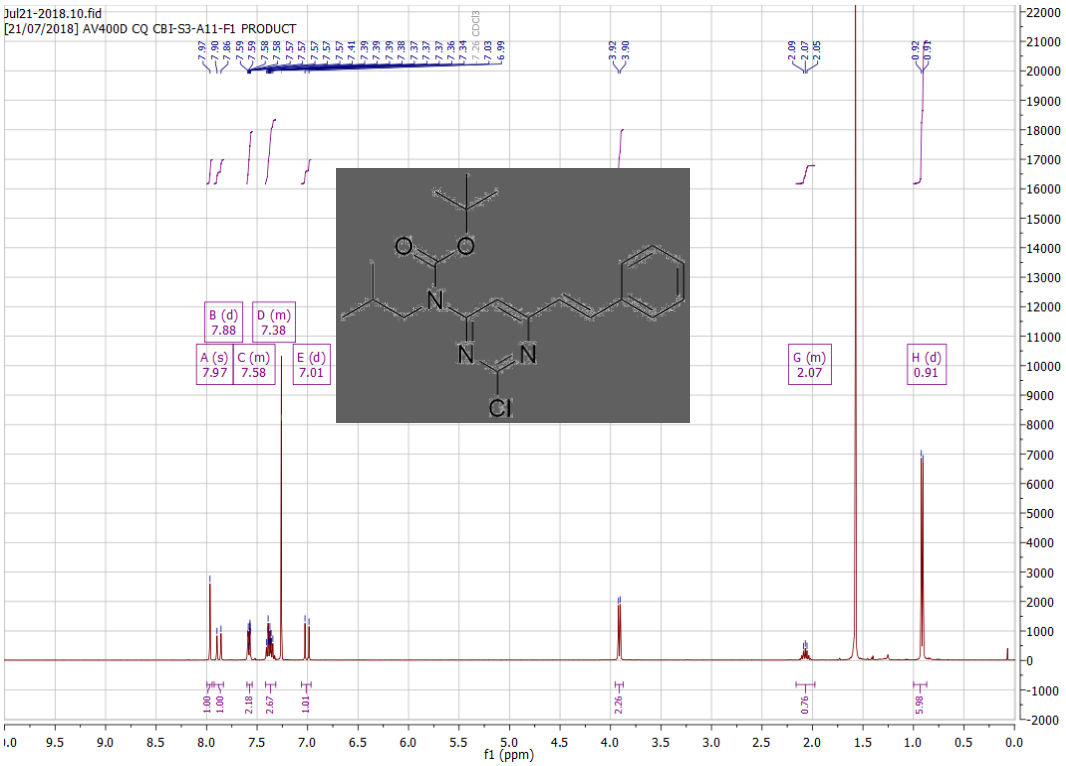
SI Figure 2.



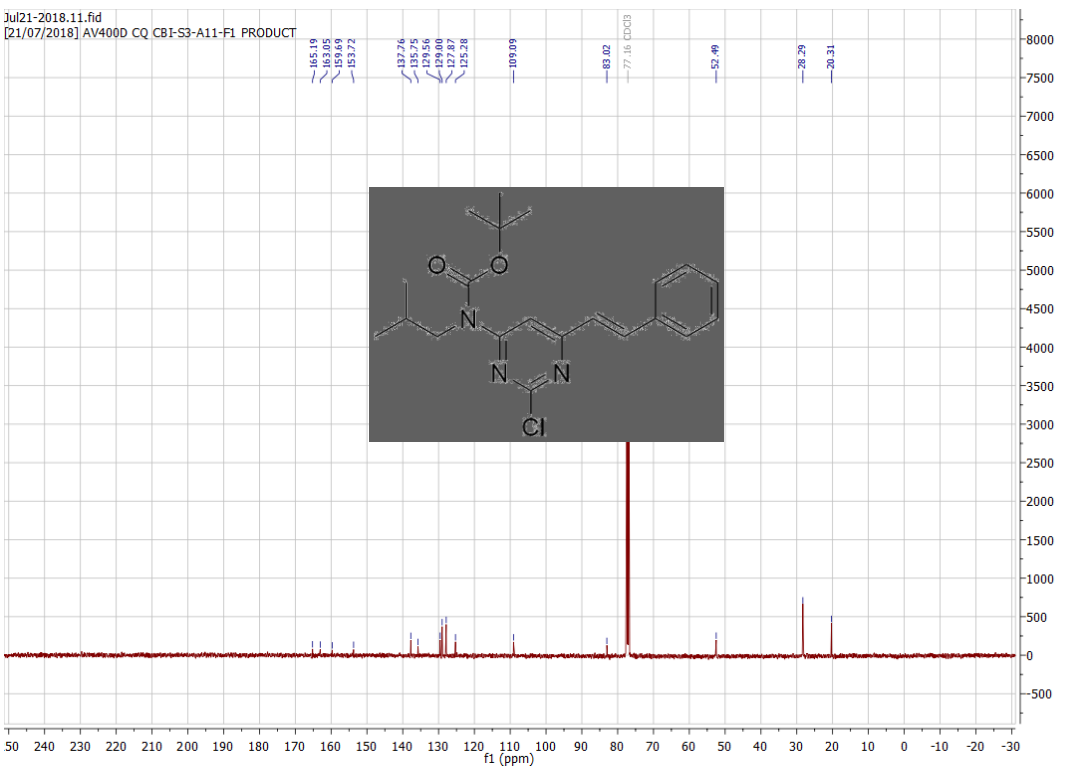
SI Figure 3.



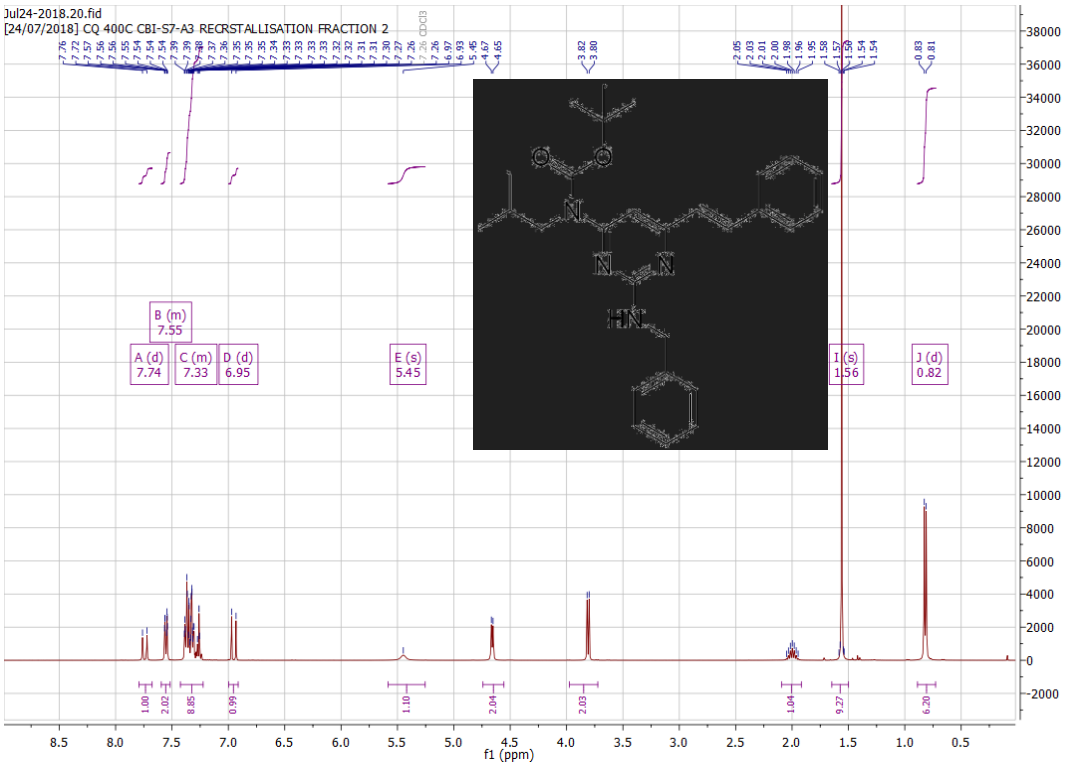
SI Figure 4.



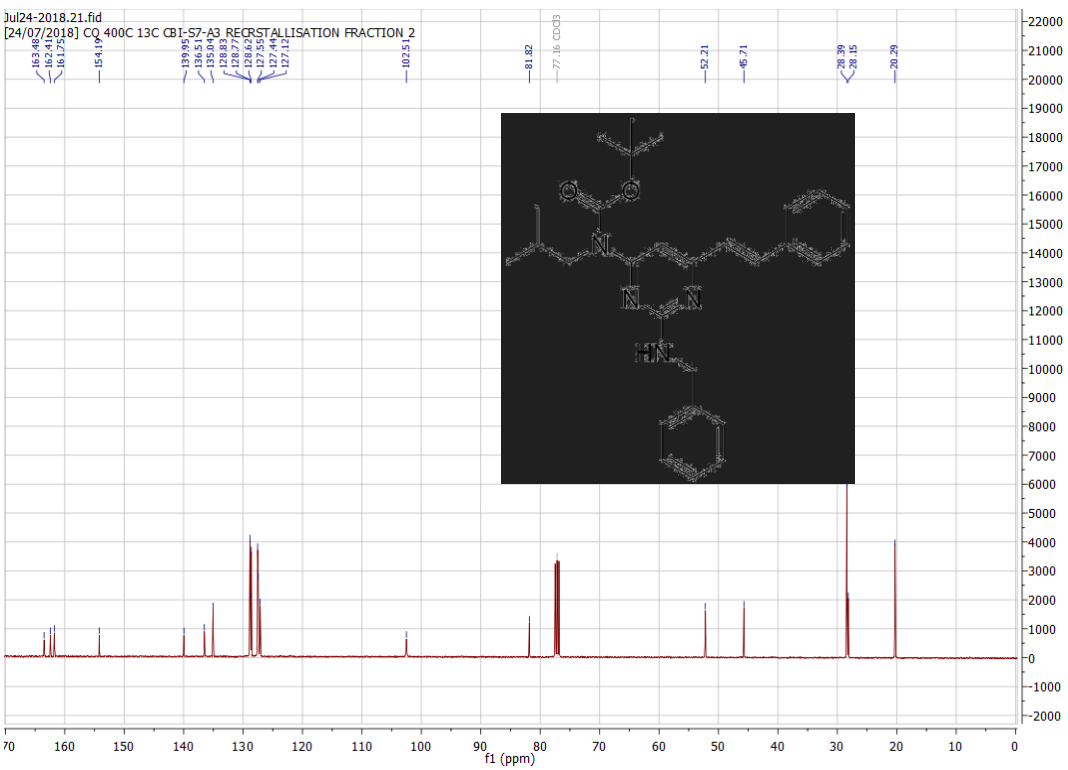
SI Figure 5.



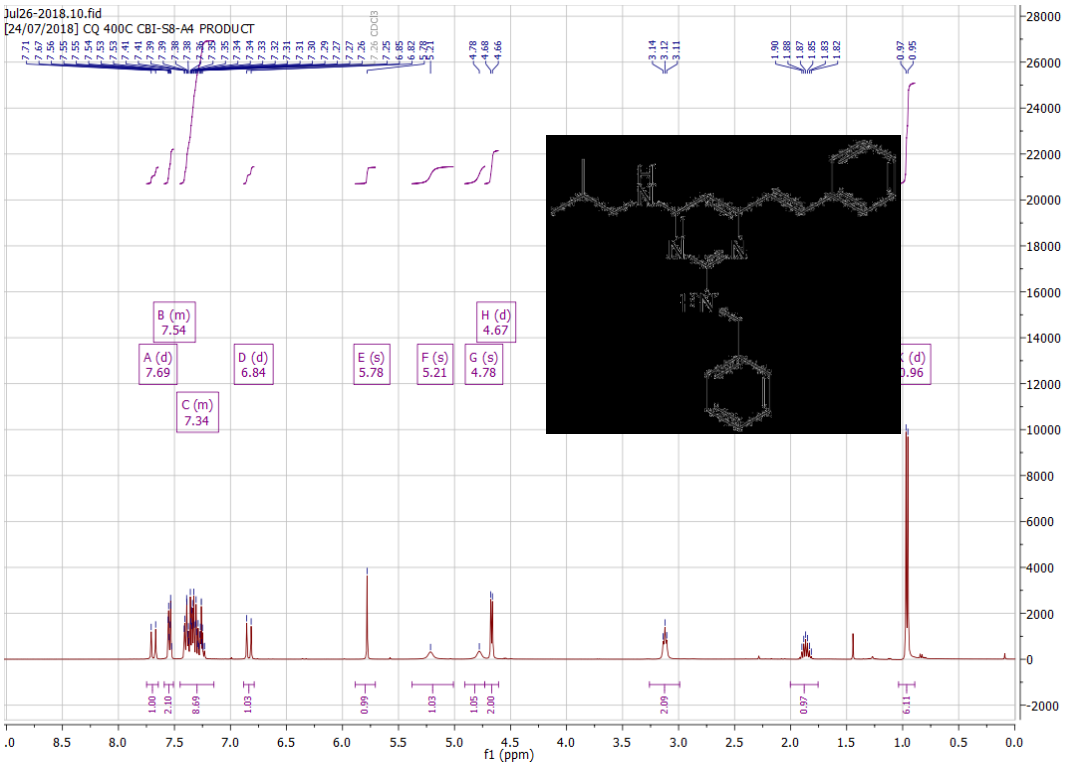
SI Figure 6.



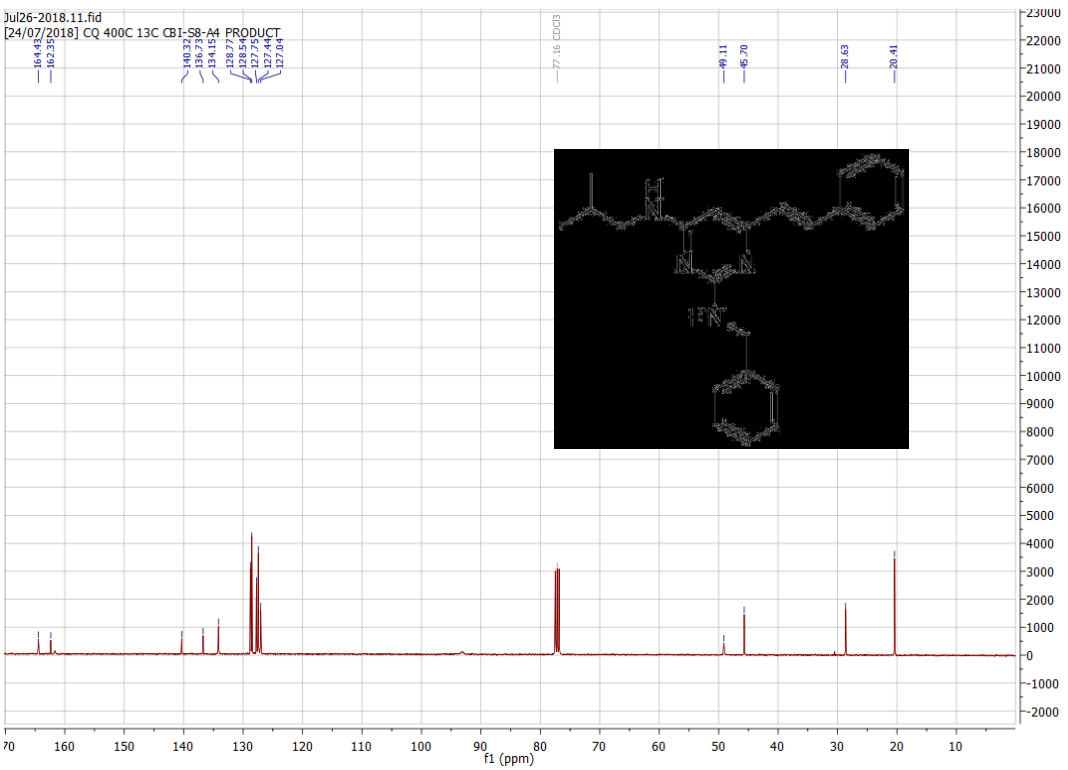
SI Figure 7.



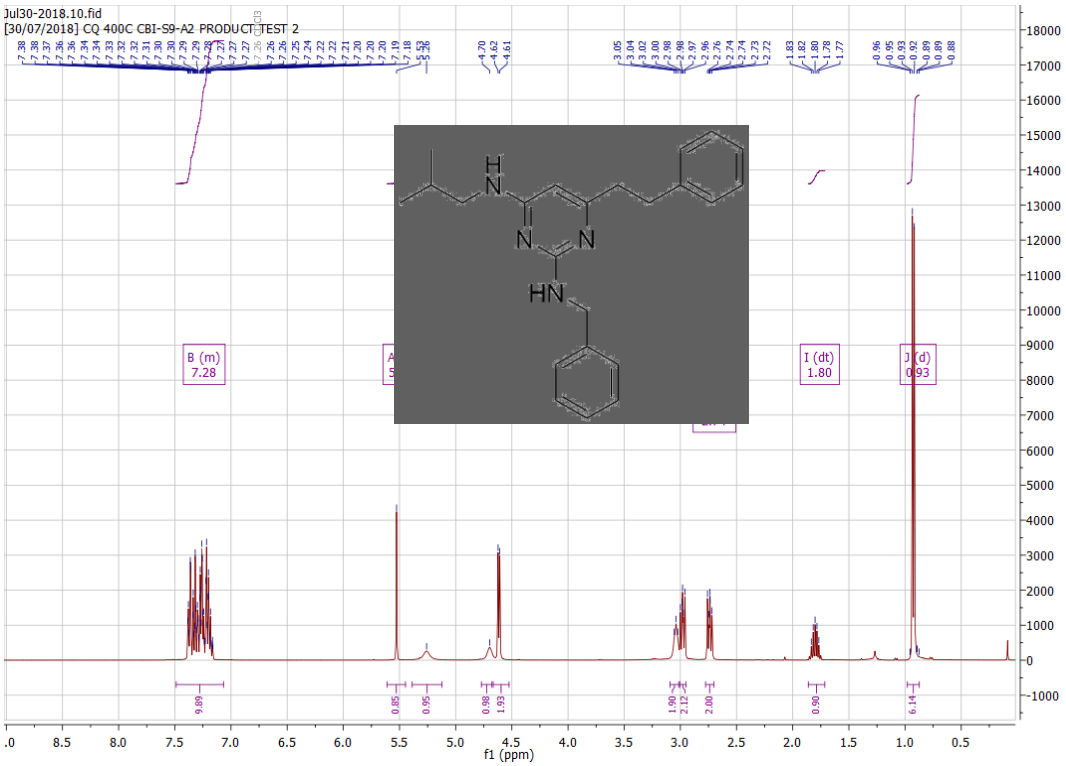
SI Figure 8.



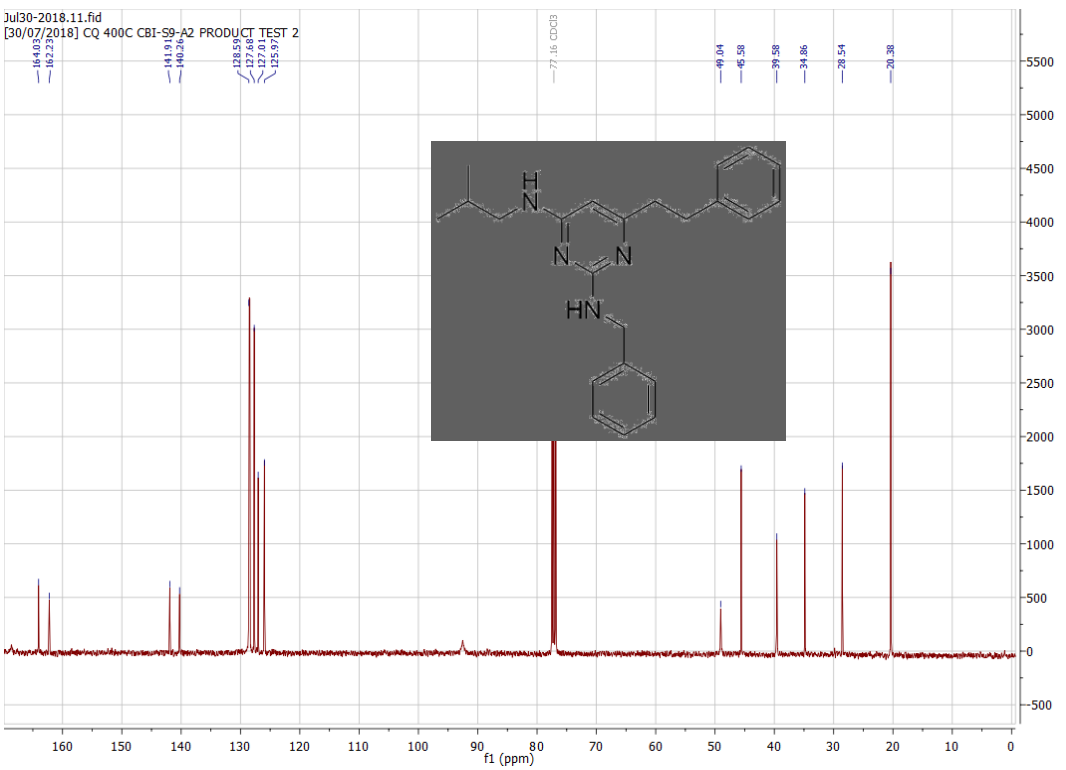
SI Figure 9.



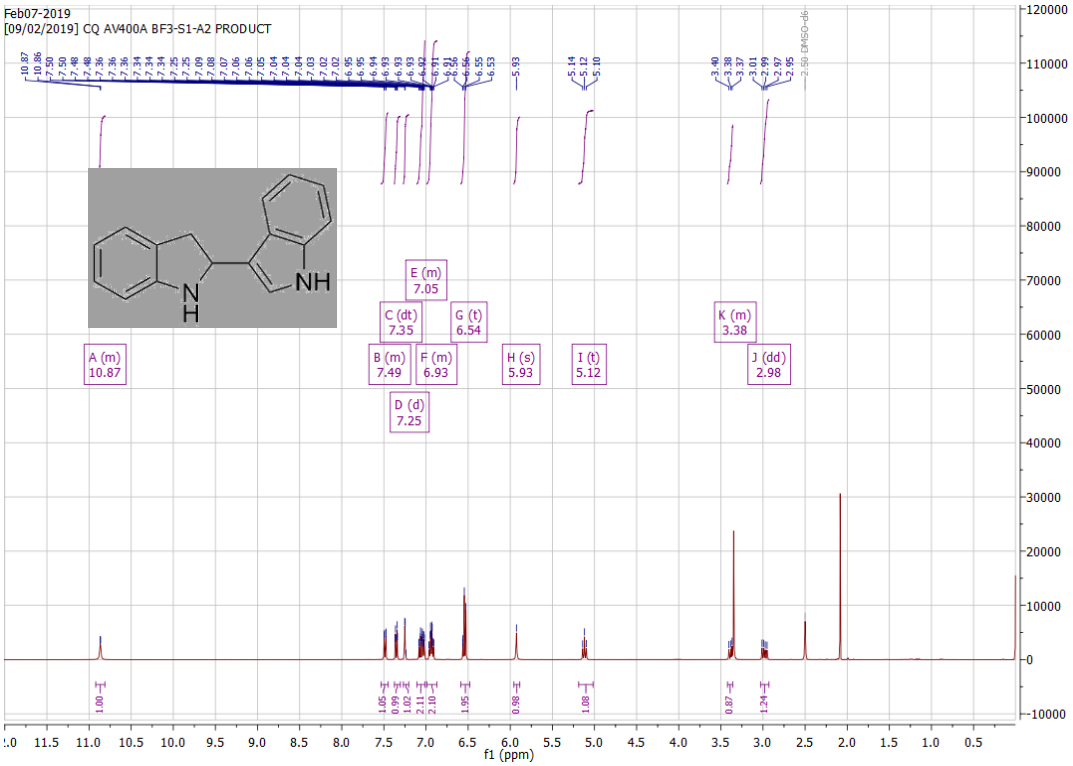
SI Figure 10.



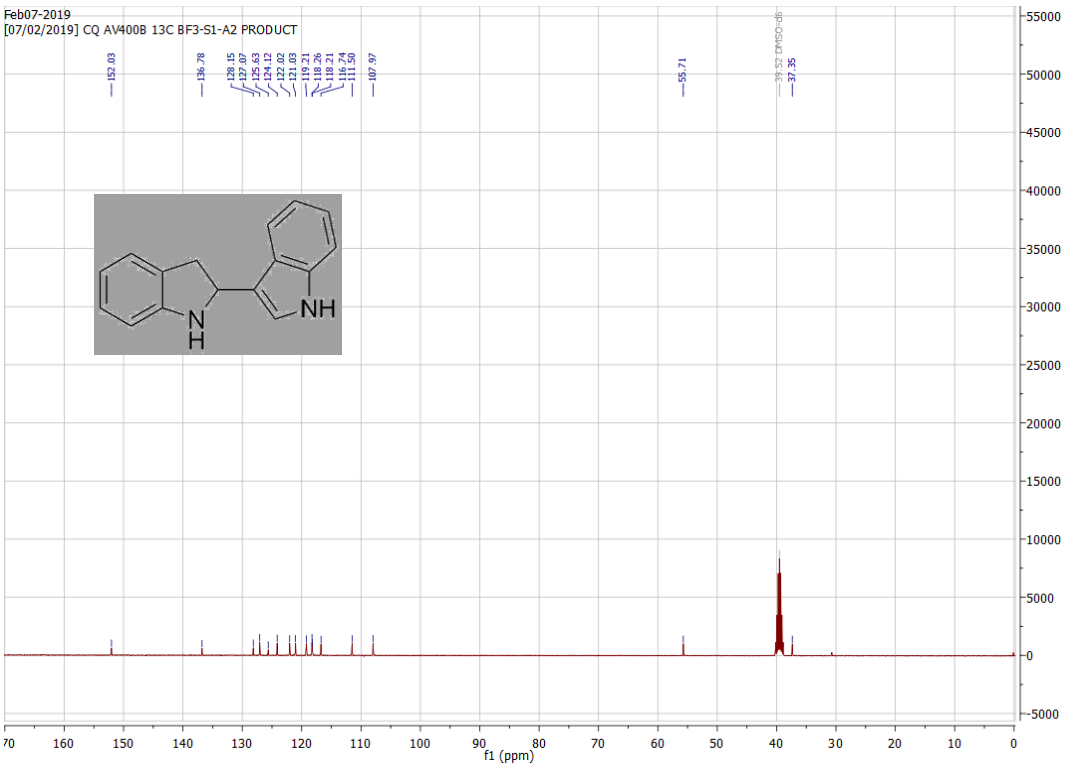
SI Figure 11.



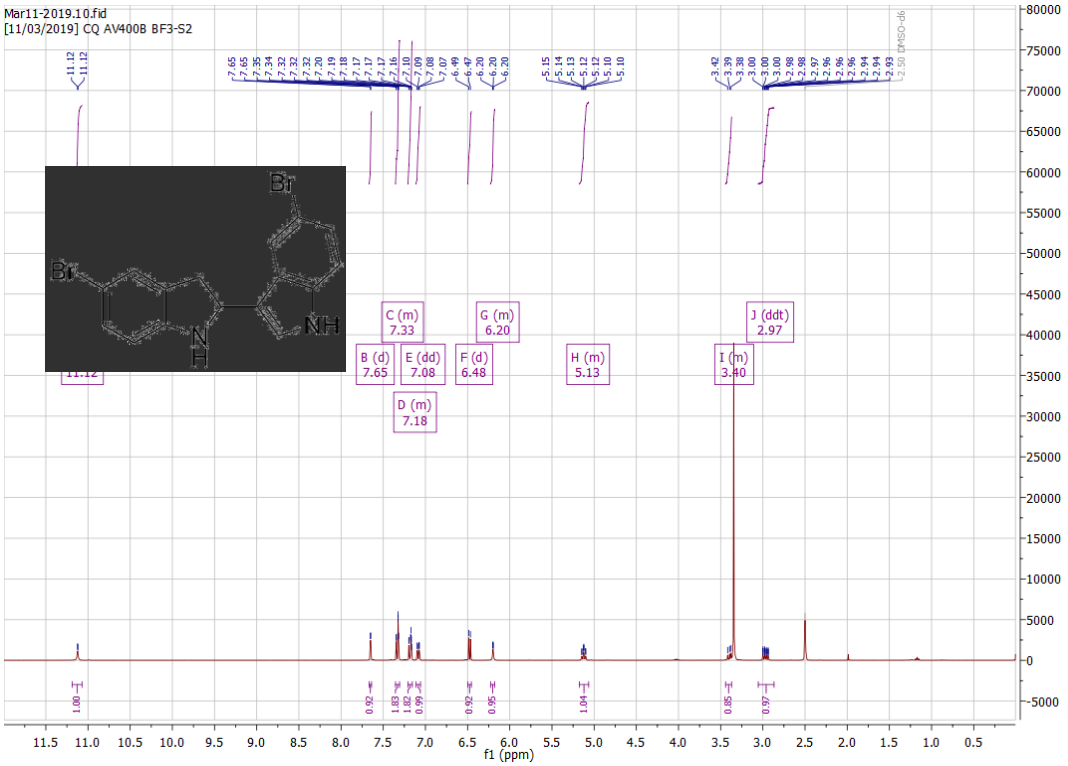
SI Figure 12.



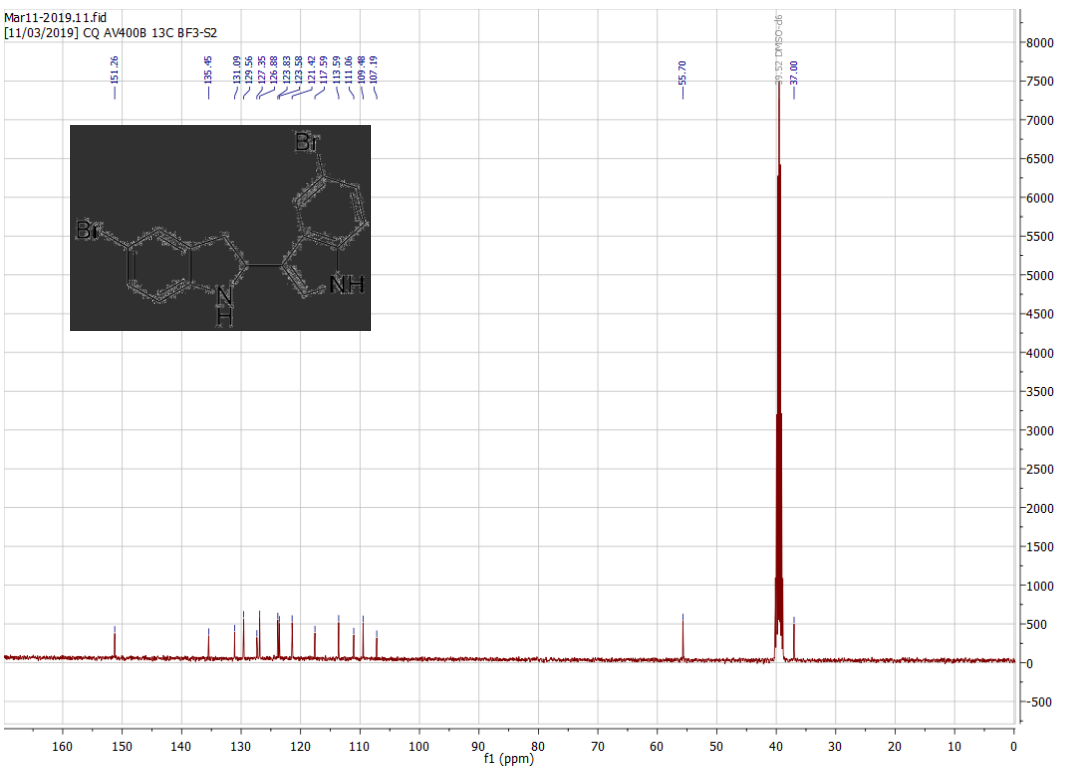
SI Figure 13.



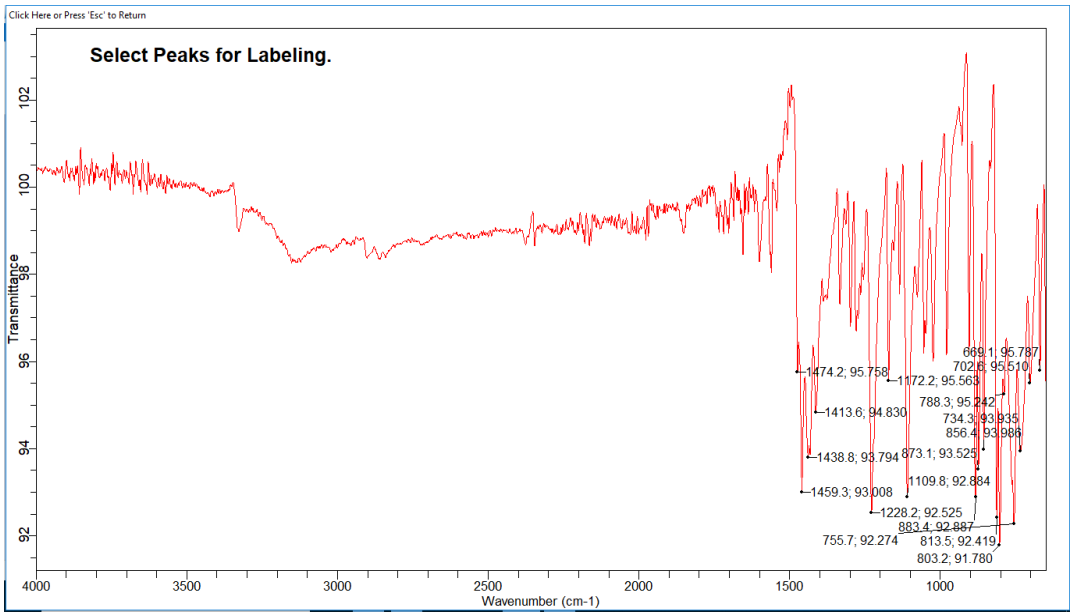
SI Figure 14.



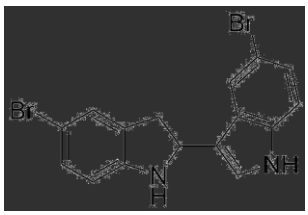
SI Figure 15.

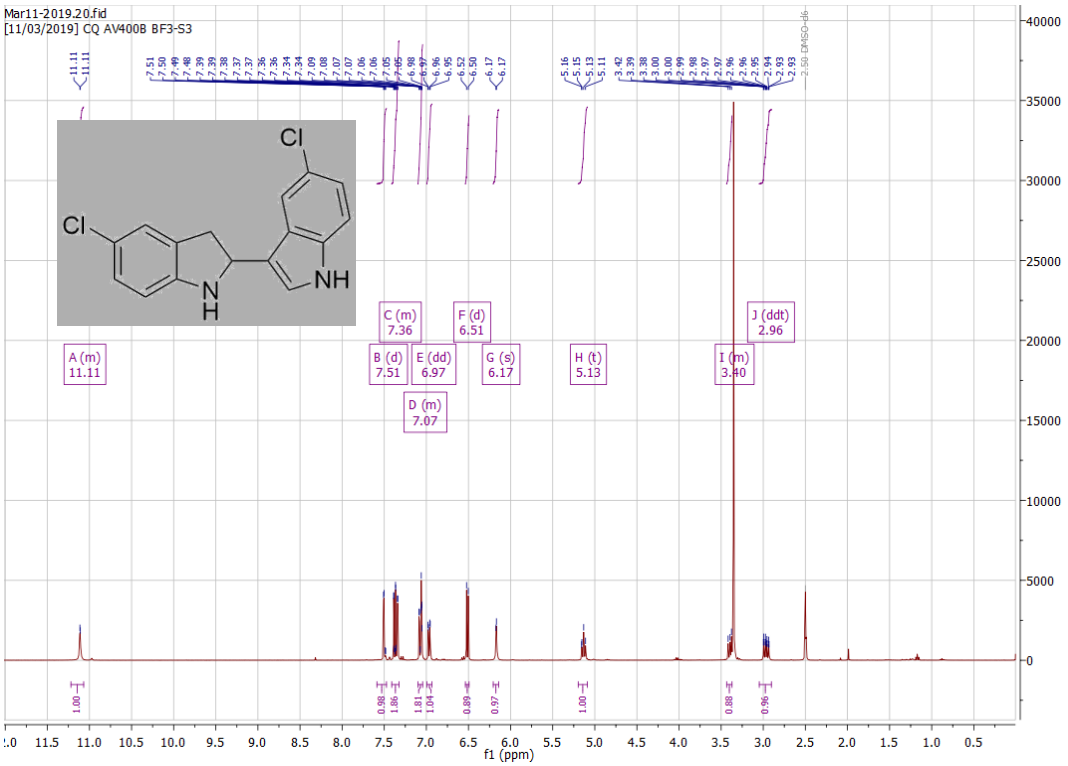


SI Figure 16.

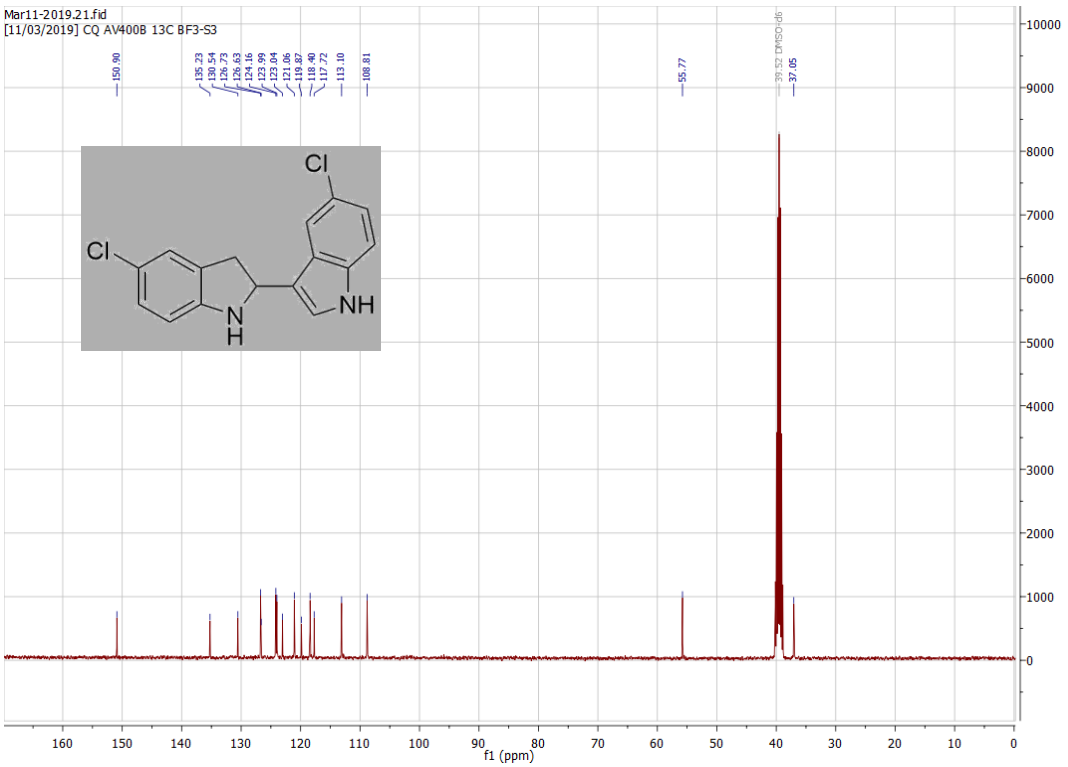

Click Here or Press 'Esc' to Return
Select Peaks for Labeling.
Transmittance
Wavenumber (cm-1)
4000
3500
3000
2500
2000
1500
1000
102
100
98
96
94
92
1474.2; 95.758
1172.2; 95.563
1413.6; 94.830
1438.8; 93.794
1459.3; 93.008
1228.2; 92.525
755.7; 92.274
803.2; 91.780
669.1; 95.787
702.6; 95.510
788.3; 95.242
734.3; 93.935
856.4; 93.986
873.1; 93.525
1109.8; 92.884
883.4; 92.887
813.5; 92.419

SI Figure 17.

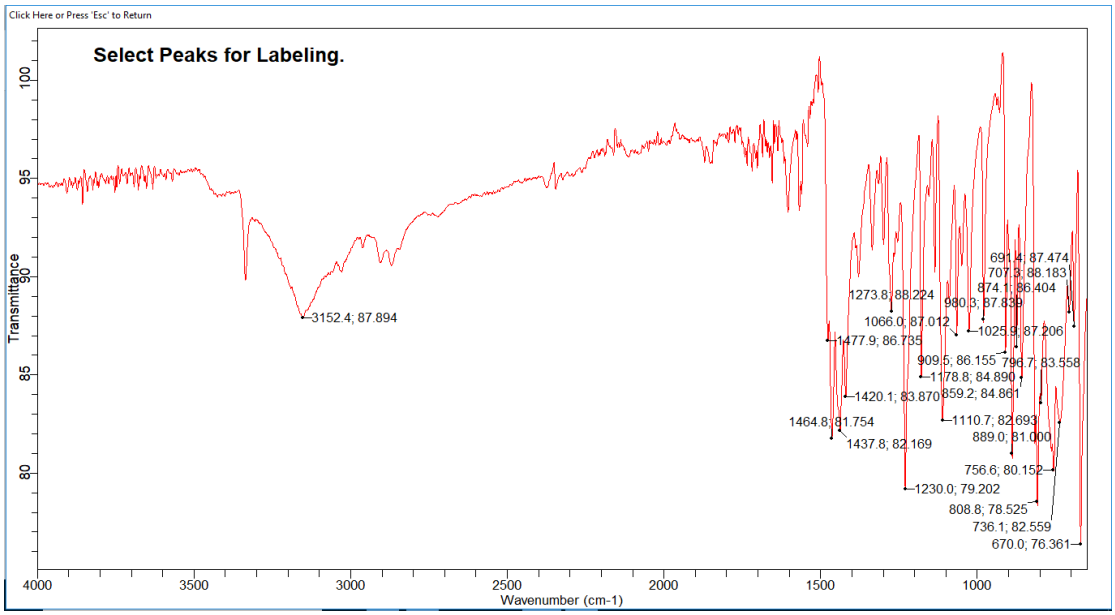

Br
Br
N
H
NH



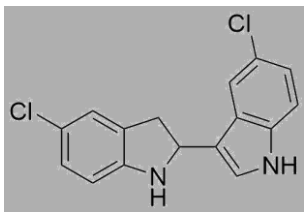
SI Figure 18.

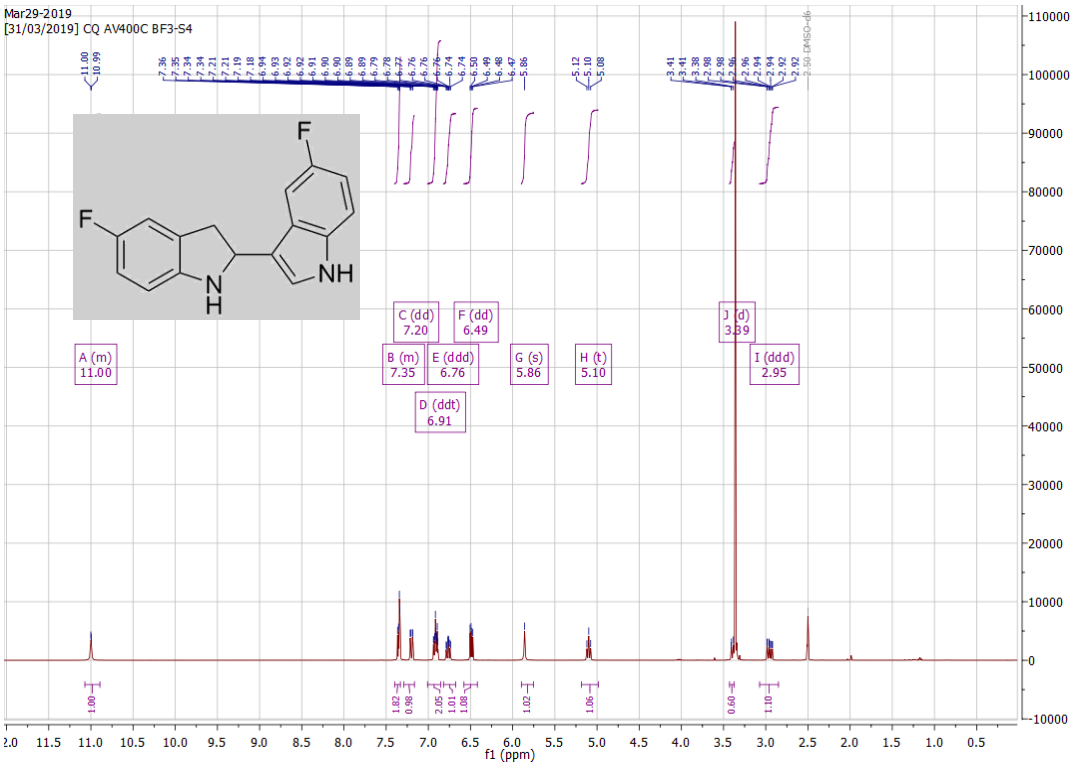


SI Figure 19.

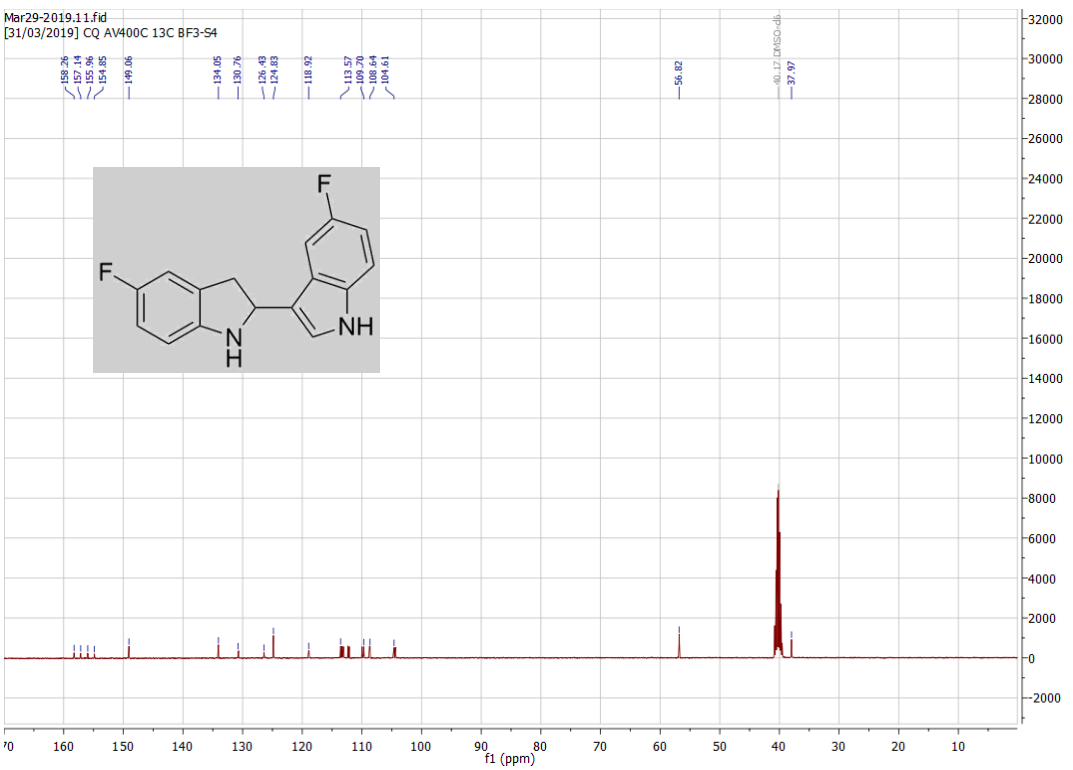

Click Here or Press 'Esc' to Return
Select Peaks for Labeling.
Transmittance
Wavenumber (cm-1)
3152.4; 87.894
1273.8; 88.224
1066.0; 87.012
1477.9; 86.735
1420.1; 83.870
1464.8; 81.754
1437.8; 82.169
1230.0; 79.202
691.4; 87.474
707.3; 88.183
874.1; 86.404
980.3; 87.839
1025.9; 87.206
909.5; 86.155
796.7; 83.558
1178.8; 84.890
859.2; 84.861
1110.7; 82.693
889.0; 81.000
756.6; 80.152
808.8; 78.525
736.1; 82.559
670.0; 76.361

SI Figure 20.

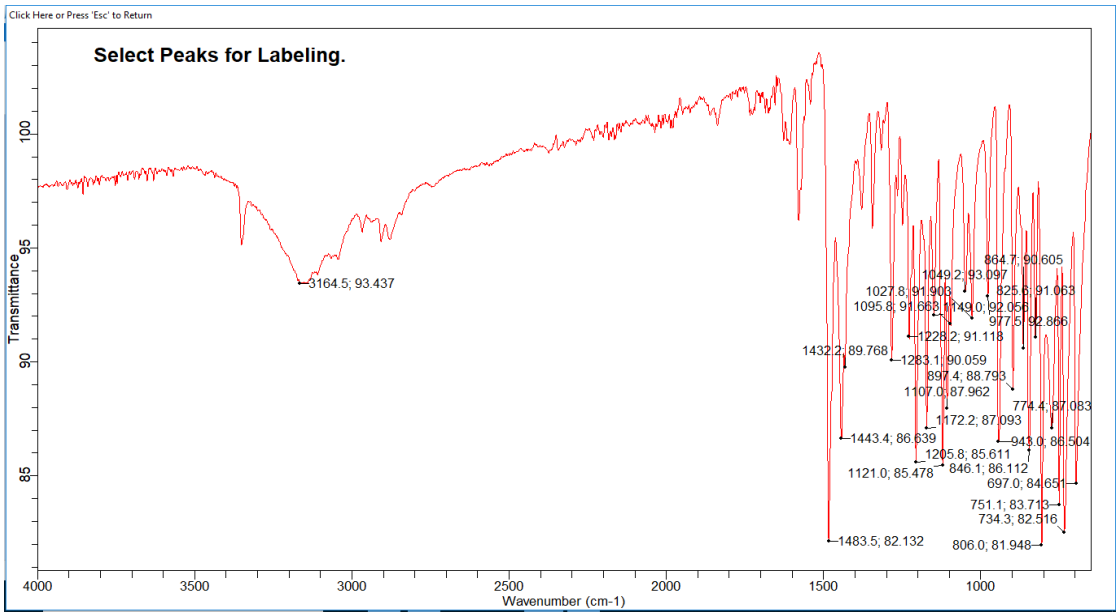

Cl
Cl
N
H
NH



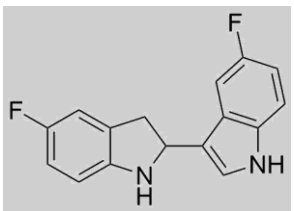
SI Figure 21.

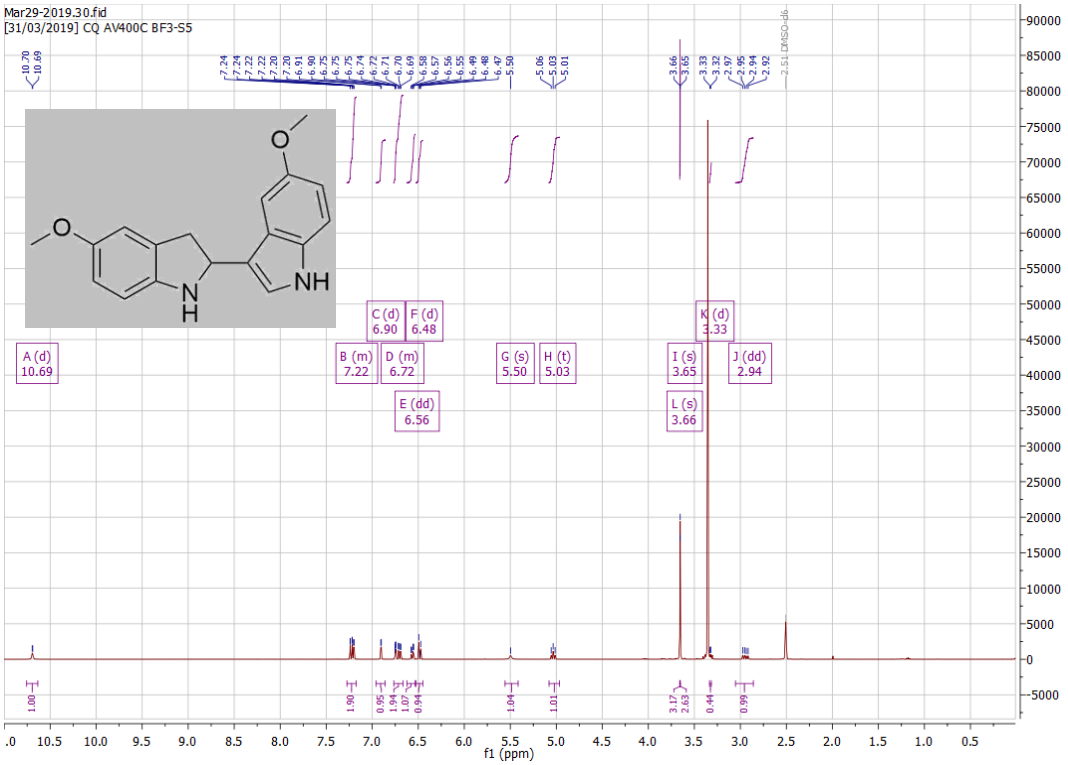


SI Figure 22.

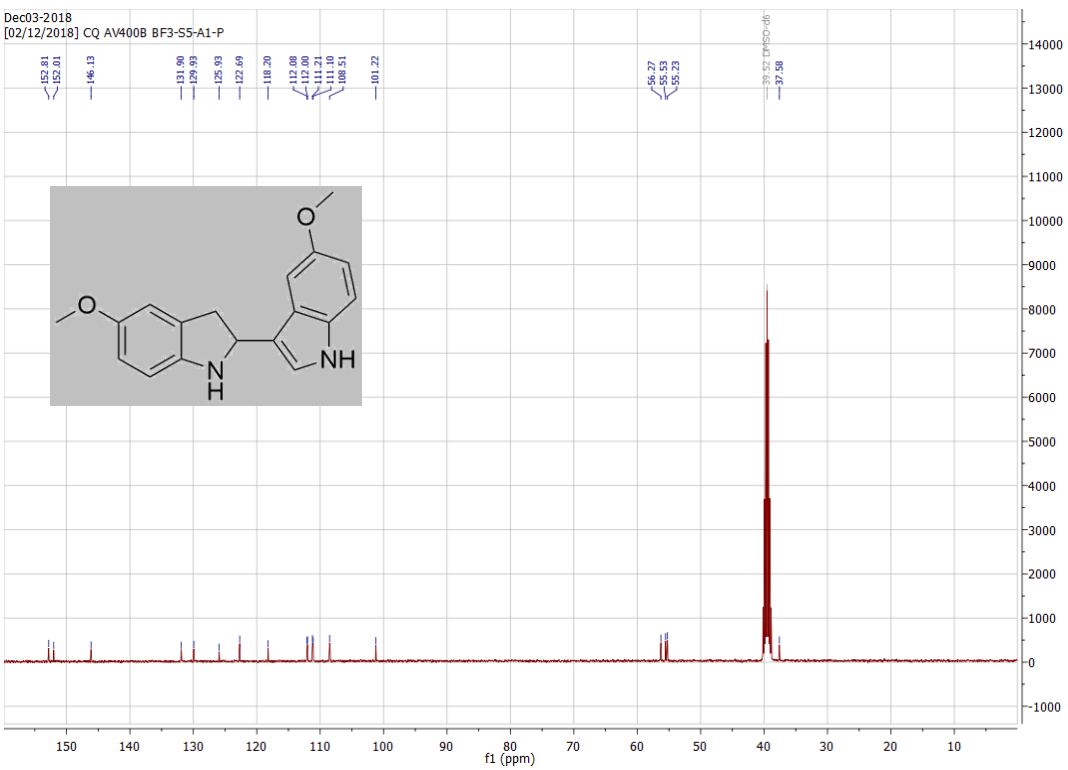

Click Here or Press 'Esc' to Return
Select Peaks for Labeling.
Transmittance
Wavenumber (cm-1)
4000
3500
3000
2500
2000
1500
1000
100
95
90
85
3164.5; 93.437
1483.5; 82.132
1443.4; 86.639
1432.2; 89.768
1283.1; 90.059
1228.2; 91.118
1205.8; 85.611
1172.2; 87.093
1121.0; 85.478
1107.0; 87.962
1095.8; 91.668
1049.2; 93.097
1027.8; 91.903
977.5; 92.866
943.0; 86.504
897.4; 88.793
864.7; 90.605
846.1; 86.112
825.8; 91.053
806.0; 81.948
774.4; 87.083
751.1; 83.713
734.3; 82.516
697.0; 84.651

SI Figure 23.

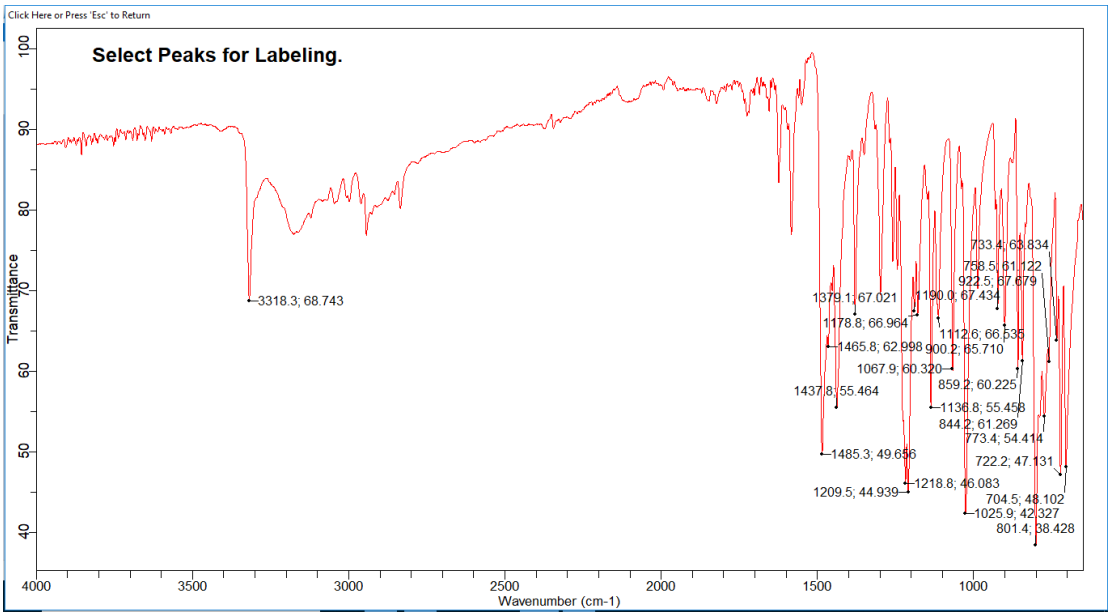

F
F
N
H
NH



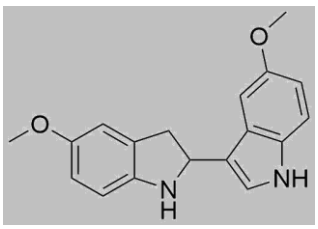
SI Figure 24.

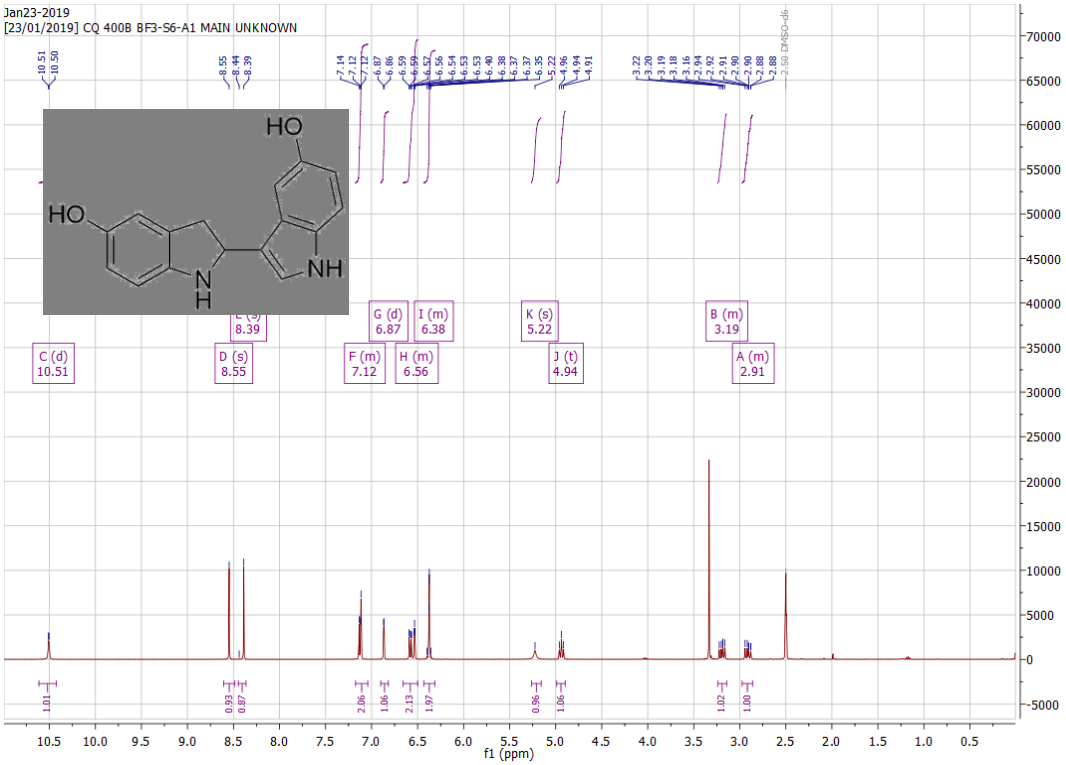


SI Figure 25.

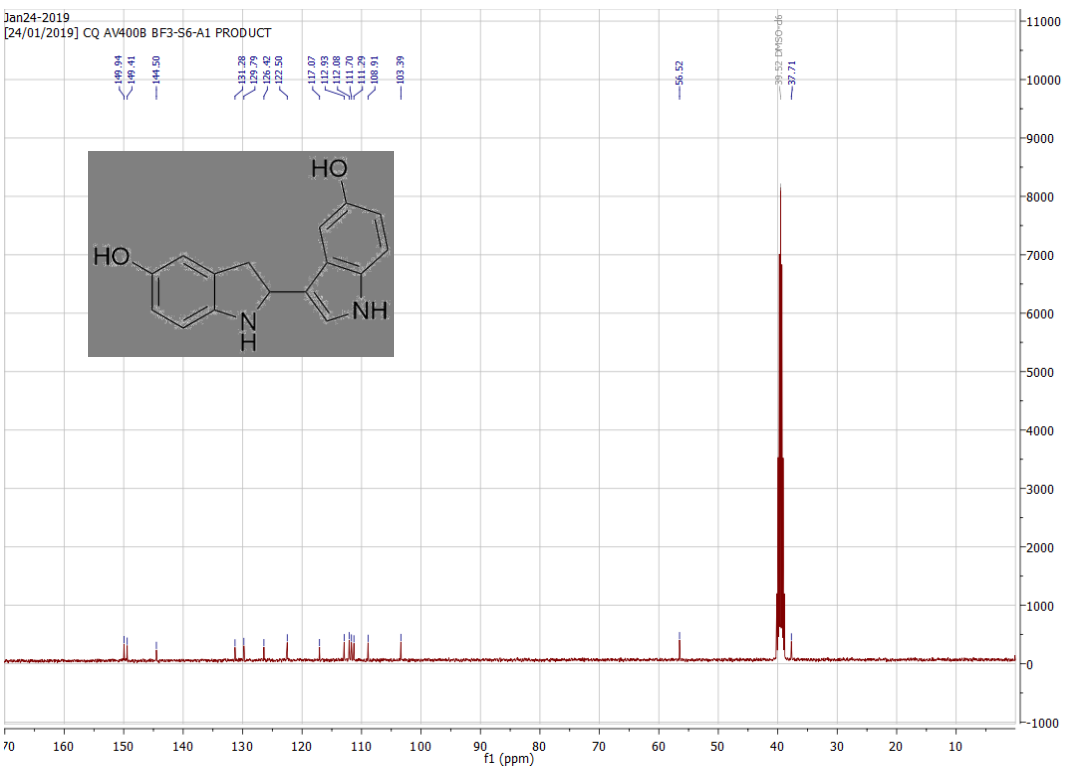

Click Here or Press 'Esc' to Return
Select Peaks for Labeling.
Transmittance
Wavenumber (cm-1)
3318.3; 68.743
1379.1; 67.021
1178.8; 66.964
1465.8; 62.998
1067.9; 60.320
1437.8; 55.464
1485.3; 49.656
1209.5; 44.939
1218.8; 46.083
1190.0; 67.434
1112.6; 66.535
900.2; 65.710
859.2; 60.225
1136.8; 55.458
844.2; 61.269
773.4; 54.414
722.2; 47.131
704.5; 48.102
1025.9; 42.327
801.4; 38.428
733.4; 63.834
758.5; 61.122
922.5; 67.679

SI Figure 26.

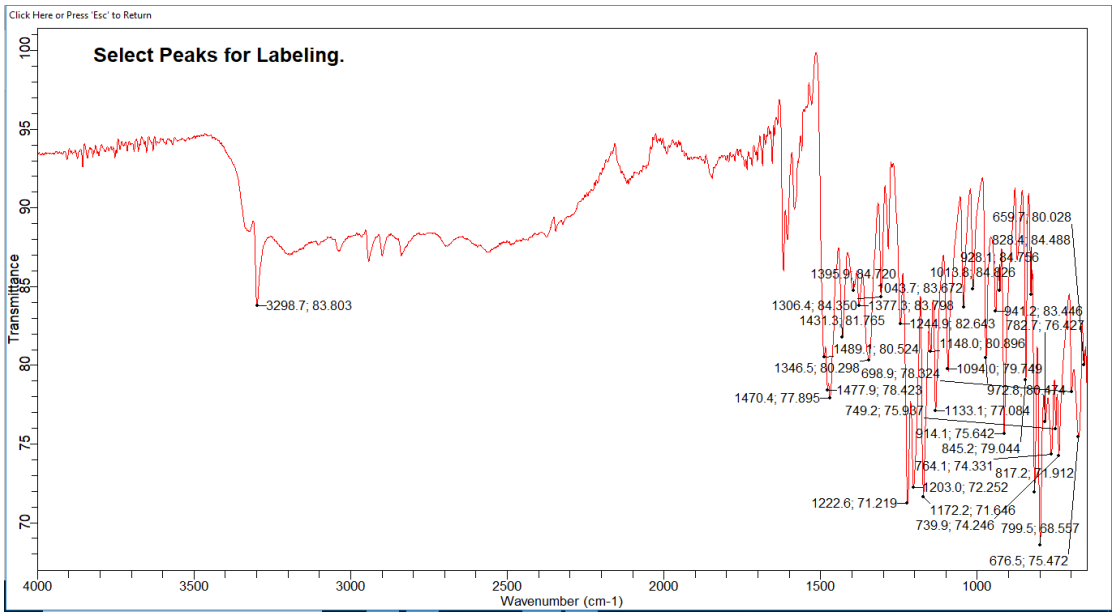

O
O
N
H
NH



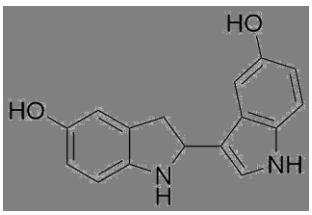
SI Figure 27.

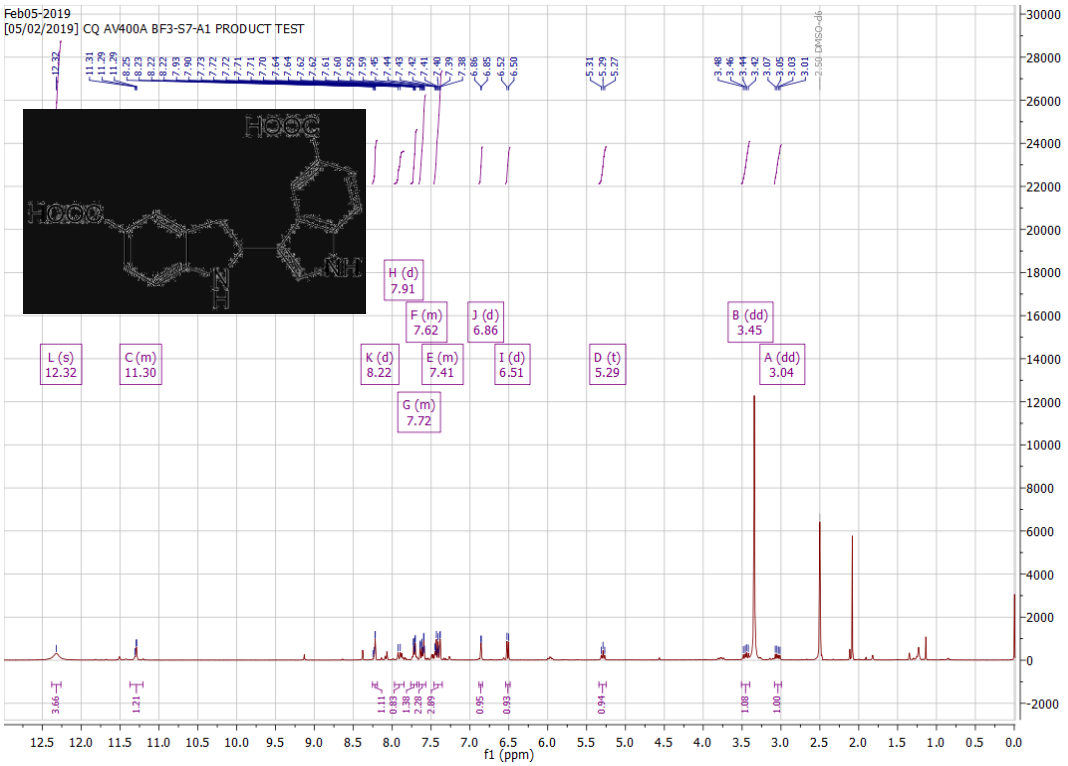


SI Figure 28.

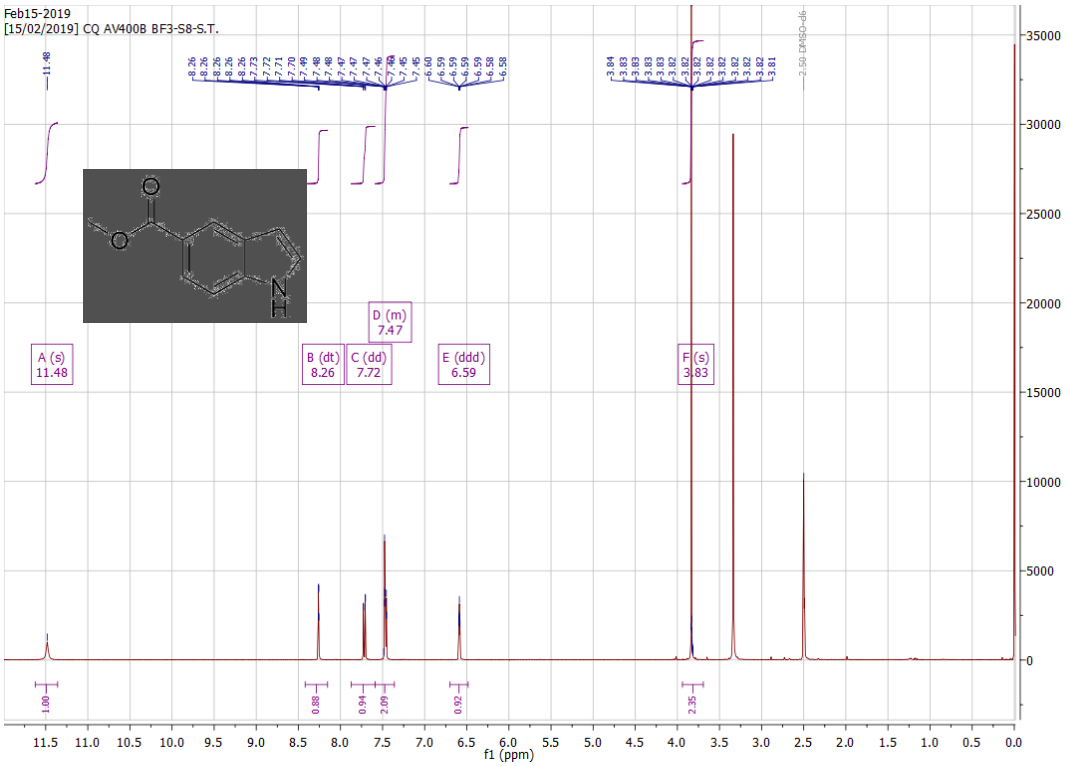

Click Here or Press 'Esc' to Return
Select Peaks for Labeling.
Transmittance
Wavenumber (cm-1)
4000
3500
3000
2500
2000
1500
1000
100
95
90
85
80
75
70
3298.7; 83.803
659.7; 80.028
828.4; 84.488
928.1; 84.766
1395.9; 84.720
1013.8; 84.826
1043.7; 83.672
1306.4; 84.350
1377.3; 83.798
941.2; 83.446
1431.3; 81.765
1244.9; 82.643
782.7; 76.427
1489.1; 80.524
1148.0; 80.896
1346.5; 80.298
698.9; 78.324
1094.0; 79.749
1470.4; 77.895
1477.9; 78.423
972.8; 80.474
749.2; 75.937
1133.1; 77.084
914.1; 75.642
845.2; 79.044
764.1; 74.331
817.2; 71.912
1203.0; 72.252
1222.6; 71.219
1172.2; 71.646
739.9; 74.246
799.5; 68.557
676.5; 75.472

SI Figure 29.

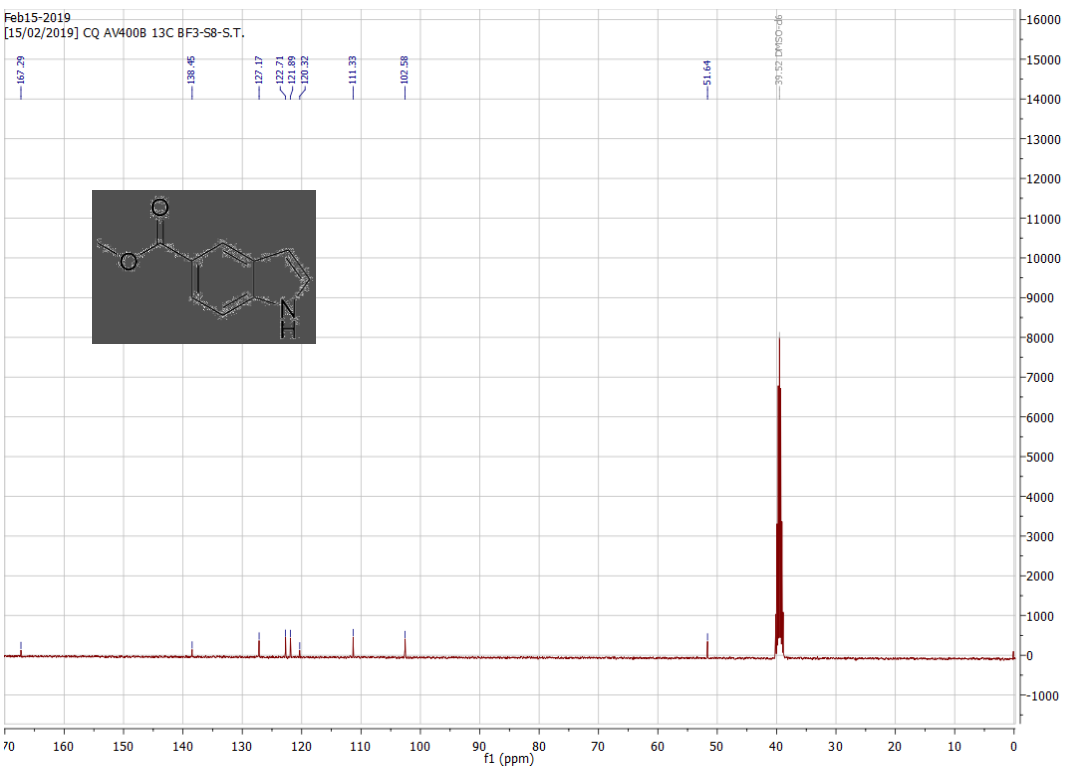

HO
HO
N
H
NH


Feb05-2019
[05/02/2019] CQ AV400A BF3-S7-A1 PRODUCT TEST
HOOC
HOOC
NH
H (d) 7.91
F (m) 7.62
J (d) 6.86
B (dd) 3.45
L (s) 12.32
C (m) 11.30
K (d) 8.22
E (m) 7.41
I (d) 6.51
D (t) 5.29
A (dd) 3.04
G (m) 7.72
f1 (ppm)

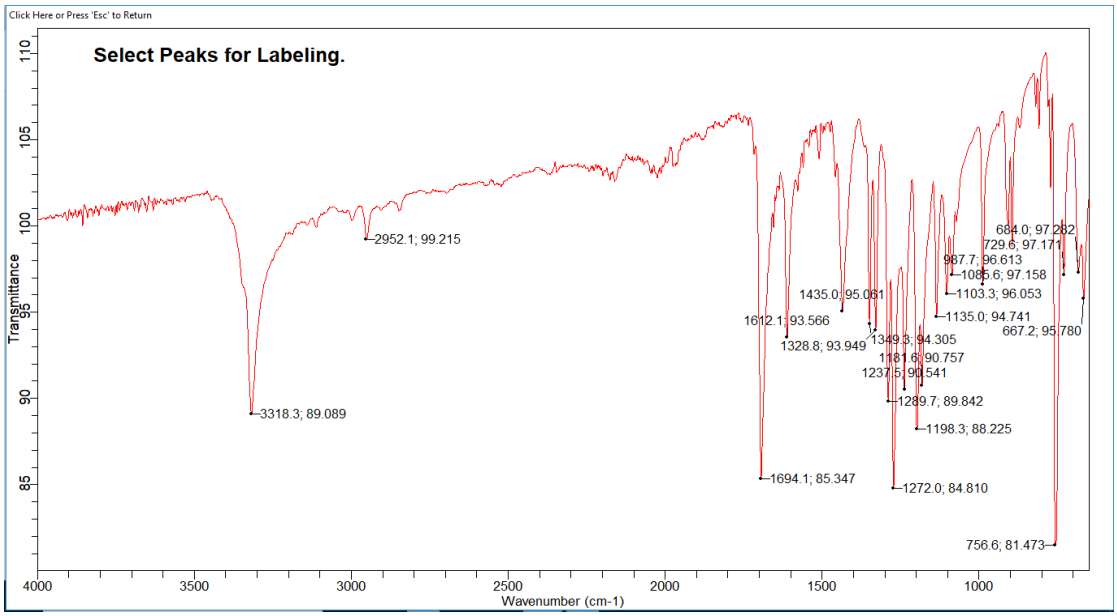
SI Figure 30.



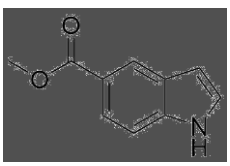
SI Figure 31.

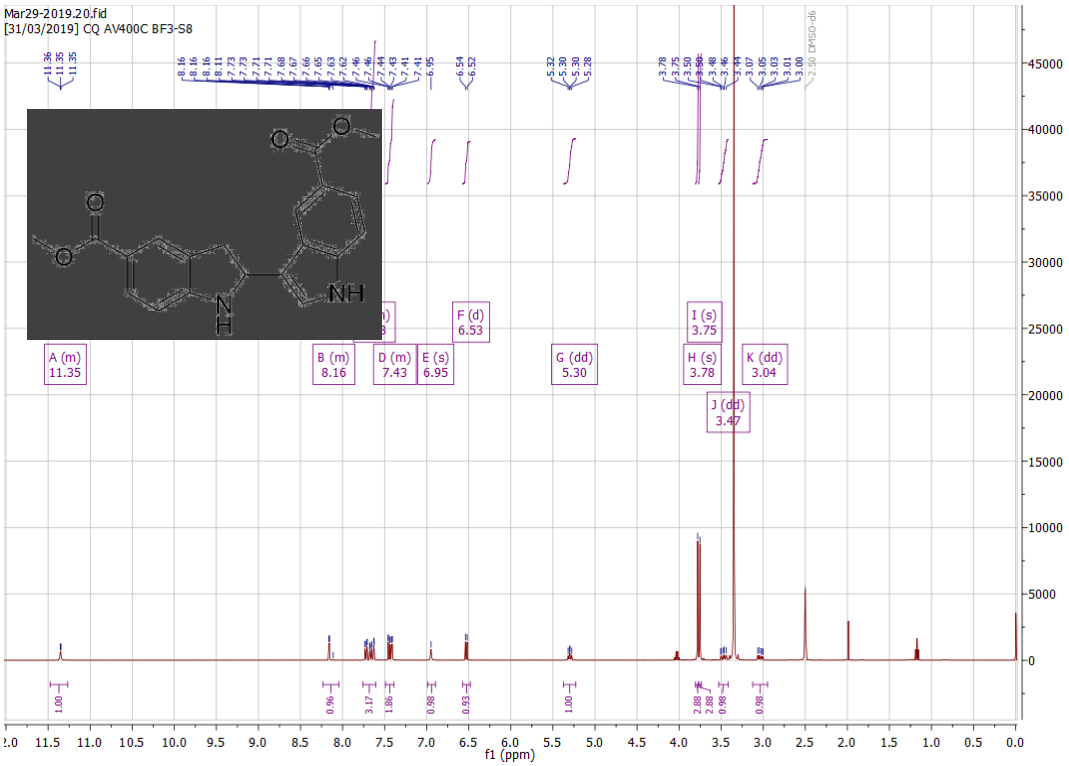


SI Figure 32.

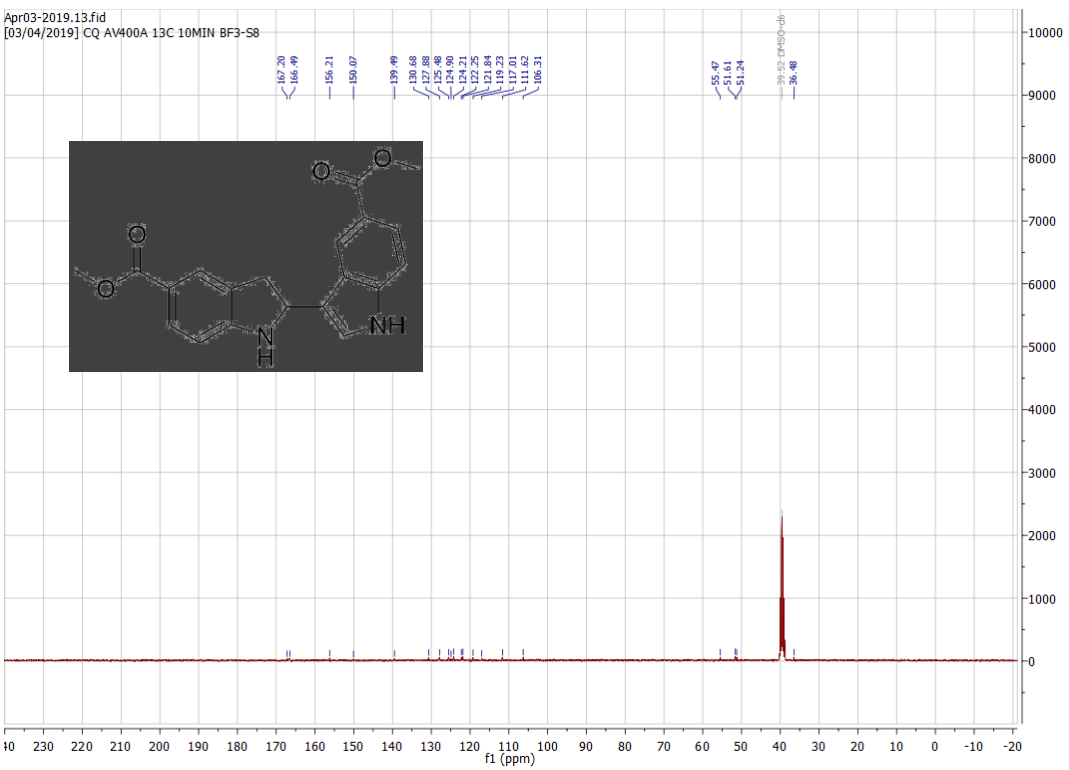

Click Here or Press 'Esc' to Return
Select Peaks for Labeling.
Transmittance
Wavenumber (cm-1)
4000
3500
3000
2500
2000
1500
1000
110
105
100
95
90
85
2952.1; 99.215
3318.3; 89.089
1694.1; 85.347
1612.1; 93.566
1435.0; 95.061
1328.8; 93.949
1349.3; 94.305
1181.6; 90.757
1237.5; 90.541
1289.7; 89.842
1198.3; 88.225
1272.0; 84.810
756.6; 81.473
684.0; 97.282
729.6; 97.171
987.7; 96.613
1085.6; 97.158
1103.3; 96.053
1135.0; 94.741
667.2; 95.780

SI Figure 33.

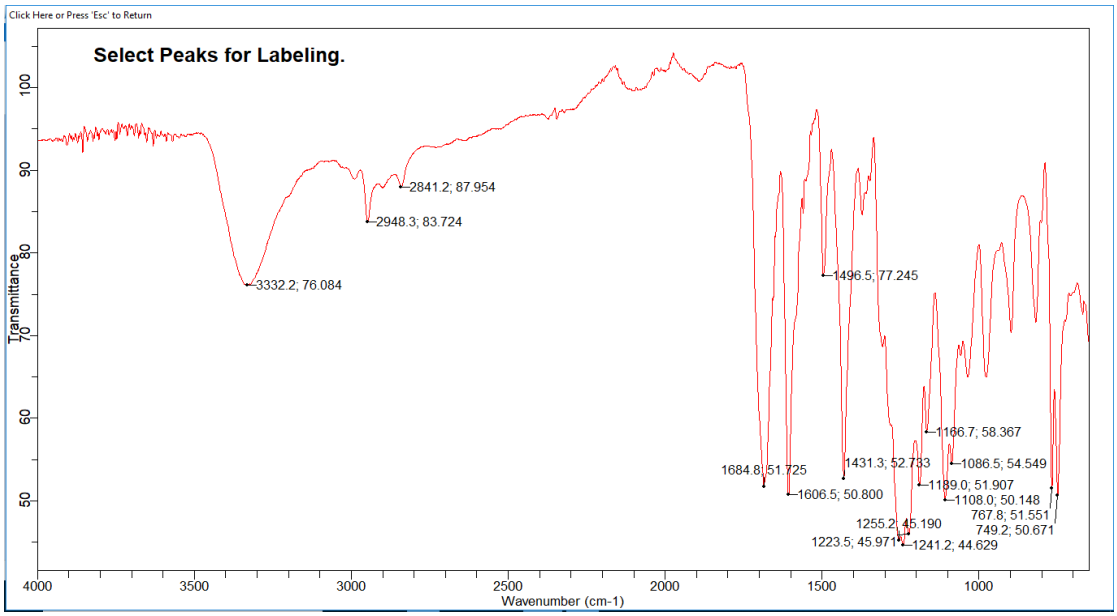

O
O
N
H



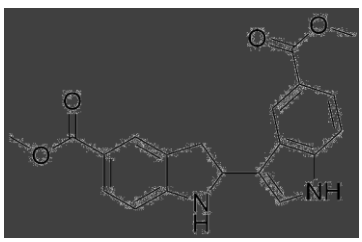
SI Figure 34.

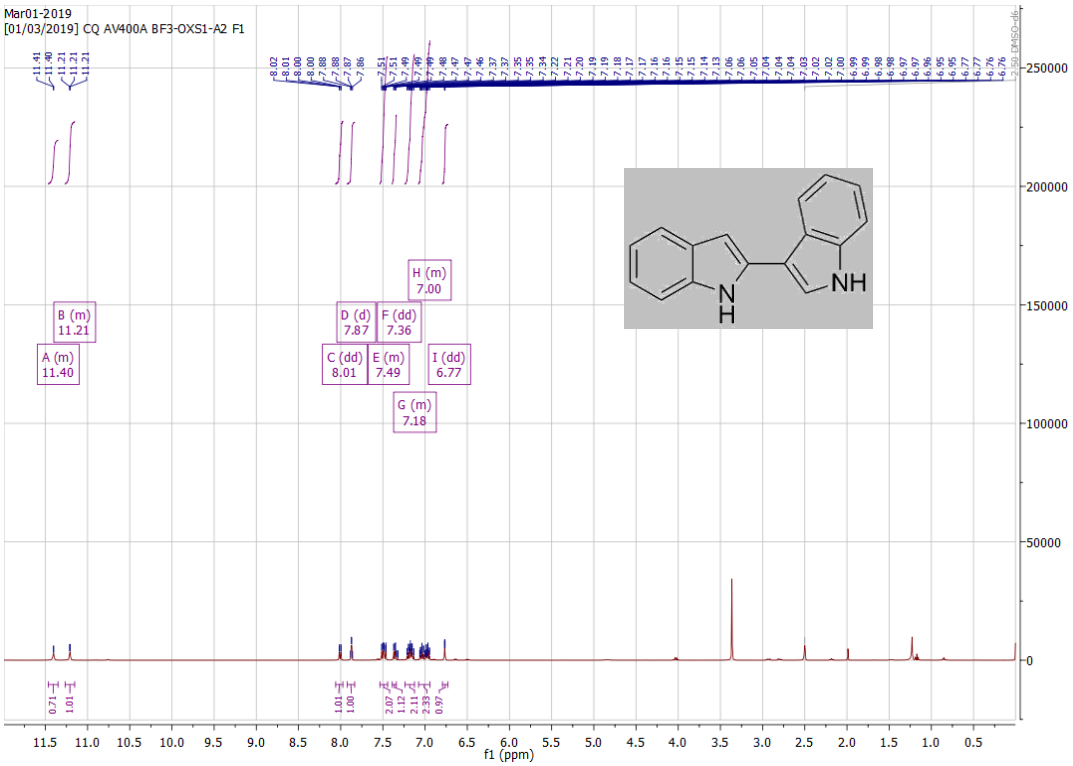


SI Figure 35.

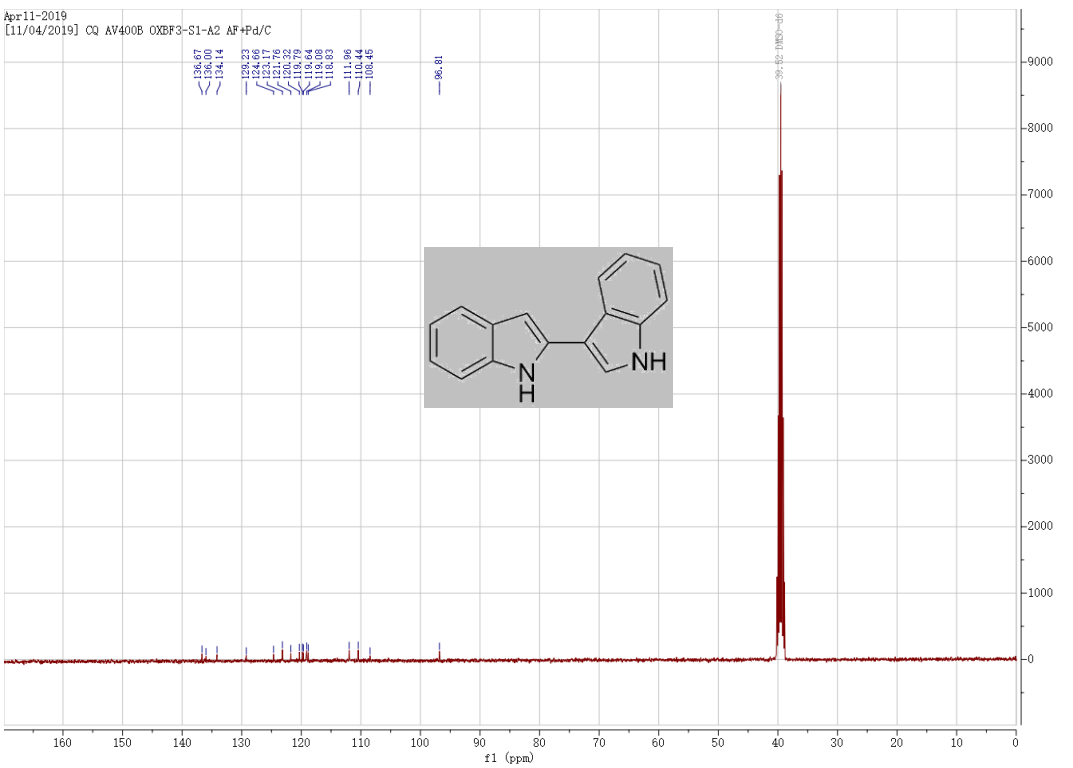

Click Here or Press 'Esc' to Return
Select Peaks for Labeling.
Transmittance
Wavenumber (cm-1)
4000
3500
3000
2500
2000
1500
1000
100
90
80
70
60
50
3332.2; 76.084
2948.3; 83.724
2841.2; 87.954
1496.5; 77.245
1684.8; 51.725
1606.5; 50.800
1431.3; 52.733
1166.7; 58.367
1086.5; 54.549
1189.0; 51.907
1108.0; 50.148
767.8; 51.551
749.2; 50.671
1255.2; 45.190
1223.5; 45.971
1241.2; 44.629

SI Figure 36.

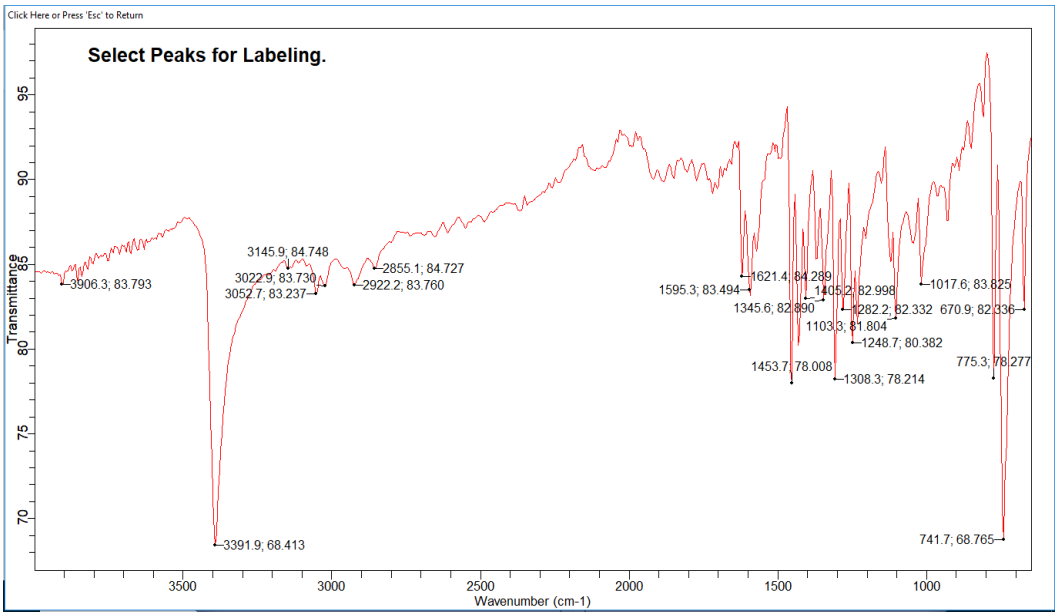

O
O
O
O
N
H
NH



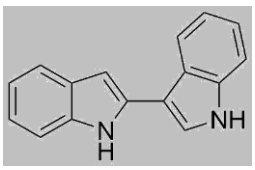
SI Figure 37.



SI Figure 38.


Click Here or Press 'Esc' to Return
Select Peaks for Labeling.
Transmittance
Wavenumber (cm-1)
3906.3; 83.793
3145.9; 84.748
3022.9; 83.730
3052.7; 83.237
2855.1; 84.727
2922.2; 83.760
3391.9; 68.413
1595.3; 83.494
1621.4; 84.289
1405.2; 82.998
1345.6; 82.890
1282.2; 82.332
1103.3; 81.804
1248.7; 80.382
1453.7; 78.008
1308.3; 78.214
1017.6; 83.825
670.9; 82.336
775.3; 78.277
741.7; 68.765

SI Figure 39.


N
H
NH

SI Table 1. Enz Serial Dilution Stock concentration (Series A & Series B) (36 in total)

	4X DMSO in NRB/ µM	4X DMSO in NRB/ nM	4X DMSO in NRB/ µM	4X DMSO in NRB/ nM
1	2.00E+02	200000.00	3.00E+02	300000.00
2	1.00E+02	100000.00	1.50E+02	150000.00
3	5.00E+01	50000.00	7.50E+01	75000.00
4	2.50E+01	25000.00	3.75E+01	37500.00
5	1.25E+01	12500.00	1.88E+01	18750.00
6	6.25E+00	6250.00	9.38E+00	9375.00
7	3.13E+00	3125.00	4.69E+00	4687.50
8	1.56E+00	1562.50	2.34E+00	2343.75
9	7.81E-01	781.25	1.17E+00	1171.88
10	3.91E-01	390.63	5.86E-01	585.94
11	1.95E-01	195.31250000	2.93E-01	292.97
12	9.77E-02	97.65625000	1.46E-01	146.48437500
13	4.88E-02	48.82812500	7.32E-02	73.24218750
14	2.44E-02	24.41406250	3.66E-02	36.62109375
15	1.22E-02	12.20703125	1.83E-02	18.31054688
16	6.10E-03	6.10351563	9.16E-03	9.15527344
17	3.05E-03	3.05175781	4.58E-03	4.57763672
18	1.53E-03	1.52587891	2.29E-03	2.28881836

5

SI Table 2. Compound 1 Stock Concentration (20 in total)

Number	4X DMSO in NRB/ µM	4X DMSO in NRB/ nM
1	3.00E+02	300000.00
2	1.50E+02	150000.00
3	7.50E+01	75000.00
4	3.75E+01	37500.00
5	1.88E+01	18750.00
6	9.38E+00	9375.00
7	4.69E+00	4687.50
8	2.34E+00	2343.75
9	1.17E+00	1171.88
10	5.86E-01	585.94
11	2.93E-01	292.97
12	1.46E-01	146.48437500
13	7.32E-02	73.24218750
14	3.66E-02	36.62109375
15	1.83E-02	18.31054688
16	9.16E-03	9.15527344
17	4.58E-03	4.57763672
18	2.29E-03	2.28881836
19	1.14E-03	1.14440918
20	5.72E-04	0.57220459

5

SI Table 3. Compound 3 Serial Dilution Stock concentration (20 in total)

Number	4X DMSO in NRB/ µM	4X DMSO in NRB/ nM
1	3.00E+02	300000.00
2	1.50E+02	150000.00
3	7.50E+01	75000.00
4	3.75E+01	37500.00
5	1.88E+01	18750.00
6	9.38E+00	9375.00
7	4.69E+00	4687.50
8	2.34E+00	2343.75
9	1.17E+00	1171.88
10	5.86E-01	585.94
11	2.93E-01	292.97
12	1.46E-01	146.48437500
13	7.32E-02	73.24218750
14	3.66E-02	36.62109375
15	1.83E-02	18.31054688
16	9.16E-03	9.15527344
17	4.58E-03	4.57763672
18	2.29E-03	2.28881836
19	1.14E-03	1.14440918
20	5.72E-04	0.57220459

5

SI Table 4. T Serial Dilution Stock concentration (22 in total)

	4X DMSO in NRB/ µM	4X DMSO in NRB/ nM
1	2.00E+02	200000.00
2	1.00E+02	100000.00
3	5.00E+01	50000.00
4	2.50E+01	25000.00
5	1.25E+01	12500.00
6	6.25E+00	6250.00
7	3.13E+00	3125.00
8	1.56E+00	1562.50
9	7.81E-01	781.25
10	3.91E-01	390.63
11	1.95E-01	195.31250000
12	9.77E-02	97.65625000
13	4.88E-02	48.82812500
14	2.44E-02	24.41406250
15	1.22E-02	12.20703125
16	6.10E-03	6.10351563
17	3.05E-03	3.05175781
18	1.53E-03	1.52587891
19	7.63E-04	0.76293945
20	3.81E-04	0.38146973
21	1.91E-04	0.19073486
22	9.54E-05	0.09536743

SI Table 5. CT Serial Dilution Stock concentration (24 in total)

	Stock B, 4X DMSO in NRB/ nM
1	800000.00
2	400000.00
3	200000.00
4	100000.00
5	50000.00
6	25000.00
7	12500.00
8	6250.00
9	3125.00
10	1562.50
11	781.25
12	390.63
13	195.31
14	97.66
15	48.83
16	24.41
17	12.21
18	6.10
19	3.05
20	1.525879
21	0.762939
22	0.381470
23	0.190735
24	0.095367